MECHANISMS OF EXTRACELLULAR MATRIX SCAFFOLD REMODELING

by

Thomas Wayne Gilbert

B.S. in Materials Science and Engineering, Carnegie Mellon University, 1998

Submitted to the Graduate Faculty of

School of Engineering in partial fulfillment

of the requirements for the degree of

Ph.D. in Bioengineering

University of Pittsburgh

2006

UNIVERSITY OF PITTSBURGH

SCHOOL OF ENGINEERING

This dissertation was presented

by

Thomas W. Gilbert

It was defended on

October 20, 2006

and approved by

Savio L-Y. Woo, PhD, DSc, Professor, Department of Bioengineering

Michael S. Sacks, PhD, Professor, Department of Bioengineering

James H-C. Wang, PhD, Associate Professor, Department of Orthopaedic Surgery

Susan J. Braunhut, PhD, Professor, Department of Biological Sciences

Dissertation Director: Stephen F. Badylak, DVM, MD, PhD, Department of Surgery

MECHANISMS OF EXTRACELLULAR MATRIX SCAFFOLD REMODELING

Thomas W Gilbert, PhD

University of Pittsburgh, 2006

Scaffolds composed of extracellular matrix (ECM) and derived from various species and various organs have been shown to promote constructive, site-specific tissue remodeling in pre-clinical studies and clinical use, including musculoskeletal, urogenital, dermal, cardiovascular, and neural applications. Despite extensive study, the mechanisms of the remodeling process are still not thoroughly understood. The goals of this dissertation were to elucidate the role of mechanical loading in the remodeling of ECM scaffolds and the role of bone marrow derived cells in the remodeling process.

To better understand the role of mechanical loading on the remodeling of an ECM scaffold, an ECM scaffold derived from the porcine small intestinal submucosa (SIS-ECM) was seeded with fibroblasts and subjected to a variety of magnitudes and frequencies of cyclic strain using a custom designed Cyclic Stretching Tissue Culture system. The magnitudes of stretch were based on a study of the collagen fiber kinematics of the SIS-ECM under uniaxial and biaxial loading conditions. The cyclic loading experiments showed that mechanical loading led to expression of matrix related genes that was consistent with a constructive remodeling response with increased expression of collagen type I (Col I), α-smooth muscle actin (SMA), and tenascin-C (TN-C), as well as decreased expression of collagen type III (Col III).

It was also found that bone marrow cells were recruited to the site of ECM remodeling and that the cells remained at the site of remodeling for 16 weeks after implantation, unlike an autologous tendon repair. Furthermore, it was found that the bone marrow derived cells did not express the hematopoietic marker CD45, but did express Col I, Col III, and SMA. The cells did not show the same expression pattern as normal tendon fibroblast (Col I^+, TN-C^+), suggesting that the cells differentiated towards a myofibroblastic cell as opposed to a normal fibroblast. The results of this study show that an ECM scaffold recruits a bone marrow derived mesenchymal progenitor to the site of remodeling, and that those cells differentiate into site specific tissue as a result of mechanical and biochemical cues.

TABLE OF CONTENTS

LIST OF TABLES

LIST OF FIGURES

PREFACE

The completion of this Dissertation would not have been possible without the efforts or support of countless individuals. First and foremost, I would like to thank my family, especially my mother, Judi Wooddy, my sister, Angela Wooddy, and my grandmother, Gertrude Kohler. Ever since I was young, they have all supported me in every endeavor I have pursued, and they have always been there to share in my success or to hold me up after my failures. Without their love and support, I could never have dreamed of being were I am today.

I would also like to thank my fiancée, Jennifer Clark. We met in the midst of my graduate work, and despite the long hours and the stressful times, she learned to love me anyway. Her support and understanding have been incredibly important to me, and she has also helped me to hold on to a little bit of sanity by giving me a reason to put my work away from time to time.

Thanks are also in order to my many friends that have stuck with me during my PhD studies. In particular, I would like to thank Marc Palmisiano, Ron Polcawich, Amy Ogan, Brad Palmisiano, Chris Wlodarczyk, Dave Kucera, Drew and Pam Shefman, and Liz Atkinson. They have always been there to keep me grounded, either by getting together for a beer to let lose, going dancing, going camping, or just to pick on me for being a professional student.

I would like to thank my highly talented Dissertation Committee for all of the time and energy they have dedicated to my education. First to Dr. Stephen Badylak, thank you for your willingness to take a chance on me, and for providing an environment in which there were endless opportunities available for the taking (as long as you were willing to work hard). All of the experiences that I have had since I joined your lab have enabled me grow immeasurably, and have given me a unique perspective as a graduate student on the field regenerative medicine. I look forward to our continued collaborations.

To Dr. Savio Woo, thank you for providing me with a strong foundation on which to begin my graduate studies. I definitely feel that your early tutelage has had a strong impact on the way that I approach my work today. To Dr. Michael Sacks, thank you for helping me to gain an appreciation for rigorous biomechanical study. I hope to delve deeper into this field of work as I begin my career. To Dr. James Wang, thank you for exposing me to the field of mechanobiology. When I first decided to pursue graduate studies, this topic was the driving force even though I did not even know the term existed. In addition, I want to thank you for all of the personal attention you provided me in the first few years of as a graduate student. Our conservations made my transition to graduate school much easier, and formed the foundation for much of my future work. Finally, to Dr. Susan Braunhut, thank you offering a different point of view with which to view my research.

I would also like to thank Dr. Harvey Borovetz. The Department of Bioengineering could not ask for a better Chairperson. He truly cares for the students in a special way. I thank him for all of the guidance he gave me over the past 6 years. I would also like it documented officially that if I had to drag my limp body across the finish line, I would not finish behind Dr. Borovetz in a marathon.

Many other Professors have had an influence on my work over the past 6+ years. Here at the University of Pittsburgh, I would like to thank Dr. David Vorp, Dr. Donna Stolz, Dr. Rich Debski, Dr. William Wagner, and Dr. Alan Russell. Elsewhere, I would like to thank Dr. David Butler (University of Cincinnati), Dr. Kathe Derwin (Cleveland Clinic Founation), Dr. Merv Yoder (Indiana University School of Medicine), and Dr. Y.C. Fung (UC San Diego).

I also was fortunate to work with a number of talented and dedicated surgeons during my time as a graduate student. I would like to thank Dr. Alex Nieponice, Dr. Thore Zantop, Dr. Sebastien Gilbert, Dr. AJ Yates, and Dr. Clark Rosen. I have learned a great deal from each of you, and I enjoyed our time in the OR.

I would also like to thank the members of the Musculoskeletal Research Center for helping me learn how to do good research, and helping me to laugh a lot while I was doing it. In particular, I would like to thank Dr. Steve Abramowitch. I still look back fondly on many of our memories in the BST. You were a great mentor and are a great friend. I look forward to much future collaboration.

Many thanks also to the members of the Badylak Lab and the Center for Pre-Clinical Studies. Special thanks to Dr. Ann Stewart-Akers, Jennifer Sydeski, and Bryan Brown for their contributions to the work that became part of my Dissertation. Thanks to Ann also for being a great sounding board for research ideas. I would also like to thank Dr. Alex Nieponice for many thought provoking conversations about research, and for teaching me some surgical skills. Thanks to Buffie Kerstetter, Shawn Bengston, Joe Hanke, and Terri Gasser for all of the support at the animal facility. We are incredibly lucky to have such a knowledgeable, dedicated, and fun loving staff. I have learned a lot from all of you. I am glad to call all of the members of the Badylak Lab both colleagues and friends, and look forward to continuing to work with all of you in the next phase of my career.

1.0 NATURALLY OCCURRING EXTRACELLULAR MATRIX

There are currently six commercially available scaffolds derived from naturally occurring extracellular matrix (ECM) that have gained approval from the Food and Drug Administration for musculotendinous applications, including GraftJacket® (Wright Medical Technology, Inc., Arlington, TN), Restore™ (DePuy Orthopaedics®, Inc., Warsaw, IN), CuffPatch™ (Arthrotek®, Warsaw, IN), TissueMend® (TEI Biosciences, Inc., Boston, MA), Zimmer® Collagen Repair Patch (Stryker Orthopaedics, Warsaw, IN), and OrthADAPT™ (Pegasus Biologics, Irvine, CA). These scaffolds vary in the species of origin, tissue of origin, means of decellularization and terminal sterilization, and extent of chemical crosslinking. Despite their clinical use, there is limited information regarding the host response to many of these products or the mechanisms by which the host response occurs. A recent study compared the host response to several of the products listed above (all except for OrthAdapt) when they were used to repair the abdominal wall in a rat model.[269] The results showed that all of the devices tended to exhibit a foreign body response to some extent, except for Restore™, which showed a constructive remodeling response. The Restore™ device is composed of porcine small intestinal submucosa (SIS-ECM) that is not chemically crosslinked. These results were consistent with a number of other studies that have shown that naturally occurring ECM scaffolds that have been minimally processed promote the formation of site specific tissue after injury in a variety of body locations in both pre-clinical animal studies and in clinical practice. The goal of this Dissertation was to elucidate some of the mechanisms by which a site specific, constructive remodeling response to a SIS-ECM scaffold occurs.

1.1 COMPOSITION AND ULTRASTRUCTURE OF SIS-ECM

Naturally occurring ECM consists of the structural and functional proteins that provide a framework for every organ. It is isolated by removing the cellular component from a tissue of interest through a series of chemical and mechanical treatments.[99] Naturally occurring ECM has been isolated from the porcine small intestine, urinary bladder, and liver, human dermis, and canine fascia lata, among others.[24] SIS-ECM is the scaffold that has been most extensively characterized. It is composed primarily of type I collagen with minor amounts of collagen types III, IV, V, and VI.[13] Despite the chemical treatments that are necessary to decellularize the SIS-ECM material, the scaffold retains a variety of glycosaminoglycans including heparin, heparin sulfate, chondroitin sulfate, and hyaluronic acid,[118] and adhesion molecules such as fibronectin and laminin.[41, 122] SIS-ECM also contains transforming growth factor-β (TGF-β),[197, 274] basic-fibroblast growth factor (b-FGF),[124, 274] vascular endothelial growth factor (VEGF),[120] and epidermal growth factor (EGF). Several of these growth factors have been shown to retain bioactivity even after terminal sterilization and long-term storage.[124, 197] The 3-D architecture and ultrastructure of SIS-ECM are largely preserved throughout various processing steps, which may explain the retained bioactivity.[41, 237] There is histologic evidence that the stratum compactum of the small intestine is intact and present in the SIS-ECM.[41] The collagen fibers of SIS-ECM generally have a preferred alignment along the longitudinal axis of the small intestine, and it appears that this preference is a composite of two populations of collagen fibers with their centroids shifted ~30° from the longitudinal axis.[237] This preferred fiber alignment gives SIS-ECM a transversely orthotropic mechanical behavior, i.e., the longitudinal axis is stiffer than the circumferential axis.[237]

A variety of forms of SIS-ECM scaffolds have shown utility as scaffolds in regenerative medicine, including, hydrated and lyophilized single layer sheets, multilaminate sheets, and powder. When constructing multilaminate sheets, it is possible to take advantage of the collagen fiber alignment of each layer to create a device with a desired mechanical behavior. For Restore™, ten layers of the ECM are used with 2 layers aligned every 72° to make an isotropic device that is strong enough to serve as a functional replacement of a tendon at the time of surgery.

In summary, a great deal is known about the composition and structure of SIS-ECM and many of its characteristics make it a favorable scaffold for regenerative medicine applications. This dissertation takes advantage of this knowledge, specifically related to the collagen fiber architecture, and attempts to develop a better understanding of the mechanisms by which ECM scaffolds promotes site specific tissue remodeling.

2.0 EXTRACELLULAR MATRIX SCAFFOLD REMODELING *IN VIVO*

When ECM scaffold material is used to replace or repair a damaged tissue, the ECM has been shown to degrade quickly, and is rapidly replaced by new host tissue that is grossly, histologically, and functionally similar to the native tissue it is intended to replace.[14] Site specific remodeling has been shown in a variety of tissues, including blood vessels,[11, 239] skin and body wall,[19, 21, 55, 115, 189, 222, 256] urinary tract,[9, 57, 162, 163, 165, 272, 295] tendons and ligaments,[13, 76, 180, 199, 206, 289] heart,[22, 26, 152, 233] digestive tract,[18, 25, 75] and bone.[258] The new host tissue that forms does not perfectly recapitulate the native tissue structure, but it does provide functionality that scar tissue lacks.

2.1 SITE SPECIFIC REMODELING OF ECM SCAFFOLDS

2.1.1 Cellular Infiltration, Collagen Deposition, and Vascularity

The remodeling process involves a characteristic cell infiltration that begins immediately after implantation.[21] Within the first few hours, an abundance of polymorphonuclear (PMN) leukocytes and mononuclear cells migrate into the ECM scaffold. The numbers of PMN leukocytes decrease so that there are only a few cells (per field) after one week and by two weeks the PMN leukocytes are almost entirely gone. The presence of mononuclear cells persists throughout the first month of remodeling, and slowly decreases thereafter until the number of mononuclear cells approaches that of normal tissue by 3 to 6 months. The morphology of the mononuclear cells tends to change with time suggesting a change in phenotype by approximately 45 days. Initially, the mononuclear cells are rounded in appearance, consistent with the classic concept of a macrophage. The macrophages that infiltrate SIS-ECM in the first two weeks have

been shown to predominantly express CD163, which is a distinct surface marker of an anti-inflammatory/immunoregulatory phenotype.[191, 270] This is consistent with the finding that the early immune response to the ECM scaffold is a TH-2 restricted response, suggesting a accommodation of the device rather than rejection.[5] Over time, the percentage of rounded cells decreases and the percentage of spindle-shaped cells increases. The spindle shaped cells represent site specific cells such as fibroblasts, endothelial cells, and smooth muscle cells. It is not known with certainty if the change in cell morphology is due to the rounded cells leaving the tissue as new spindle shaped cells migrate into the tissue, or if some portion of the rounded cells become the spindle-shaped cells. This dissertation will attempt, at least in part, to answer this question.

In addition to changes in the cellularity of tissue, the connective tissue organization and vascularity tend to follow specific trends during the course of remodeling.[21] The newly formed collagenous connective tissue is disorganized within the first weeks of remodeling. However, by one month, the tissue is moderately to well organized, with the collagen fibers tending to align along axes of stress. At longer time points, the organization continues to improve. In terms of vascularity, an aggressive angiogenic response is observed within the first week of remodeling, and the abundant vascularity tends to remain for up to three months. The causative factors and mechanisms of these changes are topics of interest in the present work.

2.1.2 Mechanical Behavior

The mechanical behavior of a remodeled ECM scaffold changes over time, and the changes are dependent on the tissue that is being replaced and the local mechanical environment. The strength of a remodeled SIS-ECM has been evaluated in a number of applications, including several tendinous and ligamentous applications. In a canine Achilles tendon, a segmental defect was created and repaired with a tube of SIS-ECM (native geometry, not laminated).[13] The joint was immobilized for five weeks, although the limb was allowed to bear weight. At 1 week after implantation, the strength of the tendon repaired with SIS-ECM was less than 100 N, or $1/10^{th}$ of the original strength. As new collagenous connective tissue was formed, the strength of the explanted tendon repaired with SIS-ECM gradually increased until the strength exceeded the strength of the insertions of the tendon to the gastrocnemius muscle and the calcaneus by 12

weeks after surgery.[13] In the rotator cuff application in a dog model, a ten layer multilaminate device (Restore™) was used to replace a completely resected infraspinatus tendon, and the animals were allowed unlimited cage activity after surgery.[76] The failure loads of the tendon repaired with SIS-ECM increased approximately three fold from the time of repair, and were comparable to failure loads for rotator cuffs subjected to a primary repair, despite having a cross sectional area that was smaller by half.[76] In the anterior cruciate ligament of a goat knee, a remodeled SIS-ECM scaffold showed a decreased strength at 3 months after surgery, followed by an increase to a level comparable to a patellar tendon autograft at one year.[16]

The mechanical behavior of remodeled ECM scaffolds has been evaluated in a number of muscular tissue applications. An 8-layer SIS-ECM device used to repair the body wall of a dog decreased to 50% of its initial strength by 10 days after implantation, but subsequently increased to twice its initial strength by 24 months.[19] After repair of the canine urinary bladder with a 3-layer SIS-ECM device,[164] it was found that the compliance of the remodeled graft increased substantially compared to the initial implant (30 fold difference), to levels that were not statistically different from the normal bladder. Furthermore, the remodeled SIS-ECM showed contractility responses that were similar to the normal bladder and the tissue was found to be innervated. A different ECM scaffold derived from the basement membrane and tunica propria of the porcine urinary bladder (UBM-ECM) was used for repair of the canine esophagus and myocardium.[25, 152] For esophageal repair, the ECM graft rapidly remodeled to approach the pressure-diameter response and compliance of the adjacent native esophagus within 90 days.[25] The newly formed esophageal tissue also showed signs of peristalsis, although the muscle contraction was not synchronous with the adjacent native esophagus.[25] In the myocardial repair in a canine model, a single layer of ECM (~100 μm) remodeled and showed evidence of contractility and improved the regional functional of the heart within 8 weeks.[152]

These examples show that in the short term after implantation, ECM scaffolds decrease in strength as the graft is rapidly degraded. However, as new host tissue is formed, the remodeled graft tends to match the mechanical behavior of the tissue that it is intended to repair. In the case of the esophagus, the graft became more compliant, while in the case of tendinous or ligamentous tissue, the load to failure increased. Furthermore, after repair of muscular tissues, the remodeled ECM scaffold does not simply serve as a passive restraint to load. New muscle tissue forms and innervation is restored so that the tissue can provide active contractility.

As stated in the previous section, ECM scaffolds exhibit a characteristic remodeling response in the first month after implantation in terms of cellularity, and yet the resulting tissue that is formed has different morphologies and mechanical behavior depending on the implantation site. Determining how this tissue differentiation occurs is one of the goals of this Dissertation.

2.1.3 Relationship between Mechanical Properties and Tissue Structure

An in depth examination of the remodeling events for a single layer of SIS-ECM has been conducted in a model of medial collateral ligament (MCL) repair in the rabbit knee,[180, 206, 289] and provides insight into some of the mechanisms by which a constructive remodeling response occurs. The SIS-ECM treated repair of a 6 mm segmental defect was compared to a non-treated control and to the sham operated contralateral MCL. At 12 weeks after surgery,[206] the SIS-ECM treated and non-treated groups both showed cross sectional areas (CSA) that were substantially larger than the sham operated control, although they were not statistically different from each other. In terms of the structural properties of the SIS-ECM treated femur-MCL-tibia complex (FMTC), the stiffness and ultimate load were both approximately double the results for the non-treated control. In terms of the mechanical properties of the remodeling SIS-ECM treated MCL, the tangent modulus and stress at failure (several failures occurred at the tibial insertion) were both approximately 50% greater than those for the non-treated MCL. This represents one of the few occasions in which a surgical treatment resulted in enhanced mechanical properties of a healing MCL, although the properties were still inferior to those for the sham operated group.

The trends observed in the early stages of remodeling continued out to 26 weeks after surgery.[289] The CSA of the SIS-ECM treated MCL had significantly decreased compared to the 12 week results, and was found to be statistically less than that of the non-treated group. The tangent modulus and tensile strength were both significantly greater than the non-treated group (33% and 50%, respectively). Interestingly, the tangent modulus for the SIS-ECM treated group at 26 weeks was found to be significantly increased compared to the 12 week results. This is contrary to previous results that showed that the mechanical properties of the MCL do not change during the course of healing, but rather the structural properties of the FMTC increase as

a result of increased CSA.[213] The tensile strength at 26 weeks could not be compared to the results at 12 weeks since only stress at failure was determined.

To develop a better understanding of the mechanisms behind the improvement in the mechanical properties of the healing MCL after treatment with SIS-ECM, the morphology and composition of the healing MCL were characterized to determine if there were any differences compared to the non-treated group.[180, 289] Histologic analysis with sections stained with Hematoxylin and Eosin (H&E) and Masson's Trichrome showed that the SIS-ECM group was composed of denser collagenous connective tissue that had more uniform alignment along the longitudinal axis of the MCL as compared to the non-treated control at both 12 and 26 weeks after surgery. Furthermore, the cells within the SIS-ECM treated ligament were more spindle-shaped in appearance and also tended to be oriented along the longitudinal axis of the ligament.

It was determined by immunostaining and collagen typing that the SIS-ECM treated group contained less collagen type V (Col V) than the non-treated group at both time points, with a Col V/collagen type I ratio that was closer to that of the sham operated control. Col V has been shown to play a role in regulation of the lateral growth of collagen I (Col I) fibrils,[34-36, 183, 285] and remains elevated in the healing MCL even after one year.[210] This leads to the formation of collagen fibrils in the healing MCL that are uniformly small,[88, 89] as compared to the normal MCL, which has been shown to have a bimodal collagen fibril diameter distribution consisting of populations of small fibrils and large fibrils.[87, 111] If the collagen fibril diameter in a healing MCL can be increased, it has been shown that there is an associated increase in the mechanical properties of the ligament substance.[207] Therefore, transmission electron microscopy (TEM) was performed in order to determine the collagen fibril diameter distributions for the SIS-ECM treated and the non-treated MCLs. At 12 weeks, both experimental groups showed uniformly small collagen fibril diameters, but the mean diameter for the SIS-ECM treated group was approximately 22% greater than the non-treated group.[289] Over time, some of the fibrils in the SIS-ECM group continued to grow such that a biomodal distribution developed that was similar to the sham operated control, although the fibrils were still smaller.[180] In contrast, the non-treated group still showed a uniformly small collagen fibril distribution.[180] These studies show that SIS-ECM contributes to constructive remodeling of the MCL at least in part by improving the collagen alignment, regulating the collagen composition, and increasing the collagen fibril diameter, all of which leads to enhanced mechanical properties of the remodeling tissue.

2.2 THE ROLE OF ECM DEGRADATION

2.2.1 Rate of ECM Degradation

As stated previously, ECM scaffolds appear to degrade quickly after implantation as determined by the morphological changes in the tissue under histologic evaluation.[14] However, histologic evaluation does not give a quantitative evaluation of the degradation kinetics, nor does it provide information on the fate of the degradation products. Both of these issues are critical aspects of the remodeling response. If the ECM degrades too quickly, then the host cannot produce matrix quickly enough to take over the mechanical burden served by the scaffold. Perhaps more importantly, since the SIS-ECM is porcine in origin, there may be unknown immunologic effects if the degradation products become part of the new tissue or are transported to another location in the body and are retained in the long-term. This would pose a significant regulatory issue.

To address these concerns, the rate of degradation of SIS-ECM and the fate of the degradation products were quantitatively determined during remodeling after repair of the canine urinary bladder.[229] In order to track the degradation, the SIS-ECM was radiolabeled with ^{14}C labeled proline, an amino acid that is the building block for hydroxyproline, which makes up about 10% of each collagen molecule. Detailed methods for labeling the ECM can be found in Section 7.1.2. Since ^{14}C labeled proline is integrally bound to every collagen molecule, a decrease in the radioactivity per unit weight of tissue corresponds directly to a decrease in the mass of the scaffold. The scaffold was found to degrade quickly after implantation with 40% of the scaffold removed from the site of remodeling within 4 weeks. The degraded ECM scaffold was replaced by new ECM (unlabeled) deposited by cells that participate in the remodeling process. ^{14}C was undetectable by 90 days. The remodeling resulted in the formation of site specific urinary bladder tissue.

With regard to the fate of the degraded ECM, radioactivity was found in blood and urine almost immediately after surgical implantation. ^{14}C was only detected in the lung and liver after repair, and was only present in small amounts detectable by accelerator mass spectrometry (AMS), an extremely sensitive method of detection. These results suggest that the primary fate of the ECM is degradation, metabolism, and excretion as urine or exhalation as CO_2.

The degradation of an ECM scaffold is extremely rapid, with nearly half of the scaffold degraded by one month, and complete degradation by 3 months. Since constructive remodeling with site appropriate mechanical behavior has been shown to be possible (as described in Section 2.1.2), the degradation kinetics also provide insight into the rate of new matrix production. In the early phase of remodeling, degradation occurs quite rapidly before cells have an opportunity to populate the scaffold and deposit new collagen, leading to the initial decrease in strength observed in many applications. However, once the cells have established residence and begin producing site specific tissue, the rapid remodeling progresses with an increase in the strength of the remodeling scaffold and site appropriate mechanical behavior. In addition, as the scaffold rapidly degrades, it is completely removed from the body so there should be no long-term effects of the scaffold. In order to determine the relevance of these results to musculotendinous applications, this Dissertation utilized the same model to quantify the degradation of an SIS-ECM scaffold used to repair a canine Achilles tendon, a tendon that is subjected to some of the highest load of any tendon in the body.

2.2.2 Bioactivity of ECM Degradation Products

Since ECM scaffold have been shown to degrade so quickly, a number of studies have evaluated the biological activity of ECM degradation products. Several *in vitro* studies have shown that low molecular weight peptides (5-16 kDa) are formed through degradation of ECM scaffolds via exposure to a mild acid and heat.[39, 176, 241] These peptides exhibit bioactivity, specifically antibacterial and chemoattractant properties.

Degradation products from SIS-ECM, urinary bladder ECM, and liver ECM have been shown to have antibacterial activity against both Gram negative *Escherichia coli* and Gram positive *Staphylococcus aureus*.[39, 241] The bacterial growth was inhibited for at least 13 hours. Interestingly, intact SIS-ECM supports bacterial growth,[125] suggesting that degradation of the ECM is necessary for the antibacterial activity to be realized. These *in vitro* studies support a number of pre-clinical and clinical studies in which infection was resisted in a surgical site repaired with SIS-ECM after deliberate bacterial or gastrointestinal contamination in the case of pre-clinical studies[12, 23, 138, 252] or prior infection in the clinical study.[268]

The chemoattractant properties of ECM degradation products have been proven for endothelial cells *in vitro* and *in vivo*.[176] In the *in vitro* experiments, a Boyden Chamber assay was performed in which endothelial cells from the heart, liver, and kidneys were added to the upper chamber and ECM degradation products (60 μg/ml), urea extract of SIS-ECM (60 μg/ml), a positive control (VEGF; 100 ng/ml), or a negative control (serum free medium) were added to the lower well. The urea extract of SIS-ECM is known to contain abundant VEGF from the scaffold, which is a powerful chemoattractant for endothelial cells.[120] After a 3-hour incubation period, the cells that had not migrated toward the chemotactic agent were removed, while the cells that had migrated through the membrane were fixed, stained, and counted. The results showed that ECM degradation products had greater chemoattractant potential than the urea extract of SIS-ECM or VEGF alone. To confirm these findings *in vivo*, ECM degradation products were loaded into a Matrigel plug and implanted subcutaneously into mice. An unloaded Matrigel plug was used as a control. The unloaded Matrigel plug exhibited no angiogenesis, while the plug loaded with ECM degradation products showed abundant blood vessel formation.

A limitation of these results is that the peptides that comprise the ECM degradation products were obtained by acid hydrolysis rather than by a biologically relevant method. However, it seems unlikely that peptides exhibiting a variety of bioactivities that are beneficial for a wound healing environment would form in an artificial situation, but would not be formed in a biological system. Studies are currently underway to confirm this hypothesis and to determine the sequence of the peptides.

These studies suggest that degradation of an ECM scaffold may be an important and necessary event in a constructive remodeling response.[20, 175, 240, 296] Stated differently, degradation of an ECM scaffold may be a requisite process with bioactive consequences that contributes to the overall remodeling phenomenon. It is logical therefore that inhibition of scaffold degradation by chemically crosslinking the ECM may decrease or eliminate the beneficial effects of ECM degradation products. This will be a topic of study in this Dissertation.

2.3 THE ROLE OF MECHANICAL LOADING

2.3.1 Effects of Immobilization on ECM Remodeling

In general, studies have shown that the choice to mobilize or immobilize a joint after ligament or tendon rupture can have a substantial effect on the healing process.[63, 64, 212, 264, 288] Several animal studies have shown better results with non-operative treatment and early mobilization than with surgical repair followed by immobilization.[213, 284, 288] In a study that compared repair versus non-repair, both with early mobilization, of a clinically relevant mop-end tear model of the rabbit MCL, there were no differences in the varus-valgus rotation of the knee, *in situ* force of the MCL, or tensile properties between the repaired and nonrepaired MCL.[284] Due to the large body of research related to the effects of early mobilization on healing, the concept of early passive range of motion after injury to a ligament or tendon (in some cases after repair) has become widely accepted. Several clinical studies have shown that after acute injury and repair of the Achilles tendon, early mobilization led to decreased time required for rehabilitation without differences in the re-rupture rate.[190, 257] However, despite the early rehabilitation, no differences were observed in the thickness of the healing tendon or the strength loss of the relevant musculature.[190]

Despite the evidence in support of early mobilization for ligaments and tendons with no repair or primary repair and the fact that most preclinical studies with SIS-ECM utilized early mobilization, some early clinical applications of SIS-ECM utilized immobilization and nonweightbearing conditions for a period of time to protect the joint during the phase of rapid ECM degradation. To determine the effects of immobilization on the remodeling of an SIS-ECM scaffold, a study was performed in which an SIS-ECM scaffold was used to repair a segmental defect in a rabbit Achilles tendon with a number of immobilization protocols.[119] Rabbits were separated into five groups. In four groups, a 1.5 cm section of the Achilles tendon was surgically removed and repaired with an SIS-ECM interpositional graft, after which the surgically repaired limb was immobilized for two weeks. The first group of animals was sacrificed at the end of two weeks as a control. The other three groups had their hind limb braced to allow full range of motion, partial range of motion (60°-90° of flexion), or no range of motion for an additional four weeks at which point all animals were sacrificed. In the control

group, a sham operation was performed in which the Achilles tendon was exposed, but no defect was created and no SIS-ECM material was implanted. The sham operated hind limb was immobilized for two weeks prior to sacrifice. Histologic analysis of the groups with partial or full range of motion showed that similar results to those described in Section 2.1.1. There was no distinguishable SIS-ECM material remaining, and the tissue was composed of dense collagenous connective tissue oriented along the longitudinal axis of the tendon. Spindle shaped cells were distributed throughout the tendon and oriented along the longitudinal axis of the tendon. The only difference between the partial and full range of motion groups was that fewer cells were found in the center of the remodeled graft with partial motion.

The SIS-ECM remodeling process was entirely different with immobilization. In both the control group and the experimental group, there was histologic evidence of the SIS-ECM scaffold at the defect site with only limited deposition of new host connective tissue that was disorganized in appearance. The cellularity was limited to the periphery of the graft, with almost no cells found in the middle of the device.

This study suggests that the constructive, site specific remodeling response that has been observed in many studies is not a result of the SIS-ECM scaffold alone. In a tendinous application, the infiltration of the scaffold by cells, deposition of collagenous connective tissue, and subsequent organization of the tissue is modulated by the mechanical environment. It appears that the lack of mechanical loading may also slow the degradation process since cells are not present throughout the scaffold, which limits the cascade of events promoted by the degradation products. One of the objectives of this dissertation is to develop a better understanding of the positive aspects of mechanical loading on the remodeling of an ECM scaffold.

2.4 THE ROLE OF BONE MARROW DERIVED CELLS

2.4.1 Recruitment of Bone Marrow Derived Cells to ECM Remodeling

The typical remodeling response for an ECM scaffold shows an abundance of mononuclear cells that are present in the remodeling ECM from the first few days through one month after

implantation. Many of these cells appear to be macrophages, which originate in the bone marrow. Since there is an abundance of cells that populate the ECM scaffold that remain at the site longer than would be expected for the normal mammalian healing response, and the remodeling response to an ECM is different than normal healing, a logical question was whether there was a population of cells originating in the bone marrow that participates in the remodeling of an ECM scaffold that does not typically participate in normal healing.

To determine if a bone marrow cell population was involved in the remodeling ECM scaffolds, scaffolds composed of bovine Type I collagen, poly(L)lactic-co-glycolic acid (PLGA), SIS-ECM, urinary bladder submucosa (UBS-ECM), and a mixture of PLGA and particulate UBS-ECM were implanted subcutaneously in a chimeric mouse model is which bone marrow derived cells expressing glucose phosphate isomerase 1a (Gpi-1^a) were implanted into a mouse that normally expressed glucose phosphate isomerase 1b (Gpi-1^b).[20] The bone marrow derived cells also expressed β-galactosidase (β-gal) to allow for histologic identification of the bone marrow derived cells. There was an abundance of bone marrow derived cells found at the implant site for all scaffolds at 7 days, after which the percentage of Gpi-1^a positive cells decreased at the implant sites of Col I and PLGA scaffolds. In contrast, the implant sites containing SIS-ECM, UBS-ECM, and the PLGA/UBS-ECM composite showed elevated Gpi-1^a activity for the entirety of the study (56 days) at about 65-75%. The expression of β-gal confirmed that these cells were marrow derived, and provided morphologic information about the location and morphology of the cells. The Col I scaffold contained very few β-gal^+ cells after 56 days that were spindle shaped in appearance and these cells were confined to the outer region of the scaffold. The PLGA scaffold also contained only a small number of β-gal^+ cells that had a rounded shape around the periphery of the scaffold after 56 days. Consistent with the Gpi-1^a results, there was an abundance of β-gal^+ cells found in the remodeled SIS-ECM and UBS-ECM. The β-gal^+ cells were distributed throughout the remodeled tissue, and exhibited a spindle-shaped morphology consistent with endothelial cells and fibroblasts. Some of the β-gal^+ cells lined primitive capillary spaces, and stained positive for PECAM-1 and von Willebrand Factor, two ubiquitous endothelial cell markers. For the PLGA/UBS-ECM scaffold, spindle shaped β-gal^+ cells were found in the proximity of the PLGA remnants, and were found throughout the thickness of the scaffold.

This study shows that ECM scaffolds recruit a population of bone marrow derived cells to the site of remodeling that participate in the long-term remodeling of the scaffold and become part of the regenerated tissue when implanted subcutaneously. There is specific evidence for these cells differentiating into endothelial cells and some of the cells exhibited fibroblastic morphology. The phenotype of the cells is not clear, but it is possible that these cells may represent the populations of endothelial progenitor cells and mesenchymal progenitor cells,[52, 126, 131, 194, 224, 228, 278] or a population of partially differentiated circulating cells such as fibrocytes.[1, 46, 59, 60, 112] The mechanism of recruitment is also not clear, but could be a function of the formation of chemoattractant peptides during degradation of the scaffold. The mechanism of recruitment and the fate of bone marrow derived cells were topics of study for this Dissertation.

3.0 EXTRACELLULAR MATRIX REMODELING *IN VITRO*

ECM remodeling *in vivo* is a complicated process regardless of whether the ECM of interest is a naturally occurring scaffold, a component of new connective tissue formed during the healing process, or part of intact tissue exposed to a new mechanical environment. Therefore, a number of *in vitro* models have been developed to facilitate a better understanding of specific aspects of ECM remodeling. Several of these models will be discussed in the following sections.

3.1 SILICONE MEMBRANE MODEL

3.1.1 Gene Expression

A variety of cell types have been seeded on elastic silicone membranes and subjected to cyclic mechanical loading to mimic physiological levels of strain and strain rate. Interpreting the effects of mechanical force on protein expression and synthesis can be difficult due to the broad range of cell types, scaffolds, and loading regimens that have been studied. It has been shown that cyclic stretching of fibroblasts and smooth muscle cells generally leads to increased production of Col I,[149, 259, 292] but when endothelial cells are exposed to cyclic mechanical stretching, Col I synthesis decreases.[260] It has also been shown that cyclic stretching of fibroblasts increased synthesis of TGF-β, b-FGF, and VEGF, but decreased production of platelet derived growth factor (PDGF).[219, 253] Several of the loading regimens utilized to study collagen and growth factor production have also been shown to increase the production of a variety of enzymes involved in the production of inflammatory mediators, including interleukin-6 and prostaglandin-E_2.[177, 254, 280] Expression of tenascin-C (TN-C) has been shown to increase substantially and rapidly in response to cyclic mechanical loading.[62]

3.2 COLLAGEN GEL MODEL

3.2.1 Static Loading

The collagen gel model, first proposed by Bell and colleagues,[28] uses Col I extracted from tissues such as rat tail tendon or bovine skin. The harvested collagen is solubilized, then polymerized to a gel composed of greater than 99% Col I. The advantage of this method is that cells can be suspended within the collagen gel, creating a tissue construct. The cells attach to the collagen fibers, and the contractile nature of the cells leads to reorganization of the matrix. In floating gels, the total area of the gel decreases uniformly and the magnitude of the change is dependent upon the contractility of the fibroblasts. As the specimen compacts, the collagen fibers and fibroblasts tend to align tangent to the perimeter of the gel. When the gel is fixated at two points, the contraction of the fibroblasts leads to the development of a tension between the two points. The resulting morphology yields fibroblasts and collagen fibers that are aligned in the direction of tension. It has been hypothesized that the fibers are aligned to the direction of tension to provide the greatest stiffness to resist load, and that the fibroblasts align with the fibers to shield from high strains. Further, it has been shown that the development of tension in confined fibroblast populated collagen gels (FPCGs) leads to modulation of matrix, adhesion, and cytoskeletal protein expression, with increased synthesis of procollagen types I and III polypeptides, fibronectin, elastin, actin and glycosaminoglycans, with decreased synthesis of procollagenase polypeptides.[127, 166]

One of the most notable models that used a confined FPCG was developed by Huang and coworkers.[127] The FPCGs were formed around stationary posts and maintained in culture for a period of 12 weeks. This study demonstrated mechanical loading of the FPCG increased matrix and glycosaminoglycan (GAG) synthesis, as well as crosslink density. The most dramatic result was a 30 fold increase in strength that was observed between week 1 and week 12.

Another important usage of the collagen gel model, named the Culture Force Monitor (CFM), was developed by Eastwood and colleagues.[79] This model incorporated highly sensitive load sensors to quantify the tension that developed in a FPCG as a means to determine the contractility of the fibroblasts. This method has been used extensively to characterize the behavior of fibroblasts. This model has been important for developing a better understanding of

the effect of biological factors on the contractility of cells and the role of cell surface receptors in the development of tension in the FPCGs.

3.2.2 Cyclic Loading

A number of systems have been developed to apply dynamic external load to a FPCG in addition to the tension that develops internally due to cell contraction.[50, 80, 141, 168, 249] These systems vary in their functionality as well as their utility. Eastwood and colleagues extended their CFM to include motor controlled displacement, naming the new system the tensioning-Culture Force Monitor (t-CFM).[80] With this system, it was determined that the geometry of the sample greatly affected the response of the fibroblasts. It was demonstrated that a FPCG with a greater aspect ratio resulted in increased cell and collagen fiber alignment due to the ability of the FPCG to contract to a greater degree in the lateral direction. Through finite element modeling, it was determined that fibroblasts align in the direction of principle stress, and the fibers also align in the same direction. Furthermore, this model showed that fibroblasts exhibit tensional homeostasis.[44] Stated differently, if fibroblasts at equilibrium are suddenly exposed to an increase in the external load, the contractile force of the fibroblasts will decrease until a new equilibrium is attained. This finding is consistent with other *in vitro* studies that show that cell behavior changes in response to the stiffness of the substrate on which it resides. The rate of fibroblast migration and magnitude of force production both increased as the stiffness of the substrate increased.[49, 78, 282] The t-CFM was also used to study the effect of mechanical loading on the synthesis of matrix metalloproteases.[220, 221] It was determined that cyclic loading of FPCGs elicited significant variations in the production of several matrix metalloproteases.

A final technique based on the collagen gel model involved forming the gel seeded with smooth muscle cells (SMCs) around an elastic silicone tube to form a tubular construct as a tissue engineered blood vessel (TEBV). In this system, circumferential strain was developed by radial distention of the silicone membrane with increased intraluminal pressure. Kanda and Matsuda were the first to present this model and demonstrated circumferential alignment of the SMCs and collagen fibers around the silicone tube.[141] Seliktar and colleagues extended this work to include mechanical testing of the scaffolds after mechanical loading.[249] In addition to confirming the SMC and collagen fiber alignment found by Kanda and Matsuda,[141] they also

demonstrated that tensile strength and modulus of the constructs increased between 4 and 8 days of cyclic loading, primarily as a result of increased crosslinking between the collagen fibers. Niklason and colleagues used this model to develop a TEBV with compliance and burst strength that were comparable to normal tissue.[209] Further, the TEBV was histologically similar to normal tissue. This was performed by contracting multiple cell populated collagen gels over a silicone tube. Each layer was seeded with either endothelial cells or smooth muscle cells in an attempt to mimic the native structure. Finally, ascorbic acid was added to the medium to promote the synthesis of new collagen.

3.3 MECHANISMS FOR ECM GEL REMODELING

3.3.1 Effects of Cell Alignment on Collagen Fiber Organization

With the development of these models to study the effect of mechanical loading on the behavior of cells, a great deal of work has begun to elucidate the mechanisms by which the observed remodeling occurs. A recently developed model examined the organization of collagen produced by cells with different orientations.[279] MC-3T3-E1 cells, preosteoblastic cells that produce abundant amounts of collagen, were seeded on smooth and microgrooved substrates, and maintained in culture for a period of four weeks, producing a layer of cell-produced collagen. The cells cultured on the smooth surface spread freely, and had no preferred orientation, while those cultured on the microgrooved surface were elongated in shape and aligned with the direction of the microgrooves. The alignment of the collagen that these cells secreted was greatly affected by the orientation of the cells. With the randomly oriented cells, although there were local areas of alignment, there was no global preferred orientation of the collagen fibers. In contrast, the collagen fibers produced by the cells aligned with the microgrooves were aligned in the same direction (Figure 3-1).

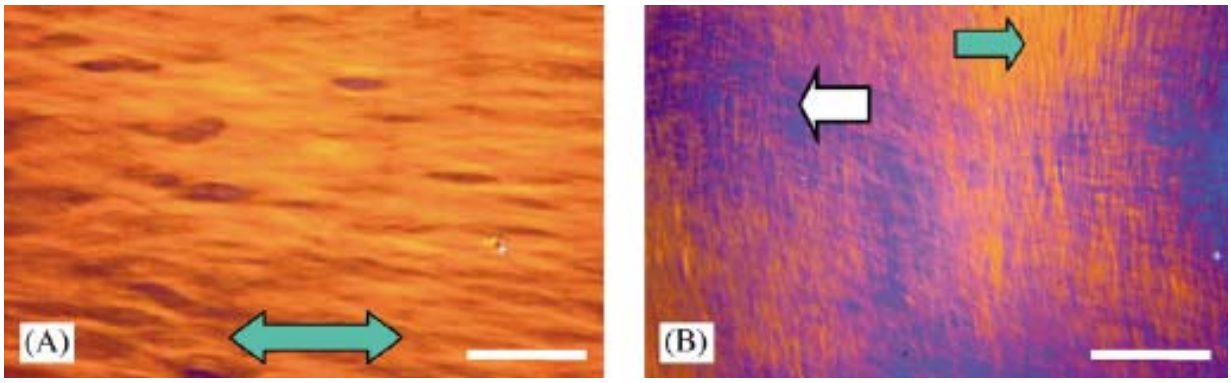

Figure 3-1. The dense collagenous matrix produced by cells on a microgrooved surface show uniformly orange under polarized light microscopy, indicating the collagen fibers were aligned in the same direction as the microgrooves (green arrow, A). The collagen matrix produced by cells on a smooth surface showed multiple colors (B), in this case orange (green arrow) and blue (white arrow), indicated multiple fiber orientations (Bar: 60µm). [279]

3.3.2 Magnitude and Direction of Force from Cells

There have been a number of studies which have modeled the forces or traction that cells exert on their surroundings.[49, 78, 94, 279, 293] The forces produced by the cell are directed. The lamellipodia of the cell exerts a "backword" directed force at the leading edge of the cell (relative to the direct of movement) or a "forward" directed force at the tail of the cell. The studies differ in their conclusions as to whether the maximum forces from the cell are produced at the leading edge of the lamellipodia[49, 78, 279] or the tail.[94] Variations are likely due to biological variations or differences in the substrate used. The magnitude of force generated by the cell was dependent on the stiffness of the substrate, with stiffer substrates associated with greater forces. While these results are not for cells seeded in collagen gels, they do provide a great deal of insight into the mechanisms involved the reorganization of collagen fibers. As cells are seeded into a collagen gel, they will attach to the fibers, and begin to exert traction to them in order to migrate. However, since the fibers are not fixed in space, they will reorient in the direction of tension. This will cause the scaffold to stiffen as more fibers become aligned, which will lead to an increase in the force produced by the cell.

3.3.3 Generation and Transmission of Force by Cells

The means by which the cells generate and transmit the traction to remodel the ECM in which they reside has been investigated. The traction from cells develops from the cytoskeletal components, such as actin and microtubules. When fibroblasts are subjected to tension, stress fibers form. These fibers resist the external load on the cell. Disruption of the actin cytoskeleton or microtubules in a collagen gel led to an inhibition of gel contraction or a subsequent decrease in the contractile force in the matrix.[43, 265]

Transmission of the force from the cytoskeleton to the local environment occurs via integrins in the cell membrane, which tie into the cytoskeleton and attach to the extracellular matrix. A number of studies have implicated different β_1 integrins in mediating cellular contraction of collagen gels, specifically $\alpha^1 \beta_1$ and $\alpha^2 \beta_1$.[54, 244] Blocking these integrins with antibodies or transfecting cells to block their synthesis led to a partial or complete inhibition of FPCG contraction. Another study demonstrated that competitively inhibiting the attachment of integrins to receptors on the ECM not only prevented contraction of a collagen gel, but led to a disruption of the actin and microtubules.[251] These findings demonstrate the importance of sound mechanical attachment between integrins and the surrounding ECM on cell function.

3.3.4 Long Range Influence of Cells

The previous section described the interaction between individual cells and the collagen fibers immediately surrounding them. However, it has also been shown that cells have the ability to influence the organization of collagen fibers some distance from their location. This phenomenon was studied by placing explanted ligament fibroblasts approximately 1 mm apart in a collagen gel. "Straps" of aligned collagen formed between the two cell explants.[242] They observed that the collagen fibers aligned quickly between the fibroblasts in the early stages of the experiment, while the speed of the advancing cells was slow. The cells only advanced approximately 10 μm, while reorganization of collagen was observed up to 1000 μm away. Therefore small movements by the cells led to rapid remodeling of the scaffold. It is suggested that the collagen gel should be considered as an interconnected meshwork of fibers, rather than a mixture of individual fibers. This meshwork concept would explain the large lateral contraction

that is observed leading to the development of "straps" between the cell explants. This phenomenon probably plays an important role in remodeling of tissues, which have a greater degree of interconnectedness. However, the effects are probably less dramatic since connective tissues are typically more robust than a collagen gel.

3.3.5 Relevance to ECM Scaffolds

Many of the mechanisms involved in the remodeling of an ECM gel *in vitro* are likely involved in the remodeling of a naturally occurring ECM scaffold *in vivo*. Cells that migrate into the ECM scaffold would initially align with the native collagen fiber alignment. The cells would then begin to deposit new collagen that would be aligned with the cell and the cells would begin to reorganize the collagen fibers within the scaffold in response to *in vivo* loading. However, the kinetics and scale of these events are probably quite different than those observed in collagen gels due to the robustness of the naturally occurring ECM scaffold. The collagen fibers within the ECM scaffold are more mature (e.g., crosslinked) than the fibers within an ECM gel, and the ECM scaffold has a greater rigidity, complex architecture, and interconnectedness. Therefore, the remodeling process probably requires an initiation of proteolytic degradation of the native ECM to allow reorganization to take place. The presence of diverse biochemical molecules (GAGs, growth factors, collagens, laminin) and the native architecture of the ECM scaffold likely have a further effect on the behavior of the cells under load, although those effects are not known.

Another important concept is the transfer of load from the collagen fiber to the cells. ECM gels are composed of isolated collagen fibers that are interwoven and have a high degree of fiber motility, while the ECM scaffolds are composed of a complex arrangement of interconnected fibers. Furthermore, the collagen fiber architecture of the ECM scaffold is designed by nature to resist the local mechanical environment of the host organ (e.g., small intestine or urinary bladder). *In vivo*, these scaffolds are being utilized in a variety of loading environments that are quite different from the organ of origin, in many cases after considerable processing of the ECM. The effects of the mechanical loading on the organization of the collagen fibers are not well understood, and it is possible that the collagen fibers within each tissue will exhibit motility and reorganize after implantation as the scaffolds are degraded. Since

the fiber kinematics is not known, it is difficult to evaluate how a strain applied to the scaffold relates to strain transmitted to the cells within the scaffold. The relationship between scaffold strain and cell strain could be an important factor in the remodeling process since cell behavior has been shown to be dependent on the magnitude of stretch. These concepts will be a topic of study in this Dissertation.

4.0 OVERVIEW

The previous sections have described the typical site specific remodeling response to an ECM scaffold and some of the potential mechanisms of this response. The cellularity of the scaffold increases dramatically after implantation and remains elevated longer than would be expected in normal mammalian wound healing. In the early phase, the cells include a large number of mononuclear cells, consistent with macrophage morphology, that exhibit an anti-inflammatory/ immunoregulatory phenotype as opposed to a proinflammatory, foreign body response. The morphology of the cells changes to that of a site-specific cell by one month after implantation. Among the site-specific cells is a population of bone marrow derived cells that participate in the long-term scaffold remodeling. It is thought that these cells are recruited to the site of remodeling by small biologically active peptides formed during scaffold degradation. The specific cells that are recruited and the fate of the cells are not yet known with certainty. Population of cells that may contribute to this remodeling response include mesenchymal progenitor cells and fibrocytes, which exhibit behavior consistent with the ECM remodeling.

The role of the mechanical environment is also important to the remodeling process. The effects of prolonged immobilization on the remodeling ECM scaffold are quite dramatic, with minimal cell infiltration into the scaffold and disorganized connective tissue formation. Early mobilization with site appropriate mechanical loading is apparently a requisite part of the constructive remodeling response. Site appropriate mechanical loading may contribute to differentiation of bone marrow-derived cells that are recruited to the site of remodeling. Furthermore, as shown in a number of *in vitro* studies, mechanical loading likely regulates matrix synthesis and improves the tissue organization, leading to tissue with site appropriate mechanical behavior.

With these previous studies in mind, the following represent the specific aims for this Dissertation.

5.0 SPECIFIC AIMS

Specific Aim 1: To investigate the expression of matrix related genes by fibroblasts seeded on SIS-ECM in response to cyclic mechanical loading at physiologically relevant magnitudes and frequencies of stretch, and characterize the associated changes that occur to the matrix organization and mechanical behavior of the SIS-ECM scaffold.

Specific Aim 1a: To determine the gene expression of collagen type I (Col I), collagen type III (Col III), matrix proteinases-2 (MMP-2), matrix metalloprotease-9 (MMP-9), α-smooth muscle actin (SMA), tenascin-C (TN-C), transforming growth factor-β_1 (TGF-β_1), and transforming growth factor-β_3 (TGF-β_3) by NIH 3T3 fibroblasts seeded on SIS-ECM and subjected to cyclic stretch at magnitudes of 5%, 10%, and 15% at frequencies of 0.1 Hz, 0.3 Hz and 0.5 Hz.

Specific Aim 1b: To investigate the effects of cyclic mechanical loading on collagen fiber architecture and kinematics, and mechanical properties of naturally derived SIS-ECM scaffolds seeded with fibroblasts.

Rationale 1: Matrix proteins and growth factors are integral to tissue remodeling as they provide signals to cells which guide tissue development and provide a structural network from which the cells can act. Therefore, it is important to understand how various cyclic mechanical loading regimens modulate fibroblast gene expression and alters the existing extracellular matrix.

Hypothesis 1: We hypothesize that the selected mechanical conditioning regimen will include increased collagen I expression, decreased collagen III expression, moderate

MMP expression, and increased expression of SMA, TN-C, TGF-β_1, and TGF-β_3. It is further hypothesized that cyclic mechanical loading of SIS-ECM seeded with fibroblasts will show increased collagen fiber alignment and increased tensile strength and tangent modulus compared with SIS-ECM alone or SIS-ECM seeded with fibroblasts without cyclic mechanical loading due to reorganization of existing collagen fibers and deposition of new collagen.

Specific Aim 2: To determine the fate of bone marrow derived cells that are recruited to the site of SIS-ECM scaffold remodeling in a mouse model of Achilles tendon repair.

Specific Aim 2a: To determine if the bone marrow derived cells recruited to the site of SIS-ECM remodeling exhibit fibroblastic characteristics after long-term remodeling.

Specific Aim 2b: To determine if a correlation exists between the process of SIS-ECM degradation and the recruitment of bone marrow derived cells to the site of SIS-ECM scaffold remodeling.

Rationale 2: Pre-clinical studies have shown that SIS-ECM remodels into site specific tissue and that bone marrow derived cells that are not typically involved in the healing process are recruited to the site of SIS-ECM remodeling. *In vitro* studies have shown that degradation products from SIS-ECM are chemoattractant, and a similar mechanism may be responsible for the recruitment of marrow-derived cells.

Hypothesis 2: We hypothesize that a portion of the bone marrow derived cells recruited to the site of SIS-ECM remodeling will show fibroblastic characteristics. We further hypothesize that by chemically crosslinking SIS-ECM, the rate of degradation will be decreased and fewer bone marrow derived cells will be recruited to the site of remodeling.

Specific Aim 3: To determine if the population of bone marrow derived cells recruited to the site of SIS-ECM remodeling includes circulating fibrocytes.

Specific Aim 3a: To determine whether mouse fibrocytes are recruited to the degradation products of a SIS-ECM scaffold via an *in vitro* Boyden Chamber Assay.

Specific Aim 3b: To determine the changes in the expression of Col I, Col III, MMP-2, MMP-9, SMA, TN-C, TGF-β_1, TGF-β_3 by mouse fibrocytes in response to a selected cyclic stretching regimen based on the results of Specific Aim 1a.

Rationale 3: Fibrocytes are bone marrow derived cells that have been shown to migrate to the site of tissue injury and exhibit fibroblastic characteristics. It is reasonable to expect that these cells may comprise a portion of the population of bone marrow derived cells that are recruited to the site of ECM remodeling. Their participation in the remodeling process may contribute to the change in the default mechanism of healing.

Hypothesis 3: We hypothesize that fibrocytes will be recruited to the degradation products of SIS-ECM *in vitro* and that they will exhibit a gene profile consistent with a constructive remodeling response.

6.0 RECRUITMENT OF BONE MARROW DERIVED CELLS TO SITE OF SIS-ECM REMODELING

This section deals with experiments that were performed to address Specific Aim 2. The first experiment was performed to determine the rate of degradation of an SIS-ECM scaffold in a musculotendinous application (canine Achilles tendon).[100] In addition, the time course of remodeling was described with a focus on the cellular infiltrate and the tissue organization. With this study as a basis for the remodeling of ECM scaffolds in a tendinous application, the second study attempted to determine whether bone marrow derived cells are involved in the long-term remodeling of tendinous tissue, and the fate of those bone marrow derived cells.[296]

6.1 DEGRADATION AND REMODELING OF SIS-ECM IN A CANINE ACHILLES TENDON MODEL

Although there are now six naturally derived ECM scaffolds on the market for musculotendinous repair, the only quantitative assessment of the rate of degradation for any ECM scaffold was performed for native SIS-ECM in the context of urinary bladder repair by integrally labeling the scaffold with ^{14}C (Details in Section 2.2.1).[229] ^{14}C is an effective tracking biomolecules in an animal model due to its stability and the development of sensitive detection methods.[47, 171] It is important to determine the rate of ECM scaffold degradation in a musculotendinous application. In the present study, ^{14}C-labelled SIS-ECM was used to determine the rate of ECM degradation and the fate of the degradation products when used as an interpositional graft in the canine Achilles tendon. In addition, a histological analysis was performed to determine the temporal changes in the appearance of the SIS-ECM scaffold during the remodeling process.

6.1.1 Animal Care Compliance

The production of ^{14}C-labeled SIS-ECM and the surgical procedure performed as part of this study were approved by the University of Pittsburgh Radiation Safety Committee and Institutional Animal Care and Use Committee of the University Pittsburgh (protocol number 0306682). The animal care complied with the NIH Guidelines for the Care and Use of Laboratory Animals.

6.1.2 Preparation of ^{14}C Labeled SIS-ECM

The methods for labeling the SIS-ECM with ^{14}C have been reported previously.[229] Briefly, piglets were given weekly intravenous injections of 10μCi of ^{14}C labeled proline (Amersham Life Science; 256mCi/mmol, 50μCi/ml) beginning at 3 weeks of age and continuing until the time of sacrifice. At approximately 26 weeks of age, the animals were sacrificed and the small intestine was harvested. The small intestine was mechanically abraded to remove the tunica muscularis externa and the majority of the tunica mucosa. The remaining tunica submucosa and basilar portion of the tunica mucosa was then disinfected and decellularized in a 0.1% PAA solution followed by two rinses PBS and deionized water.

To produce each Achilles tendon repair device, a ten layer construct of the hydrated sheets of ^{14}C labeled SIS-ECM was created such that each sheet was oriented with the longitudinal axis of the small intestinal submucosa oriented in the same direction. SIS-ECM has a preferred collagen fiber orientation along the long axis of the small intestine,[237] therefore creating the construct in this uniaxial orientation provided increased strength in the direction aligned with the repaired tendon. The ten layer construct was then laminated by a vacuum-pressing technique.[90] The construct was placed between two perforated stainless steel sheets, and the stainless steel plates were placed between sheets of sterile gauze. The entire construct was then sealed in vacuum bagging, and subjected to a vacuum of 710-730 mm Hg for approximately 8 hours. The multilaminate device was cut into 2 cm x 3 cm sheets, with the preferred fiber direction corresponding to the 2 cm axis. The final construct was terminally sterilized by exposure to ethylene oxide.

6.1.3 Study Design and Surgical Procedure

Twelve adult female mongrel dogs weighing approximately 20 kg were divided into six groups of 2 dogs each. All dogs were subjected to segmental resection of 1.5 cm of the Achilles tendon, and the defect was repaired with the bioscaffold composed of ^{14}C-labeled SIS-ECM. One group of animals was sacrificed at each of the following time points: 3, 7, 14, 28, 60, and 90 days post-surgery.

Surgical plane anesthesia was produced in each dog by induction with sodium thiopental (12-25 mg/kg IV) followed by intubation and maintenance with 2-3% Isofluorane. The animals were prepared for surgery by shaving the surgical site and scrubbing with Betadine solution. Antibiotics (Cephalexin) were administered intramuscularly pre-operatively and then post-operatively twice a day for 7 days. For each dog, the Achilles tendon of a randomly selected hind limb was dissected free of surrounding tissue and a 1.5 cm segment was excised from the mid-tendinous region. The tendon defect was repaired with a 2 cm x 3 cm graft of the ^{14}C labeled SIS-ECM scaffold folded accordion style, such that 2-3 mm of the 2 cm length overlapped each end of the tendon defect, using 4-0 proline suture to mark the ends of the defect (Figure 6-1). The paratenon was sutured with 4-0 PDS suture and the skin incision closed using standard surgical technique. The animals were placed in a tube splint (modified Robert Jones bandage) to allow immediate partial weight bearing without allowing the tendon unit to stretch (Figure 6-2). The splint was removed after 28 days and the dogs were allowed free ambulation without external support.

At regular time intervals after surgery, urine, blood, and fecal samples were collected to determine the route of elimination of the degraded ^{14}C-labeled materials from the body. At the time of sacrifice, the remodeled SIS graft and the contralateral non-operated control were harvested for microscopic examination and quantification of the ^{14}C concentration within the tissue. The specimen prepared for histology contained remodeled normal tendon and remodeled ECM so that the transition between the two tissues could be evaluated. The specimen for ^{14}C analysis was taken from the middle of the remodeled ECM graft. Tissue samples were collected from the skin, skeletal muscle, mesenteric fat, spleen, liver, kidney, pancreas, lymph nodes, lung, heart, and brain to determine if ^{14}C had collected in these organs.

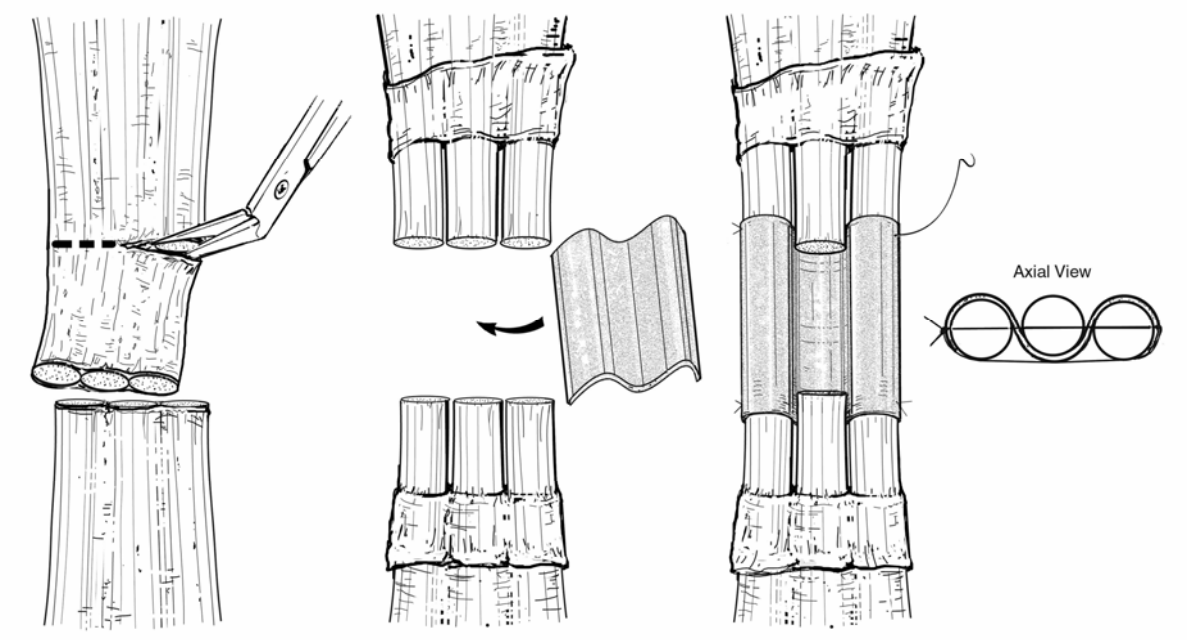

Figure 6-1. Schematic of the surgical placement of the SIS-ECM graft in the Achilles tendon defect. The 2 cm x 3 cm graft was folded accordion style, and woven through the bundles of the Achilles tendon and fixed with a mattress suture.

Figure 6-2. Modified Robert Jones bandage utilized to splint the repaired Achilles tendon for 28 days post-operatively.

6.1.4 Liquid Scintillation Counting of ^{14}C

The radioactivity in each sample was measured by liquid scintillation counting using a LS1800 B-counter (Beckman Coulter, Somerset, NJ). For urine, 0.2 ml urine was added directly to 10 ml scintillation fluid (Ultima Gold, Perkin Elmer, Boston MA). The radioactivity in urine was reported as CPM/ml. For the SIS-ECM graft at time zero, the remodeled tendon, and all other harvested tissues, approximately 80 mg of tissue was incubated with 1 ml of Solvable (Packard Instruments, Meriden, CT) at 50°C for 2-4 hours. Ten ml of scintillation fluid was then added to each sample and the radioactivity was determined. The tissue radioactivity was reported as CPM/g.

Blood samples were incubated with 1:1 mixture of Solvable:Isopropanol (Fisher Scientific, Pittsburgh, PA) at 60°C for 30 minutes. The samples were the treated with 30% H_2O_2 (Spectrum, Gardena, CA) to quench endogenous peroxidase activity and incubated at 60°C for an additional 30 minutes. Fifteen ml of scintillation fluid was added to each sample and the radioactivity was measured. The blood radioactivity was reported as CPM/ml. To measure the radioactivity in a fecal sample, approximately 20 mg of feces was rehydrated with 0.1 ml of water for 30 minutes at room temperature. One ml of Solvable was added to each sample, and the samples were incubated in a 50°C oven for 1-2 hours. 0.5 ml of Isopropanol was added before the final 2 hour incubation at 50°C. Peroxidases were quenched with 0.2 ml of 30% H_2O_2, and 10 ml of Ultima Gold was added. The radioactivity of the feces was reported as CPM/g.

6.1.5 Histologic Analysis Methodology

A portion of each tendon was harvested and trimmed to include the remodeled SIS-ECM graft and the adjacent native tendon proximal and distal to the remodeled graft. The tissue was fixed in 10% neutral buffered formalin, sectioned longitudinally, and stained with both Hematoxylin and Eosin and Masson's Trichrome stains for microscopic examination. The cellularity of the remodeled graft was assessed by obtaining five microscopic images from each section at 40x magnification for subsequent counting using MetaVue Software (Universal Imaging

Corporation, Downingtown, PA). The cells were classified as neutrophils or mononuclear cells. The data is presented as the average number of cells per 40x field. For statistical comparisons, a student t-Test was performed between groups with statistical significance set at a p-value < 0.05.

6.1.6 Surgical Outcomes

All animals recovered well from surgery, and tolerated the splinting for one month. After removal of the splint, all animals returned to normal gait. Gross evaluation of the remodeled tendons after sacrifice showed no evidence of tendon rupture at any time during the postoperative period. By visual inspection, there did not appear to be any change in the total tendon length or length of the repair site.

6.1.7 Time Course of Degradation and Fate of Labeled ECM

The values for ^{14}C concentration of the remodeling SIS-ECM tissue for each dog are listed and the average values at each time point are plotted in Figure 6-3. Approximately 10% of the scaffold material had been degraded and removed from the site of remodeling by as early as 3 days post-surgery. By 14 days, approximately 20% of the scaffold material had been degraded and at 28 days, approximately 60% of the scaffold material had been degraded. By 60 days post-surgery, the amount of ^{14}C in the remodeled tissue was equal to background levels (<8%) indicating complete scaffold degradation and removal from the site of remodeling.

The only other tissues in which ^{14}C activity could be detected were blood and urine. The blood showed positive ^{14}C activity at 3 days and 7 days after surgery. ^{14}C activity could be detected in the urine at 3, 7, and 14 days post-surgery. All other tissue samples were negative (i.e., below background values) for ^{14}C activity at all time points.

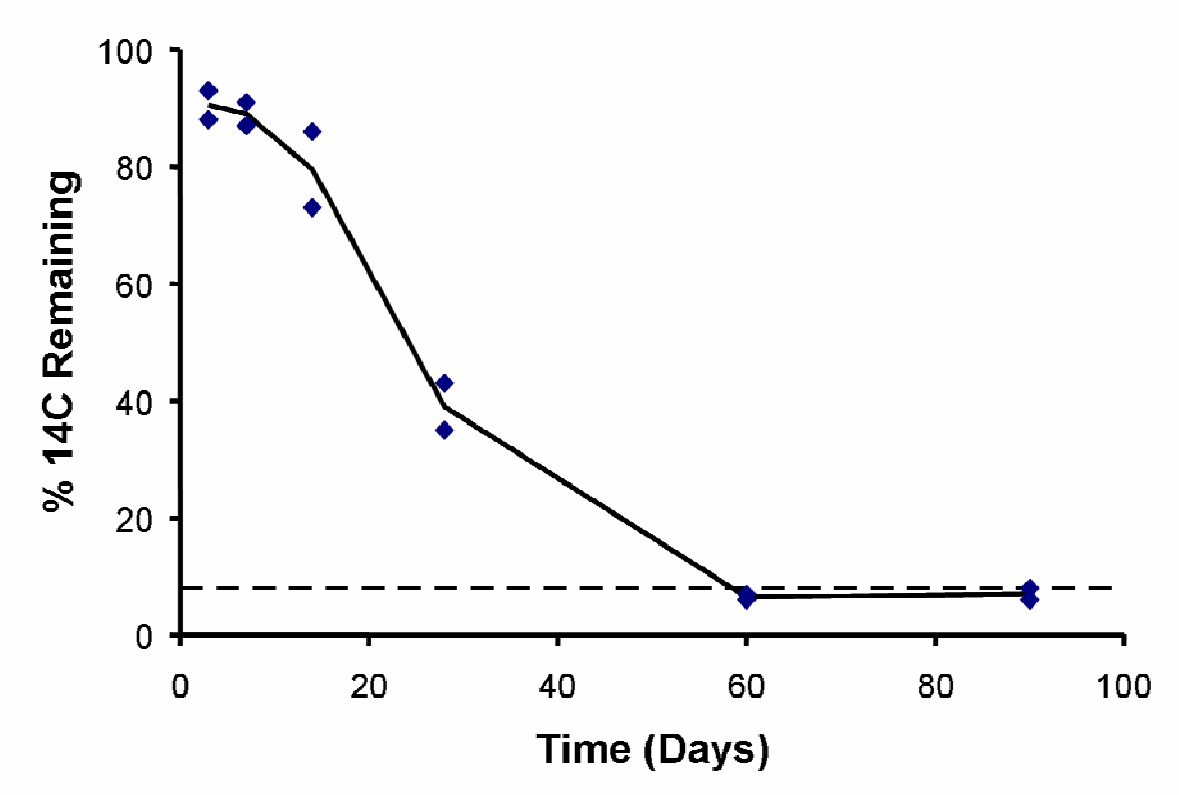

Figure 6-3. Graphical representation of the average ^{14}C% remaining at the graft site at each time point. The shaded area indicates the background ^{14}C level observed at approximately 8%. The actual measurements for ^{14}C% is included next to each data point.

6.1.8 Histologic Description of Remodeling

Histologic examination of the SIS-ECM graft prior to implantation showed a laminate structure of dense, organized, collagenous tissue with no cellularity (Figure 6-4).

Tissues harvested from the remodeling SIS-ECM tendon tissue showed that at 3 days post-surgery, the acellular scaffold material had been infiltrated with a large number of host inflammatory cells characterized by an approximately equal number of neutrophils and mononuclear cells ($p = 0.55$) (Table 6-1). Early evidence for scaffold degradation included the separation of the individual sheets within the multilaminate structure by infiltrating host cells and loss of distinct scaffold architecture at the periphery of the graft material. There was no histologic evidence for deposition of new host ECM based upon the distinct margins of the graft and cut end of the native tendon.

By 7 days (Figure 6-5), the cellular infiltrate had increased in amount and consisted almost exclusively of mononuclear cells (Table 6-1). A moderate degree of scaffold degradation was present and the host-cell infiltrate progressed from the periphery of the SIS-ECM graft material to the center of the graft material. New host ECM was present at the remodeling site based upon the presences of amorphous connective tissue between the native tissue and the SIS-ECM graft material.

By 14 days (Figure 6-6), the entire SIS-ECM scaffold material was infiltrated with host cells that were primarily mononuclear in morphology with only a few scattered neutrophils present. This time point showed the greatest cellularity over the time course of remodeling with an average 271 ± 133 cells per 40x field (Table 6-1). Graft degradation was characterized by separation of the various layers of the multilaminate sheet and loss of a distinct boundary between newly deposited host ECM and the original SIS-ECM graft material. New host ECM deposition was present, especially at the periphery of the graft. The distinct line of demarcation between the SIS-ECM scaffold material and the cut end of the native Achilles tendon to which it was attached was no longer evident by 14 days.

By 28 days (Figure 6-7), there was a decrease in the cellularity similar to the numbers observed at 7 days after implantation (Table 6-1). The mononuclear cells were still abundant,

and were uniformly distributed throughout the remodeled ECM graft. No neutrophils were observed. There was loss of almost all morphologic evidence of the SIS-ECM graft material which was replaced by a relatively homogeneous deposition of new host derived ECM material. The remodeled ECM was beginning to show regions of organization by this time point.

At 60 days (Figure 6-8), there was replacement of the SIS-ECM by organized, aligned host ECM and spindle cells consistent with the morphologic appearance of fibroblasts. The total cellularity was not statistically different from the cellularity at 28 days (Table 6-1). The remodeled SIS-ECM graft was replaced by organized connective tissue and the site could only be identified from the native tissue by the presence of the Prolene suture.

The 90 day tissue samples (Figure 6-9) showed a slight decrease in the number of spindle cells present within the graft material compared to the 60 day sample and the cellularity was not statistically different from the normal Achilles tendon (Table 6-1). The collagen fiber organization and vascularity was also qualitatively similar to that of normal tendon tissue.

6.1.9 Significance of Degradation Results

The results of this study show that SIS-ECM, when used as a biologic scaffold for Achilles tendon reconstruction is rapidly degraded after implantation, with approximately 60% of the mass degraded and resorbed within 4 weeks. Degradation of the SIS-ECM appears to be complete by 3 months. These findings are almost identical to the degradation rate of SIS-ECM when this biologic scaffold was used for reconstruction of the urinary bladder.[229] The resorbed ^{14}C labeled degradation products in the present study were eliminated from the body primarily via urinary excretion. No detectable ^{14}C was found in any of the parenchymal organs that were examined.

The non-linear temporal degradation of the SIS-ECM correlated with the extent and distribution of the host cellular infiltrate. At the time of implantation, there were no cells present within the SIS-ECM scaffold. As cells infiltrated the graft, the rate of scaffold degradation increased. By four weeks post surgery, the cell infiltrate lessened and the rate of scaffold degradation began to diminish. The distinctive laminated architecture of the SIS-ECM graft was no longer distinguishable by 28 days, and the remodeled scaffold showed a relatively uniform accumulation of homogenous collagenous connective tissue.

The Achilles tendon is subjected to some of the highest stresses of any tendon in the body.[96, 145, 156, 291] It would therefore seem logical that an ECM scaffold which is subjected to rapid degradation, such as SIS-ECM, would be at risk of failure when used as a repair device for the Achilles tendon under physiologic loading, especially during the first 4-8 weeks after surgery. In fact, this concern has been the rationale for chemically crosslinking many ECM scaffolds including one commercially available device derived from SIS-ECM (CuffPatch™, Arthrotek, Inc.).[2, 173, 271] In the present study, a tube splint that allowed for partial weight bearing was utilized for the first month after implantation to prevent failure due to suture pull-out while still allowing the ECM scaffold to bear load. The application of load early in the remodeling process has been shown to be important for constructive tissue remodeling.[119] It is also likely that other tendons that run parallel to the Achilles tendon, such as the flexor hallucis longus tendon shared some of the load across the SIS-ECM graft. After removal of the splint, the remodeled SIS-ECM scaffold was sufficiently strong to withstand unrestricted cage activity in this animal model without evidence of rupture. The remodeled scaffold showed organized, aligned collagenous tissue after removal of the tube splint at 28 days. Although mechanical testing was not performed in this study, a previous study using the same canine model of Achilles tendon repair showed that the strength of the remodeled Achilles tendon exceeds the strength of the insertion to the gastrocnemius muscle and the calcaneus by 12 weeks after repair with SIS-ECM.[13]

6.1.10 Limitations

A limitation of the present study is the small number (n=2) of animals that were evaluated at each time point. The low numbers were a result of practical considerations including the cost of the study and the complexity involved in producing the SIS-ECM labeled with ^{14}C. Despite these limitations, this study showed rapid degradation of an SIS-ECM scaffold used for repair of a musculotendinous tissue, an application for which SIS-ECM is currently in clinical use. This study also shows that as degradation occurs, the graft remodels into dense collagen rich connective tissue with an organization, cellularity, and vascularity similar to that of native tendon tissue.

Table 6-1. Cellularity of normal tendon and the remodeled SIS-ECM graft. All data is presented as the average number of cells in five 40x field. Statistical significance was set at $p<0.05$. † indicates statistical significance compared to the cellularity for the native tendon.

Tissue	Mononuclear Cells	Neutrophils	Total Cells
Native Tendon	54 ± 17	0	54 ± 17
SIS-ECM Device	0	0	0
Day 3	53 ± 15 58 ± 8	49 ± 10† 86 ± 34†	102 ± 15† 144 ± 29†
Day 7	154 ± 35† 166 ± 30†	4 ± 6 0	158 ± 31† 166 ± 30†
Day 14	377 ± 15† 152 ± 38†	14 ± 8† 0	390 ± 23† 152 ± 38†
Day 28	105 ± 31† 184 ± 24†	0 0	105 ± 31† 184 ± 24†
Day 60	116 ± 24† 146 ± 67†	0 0	116 ± 24† 146 ± 67†
Day 90	63 ± 5 82 ± 24	0 0	63 ± 5 82 ± 24

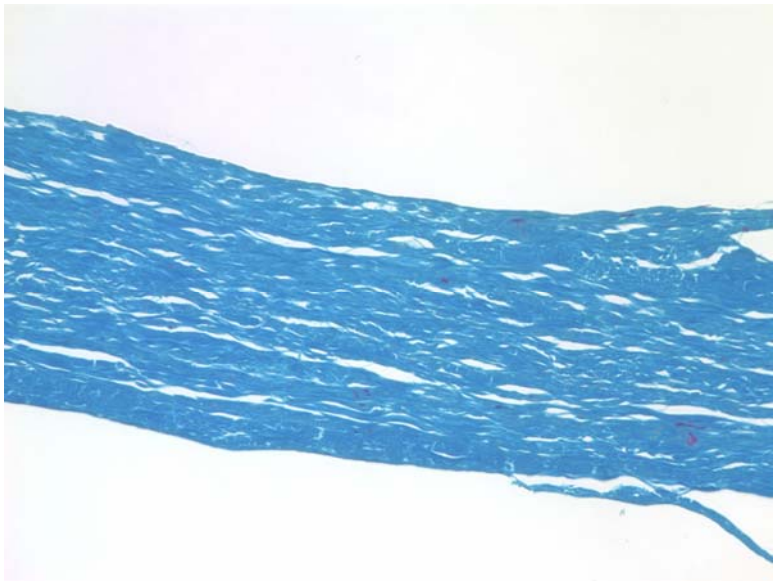

Figure 6-4. Histological section of the SIS-ECM device prior to implantation. The section shows a laminate structure of dense organized collagen and no cellularity. (20x)

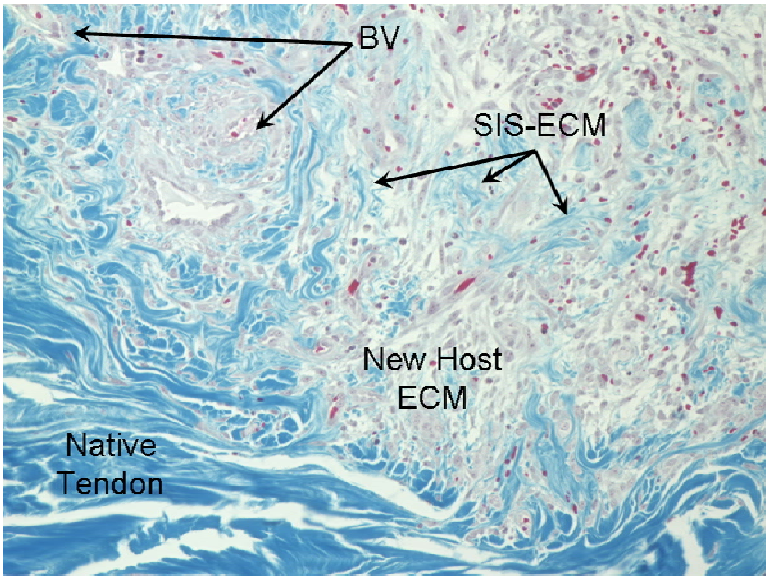

Figure 6-5. Histological section of the interface between the remodeled SIS-ECM graft and the remodeled Achilles tendon at 7 days after surgery stained with Masson's Trichrome. The section showed an abundant cellular infiltrate that consisted almost exclusively of mononuclear cells surrounded by new host ECM. There was also evidence of angiogenesis, with blood vessels indicated by 'BV'. A moderate degree of scaffold degradation was indicated by the marked change in the architecture of the SIS-ECM graft. (40x)

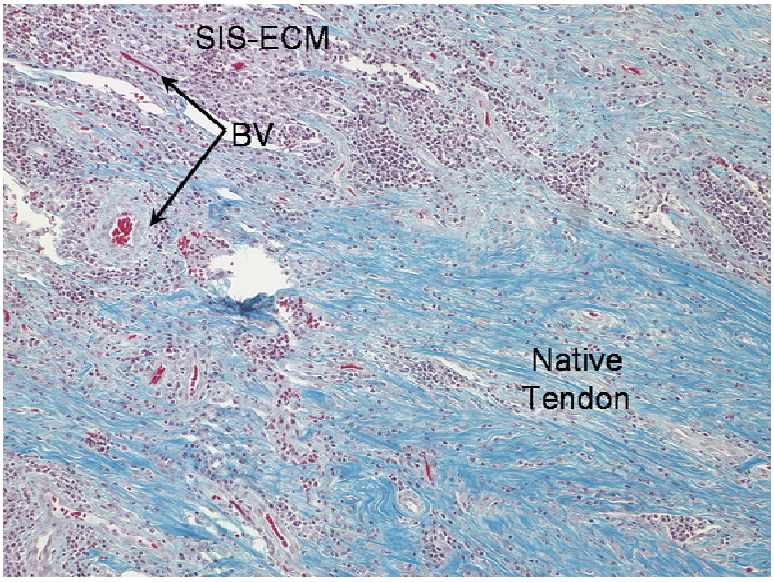

Figure 6-6. Histological section of the interface between the remodeled SIS-ECM graft and the remodeled Achilles tendon at 14 days after surgery stained with Masson's Trichrome. The section showed that the entire SIS-ECM scaffold material was infiltrated with host cells that were almost exclusively mononuclear in morphology. There was also evidence of angiogenesis, with blood vessels indicated by 'BV'. The graft was well integrated with the newly deposited host tissue. (20x)

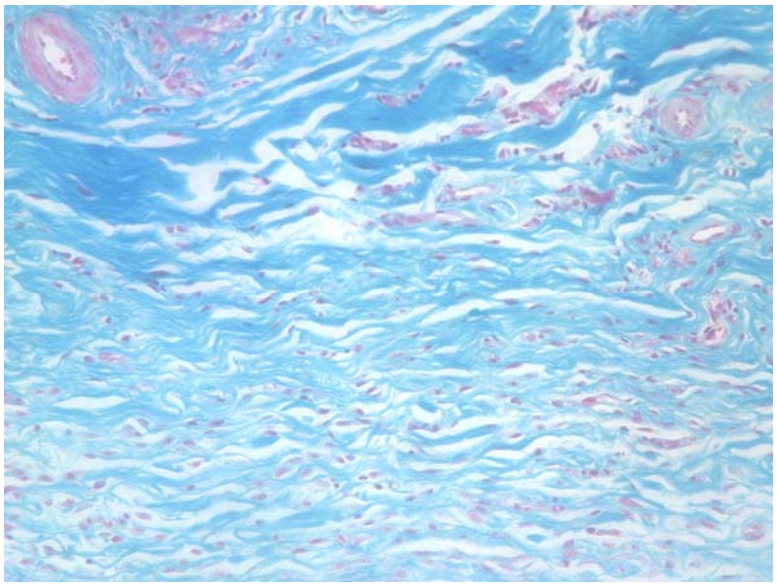

Figure 6-7. Histological section of remodeled SIS-ECM at 28 days after surgery stained with Masson's Trichrome. Dense sheets of exclusively mononuclear cells populated the remodeled ECM scaffold. There was a loss of morphologic evidence of the SIS-ECM scaffold with relatively homogeneous deposition of new host derived ECM that was disorganized in its orientation. (20x)

Figure 6-8. Histological section of remodeled SIS-ECM graft at 60 days after surgery stained with Masson's Trichrome. The section showed that the SIS-ECM graft was replaced with organized, aligned host ECM and spindle cells consistent with the morphologic appearance of fibroblasts. The repair site between the SIS-ECM graft and the native tissue could not be identified and was replaced by a uniform and organized connective tissue. (20x)

Figure 6-9. Histological section of remodeled SIS-ECM graft at 90 days after surgery stained with Masson's Trichrome. The section showed that the remodeled SIS-ECM graft was completely replaced with dense, organized, aligned host ECM and spindle-shaped cells consistent with fibroblast morphology. The cellularity and vascularity were qualitatively similar to that for normal tendon tissue. (20x)

6.2 RECRUITMENT OF BONE MARROW DERIVED CELLS TO THE SITE OF SIS-ECM REMODELING IN A MOUSE ACHILLES TENDON MODEL

It is generally accepted that following tendon injury, the healing process is characterized by an infiltration of inflammatory cells that shift from primarily neutrophils during the acute phase (e.g., first 6-72 hours) to a primarily mononuclear macrophage population thereafter. In the absence of complicating factors such as infection, the inflammatory cells become less abundant within 10-14 days as fibroblasts migrate into the remodeling tendon from the adjacent tissue.[8, 48, 81] However, the cells that populate the SIS-ECM scaffold after surgical implantation are almost exclusively mononuclear in morphology after day 3 and these mononuclear cells progressively increase in number for at least 14-28 days. This unusual cellular response is associated with new ECM deposition by the host and a site specific constructive remodeling process. In a previous study in which SIS-ECM was implanted subcutaneously,[20] it was shown that a portion of the cells that participated in the remodeling of SIS-ECM were bone marrow-derived cells, and they participated in the remodeling beyond the immediate post surgical inflammatory response. The objective of the present study was to determine if bone marrow-derived cells participate in the long term remodeling of a musculotendinous tissue when SIS-ECM is used in a mouse model of Achilles tendon repair.

6.2.1 Preparation of SIS-ECM

Briefly, the small intestine was mechanically delaminated to remove the tunica muscularis externa and the majority of the tunica mucosa. The remaining tunica submucosa, muscularis mucosa, and basilar portion of the lamina propria was then disinfected and decellularized in a 0.1% peracetic acid solution followed by two rinses each in phosphate buffered saline and deionized water. This process yielded an acellular material, which was then lyophilized and

terminally sterilized with ethylene oxide. A single layer form of SIS-ECM was used such that the long axis of the device corresponded with the direction of preferred fiber alignment of SIS.[237]

6.2.2 Chimeric Mouse Model

Six to eight-week-old female C57BL/6J mice were lethally irradiated with 11Gy of gamma irradiation (96cGy/per minute) administered in 2 doses divided by 4 hours using a ^{137}Cs irradiator (Nordion, Kanata, Canada). The lethally irradiated C57BL/6J mice were transplanted via tail injection with 5 X 10^6 low-density mononuclear cells isolated from female B6.ACTbEGFP mice that express green fluorescence protein (GFP) in all of their cells. Recipient animals were tested at monthly intervals to assay for the level of donor cell chimerism via sampling of peripheral blood cells. Stable chimerism post-transplant was achieved in four months. When the blood of the host animals was 100% donor origin (GFP positive), the mice were considered ready for use in the scaffold implantation study.[294]

6.2.3 Study Design and Surgical Procedures

All procedures were performed as approved by the *Institutional Animal Care and Use Committee at the University Pittsburgh* (Protocol #0405959) and the animal care complied with the *NIH Guidelines for the Care and Use of Laboratory Animals*.

Forty chimeric mice that expressed GFP in all of their bone marrow-derived cells were anesthetized with inhalant Isofluorane using a nose cone. The right hind limb of each animal was shaved and prepared for surgery using sterile technique. Under magnification, the Achilles tendon was exposed through an anterolateral skin incision and the surrounding paratenon incised. Two 7-0 Vicryl sutures (Ethicon, Somerville, NJ) were placed proximal and distal in the Achilles tendon. The spacing of the two sutures was 3 mm. In group one (n=20), the proximal and distal suture were stitched through the intervening tendon tissue creating two loops of suture (Figure 6-10A). The tendon was then transected within each loop, creating the autologous tendon graft. The two suture loops were pulled tight and knotted to secure the graft. In group two (n=20), a 2 mm segment of the tendon was resected and a 3 x 2 mm single layer sheet of lyophilized SIS-ECM was attached to the free ends of the tendon via the two placed sutures (Figure 6-10B).

Prior to closing the skin, the graft was rehydrated with sterile saline and the graft was tubularized around the free ends of the tendon (Figure 6-10B). In both groups the wound was closed in layers using 7-0 Vicryl sutures. Remodeling was evaluated in four animals in each group at time points of 1, 2, 4, 8 and 16 weeks after surgery.

After sacrifice, the experimental and contralateral Achilles tendons were harvested from each animal and fixed in 4% paraformaldehyde. The tissue was then embedded in paraffin and 5μm sections were obtained. Unstained sections were used to visualize the GFP protein, and adjacent sections were processed for staining with H&E or Masson's Trichrome. The unprocessed section was examined with fluorescent microscopy for the presence of GFP^+ cells, and photomicrographs were obtained at 20x. A photomicrograph was also obtained for the same area of the tendon from adjacent tissue sections that were stained with H&E or Masson's Trichrome to assess the histological appearance in the vicinity of the cells expressing GFP.

6.2.4 Surgical Outcomes

All animals tolerated the surgical procedure without adverse events and all animals were ambulatory immediately after surgery without apparent lameness.

6.2.5 Histologic Findings for the Native Murine Achilles Tendon

Histologically, the native Achilles tendon was composed of a highly organized collagenous matrix. Scattered spindle-shaped fibroblasts could be seen between highly aligned collagen fibers. In the paratendinous tissue, vascular structures were aligned longitudinal to the tendon. No GFP expressing marrow-derived cells were found in the intact Achilles tendon.

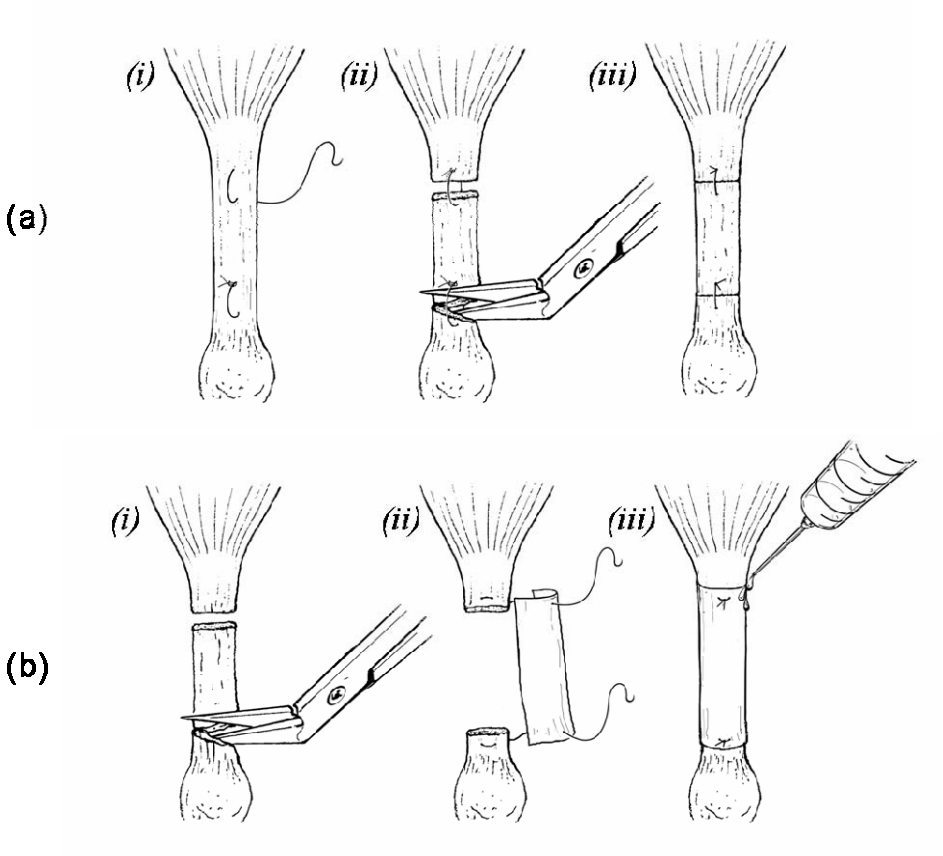

Figure 6-10. (A) The control procedure was performed by first *(i)* placing 7-0 prolene suture loops 2 cm apart in the midsubstance of the tendon. The tendon was then *(ii)* cut within the suture loops to hold the explanted tendon in place. The sutures were finally *(iii)* pulled taught and knotted to secure the autologous tendon graft. (B) The SIS repair procedure was performed by first *(i)* cutting a 2 cm length from the midsubstance of the tendon. *(ii)* A single layer of lyophilized SIS-ECM was then secured to the cut ends of the tendon with 7-0 prolene suture. Finally, the sutures were finally *(iii)* pulled taught and knotted to secure the SIS-ECM graft and the graft was hydrated with saline.

6.2.6 Histologic Findings for the Autologous Tendon Repair Group

At necropsy, all tendon repairs remained intact. Gross examination showed that the reconstructed tendon of both groups had a slightly increased diameter when compared to the intact contralateral tendon at all time points. One week after surgery, the autologous tendon implant was difficult to identify because of the presence of dense granulation tissue. Histological examination at 1 and 2 weeks after surgery showed a dense infiltration of mononuclear cells and abundant new blood vessels (Figure 6-11A). A robust accumulation of GFP-expressing marrow-derived cells was observed at the site of remodeling, generally associated with areas of angiogenesis and inflammation (Figure 6-11B). By four weeks after surgery, the remodeled tendon consisted of organized collagenous tissue, and the cellularity had diminished to near normal. At 4, 8, and 16 weeks, no GFP expressing marrow-derived cells were observed in the tendon body, but occasional green fluorescent cells could be identified around or within vascular structures of the paratendinous tissue. Representative photomicrographs of the autologous repair group 4 weeks after surgery are shown in Figure 6-12. Figure 6-13 shows the histologic appearance of remodeled tissue 16 weeks after surgery. Table 6-2 provides a semi-quantitative summary of the inflammatory cells, bone marrow-derived cells, mononuclear cells, and collagenous tissue of the autologous tendon repair and SIS-ECM repair groups compared to normal tendon at each time point.

6.2.7 Histologic Findings for the SIS-ECM Repair Group

As with the autologous tendon repairs, no graft ruptures were observed at any time point. The SIS-ECM graft was still distinguishable 1 week after surgery, but by 2 weeks the SIS-ECM was incorporated into the remodeling tendon and could not be identified as a discrete entity. Similar to the autologous tendon repair group, the SIS-ECM repair group showed a dense mononuclear cell infiltration and a rich blood supply at 1 and 2 weeks after surgery. An abundant population of GFP expressing marrow-derived cells was observed in the remodeling tendon both in the vicinity of vascular structures and in the tendon body (Figure 6-14). At 4 weeks post surgery (Figure 6-15), a dense mononuclear cell population persisted at the site of scaffold placement, and these cells consisted of both mononuclear round cells and spindle-shaped cells. There was

no morphologically distinguishable SIS-ECM scaffold material remaining and the suture lines between the native tissue and the healing tissue could not be identified. The SIS-ECM repair group showed more marrow-derived green fluorescent cells when compared to the autologous tendon repair group at 4 weeks. The cellularity of the SIS-ECM scaffold site had diminished by 8 weeks after surgery, but was still greater than would be found in normal tendon tissue. No obvious inflammatory response could be seen at the 8 week time point. At both eight and sixteen weeks, the remodeled tendon of the SIS-ECM group continued to show GFP positive marrow-derived cells distributed uniformly throughout the graft segment. The green fluorescent marrow-derived cells within the body of the tendon were typically spindle-shaped and GFP positive cells were also noted in the paratendinous tissue (Figure 6-16).

6.2.8 Significance of the Presence of Bone Marrow Derived Cells

This study confirms that SIS-ECM supports constructive remodeling of the Achilles tendon in a mouse model, and showed that a bone marrow-derived cell population was involved in the long-term remodeling process. While the role of these cells in the remodeling process is not yet fully understood, it has been observed that they remain beyond the inflammatory stage of healing and are found throughout the midsubstance of the tendon when healing is complete. At least some of these cells differentiate along a site appropriate fibroblastic lineage and become part of the new tissue. It is possible that the cells may also differentiate down other cell lineages. The recruitment, persistence, and site specific differentiation of bone marrow derived cells is not generally observed during "normal" adult mammalian tissue remodeling. These findings suggest that the bone marrow-derived cells that populate the SIS-ECM may represent a population of cells that can become appropriate site specific cells that reside in normal tendon tissue, such as fibroblasts and/or endothelial cells. In the absence of SIS-ECM, no bone marrow-derived cells are found within the body of the remodeled tendon. In the current model, it was expected that the autologous tendon control would heal well because the tissue used in the repair was healthy, and the devitalized autologous tendon graft was replaced immediately after the defect was created. In the clinical scenario, the control group would more closely resemble an acute Achilles tendon injury and repair. A neglected Achilles tear with tendon retraction would require a method to "fill" the gap. In these cases of neglected repair and retraction, the presence

of a bone marrow derived cell with the potential to differentiate into a tissue specific cell may have a beneficial effect on tissue healing and remodeling.

Marrow-derived mesenchymal progenitor cells have been identified to have the potential to differentiate into a variety of types of cells *in vitro* and *in vivo*.[52, 224] Their potential to improve healing is part of the rationale for autologous transplants of bone marrow aspirates for bone repair in the clinical setting.[185, 287] There is increasing evidence that marrow-derived mesenchymal progenitor cells can enter circulation and participate in remodeling of tissue during development and homeostasis, or following injury.[84, 161, 181, 263] A chimeric mouse model in which all of the bone marrow derived cells expressed green fluorescent protein (GFP) showed that marrow-derived cells populated a number of organs, including the heart, lung, kidney, small intestine, and skin due to normal homeostasis.[84] When an injury was created in the skin, it was observed that a population of non-hematopoietic bone marrow-derived cells was present in the wound site, was synthesizing collagen types I and III, and had a histological resemblance similar to fibroblasts. In another study,[144] a portion of fetal mouse small intestine was transplanted into a chimeric mouse expressing GFP in all of its bone marrow cells. Non-hematopoietic marrow-derived cells were observed in the lamina propria of the implanted intestinal tissue. This same layer of the small intestine, i.e., the lamina propria, is included in the SIS-ECM scaffold material. Similar findings were observed in both mice and humans in which female recipients received bone marrow from a male donor.[40] Myofibroblasts positive for the Y chromosome were observed in the lamina propria of the small intestine. The same events that recruit these bone marrow derived cells to the site of injured and remodeling tissue may also be involved in the recruitment of the same cells to the site of ECM scaffold remodeling.

In the present study, no GFP expressing marrow-derived cells were observed within the native tendon or within the fully remodeled autologous tendon tissue graft. Occasional marrow-derived cells were observed in the vicinity of new blood vessels and in the paratendinous tissue of the Achilles tendon repaired with autologous tendon tissue. These findings suggest that the marrow-derived cells are not typically involved in the homeostasis or long-term remodeling after injury of the native Achilles tendon.

As described in Section 1.2.5, it has recently been shown *in vitro* that small peptides (5-16 kDa) formed during chemical and physical degradation of ECM bioscaffolds, including SIS-ECM, are chemoattractant for numerous cell types, including endothelial cells.[175] A similar

chemoattractant mechanism may also be responsible for the recruitment of marrow-derived mesenchymal progenitor cells to the site of the ECM remodeling. We speculate that the constructive remodeling process associated with naturally derived ECM scaffolds is due at least in part to the participation of autogenous circulating marrow-derived progenitor cells that are recruited by the degradation products of the SIS-ECM. It is plausible that such cells would then differentiate in response to local environmental cues and thus contribute to tissue organization and differentiation. Factors that inhibit the ECM degradation process, such as chemical crosslinking, may interfere with the biological activities that have been demonstrated by the products of ECM degradation.

The results of this study show that a population of marrow-derived cells participates in the long-term remodeling of a degradable ECM scaffold when used as a repair device in this murine model of Achilles tendon repair. It further suggests that at least a portion of these cells differentiate down a fibroblastic lineage, and it has been shown previously that these cells can also differentiate down an endothelial cell lineage.[20] Such cells do not contribute to tendon healing in the absence of the ECM biologic scaffold. The translation of these findings to the tendon healing process in humans remains to be shown.

Table 6-2. Qualitative prevalence of inflammatory cells, bone marrow derived cells, mononuclear cells, and collagenous tissue in the autologous tendon repair group (Control) and the SIS-ECM group compared to normal tendon.

	Inflammatory Cells		Bone Marrow Derived Cells		Mononuclear Cells		Collagenous Tissue	
Weeks	Control	SIS-ECM	Control	SIS-ECM	Control	SIS-ECM	Control	SIS-ECM
1	+++	+++	+++	+++	+++	+++	↓	↓↓
2	+++	+++	+++	+++	+++	+++	↓	↓
4	++	+	+	++	++	++	—	—
8	+	—	—	+	+	+	+	+
16	—	—	—	+	+	+	+	+

+++, robust increase; ++, moderate increase; +, slight increase; —, normal level; ↓, slight decrease; ↓↓, moderate decrease

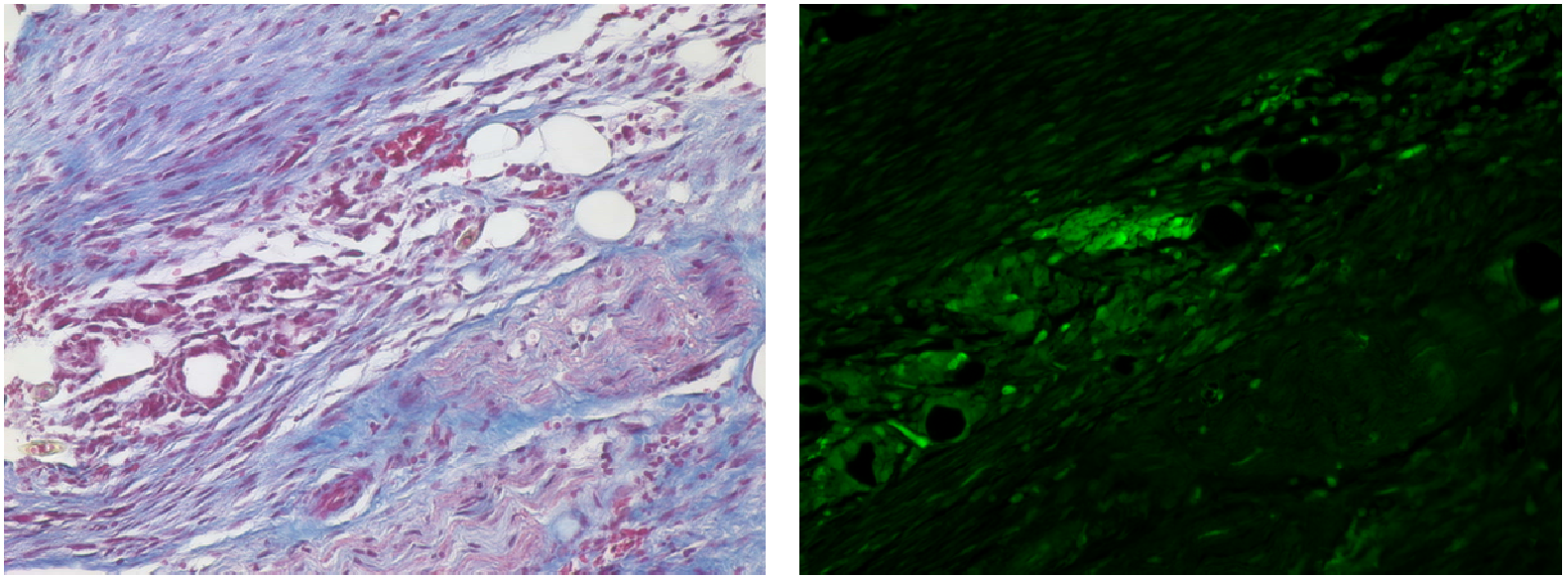

Figure 6-11. (A) At two weeks after surgery, the autologous tendon repair group showed a dense mononuclear cell infiltration, abundant blood vessels, and acute inflammation (Masson's Trichrome 20x). (B) A robust accumulation of GFP expressing marrow-derived cells were found in the vicinity of new blood vessel formation and inflammation (FITC 20x).

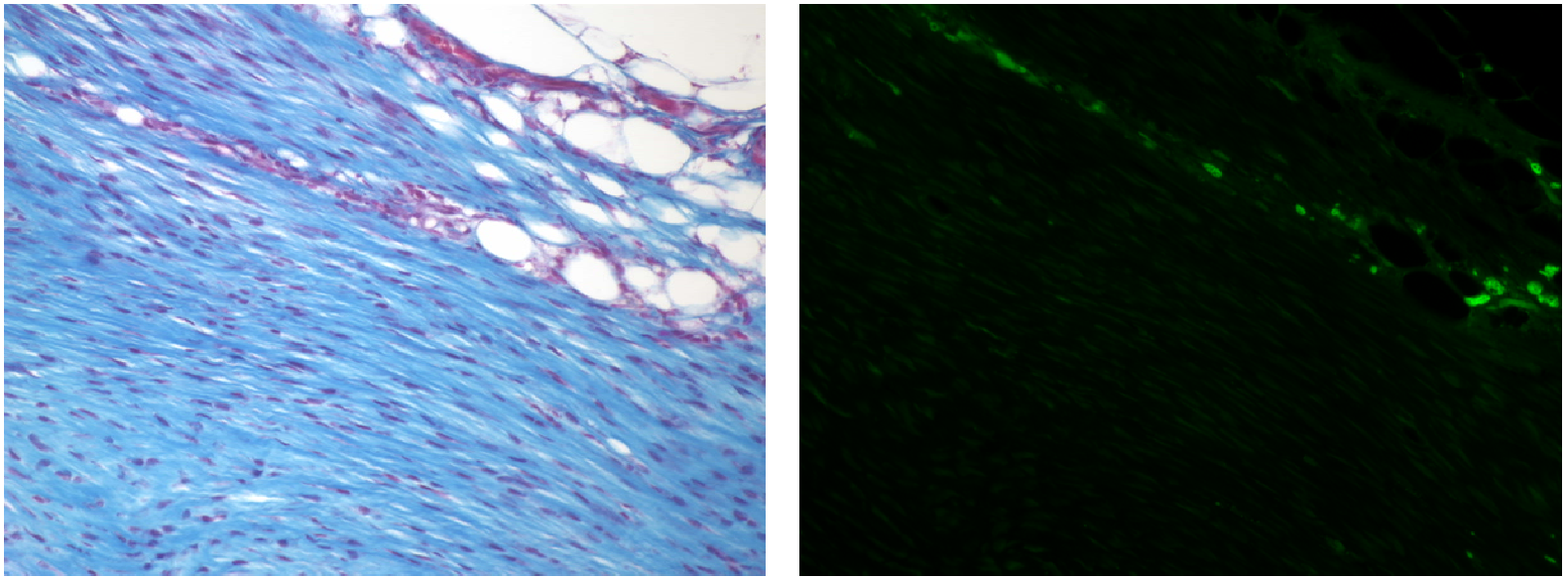

Figure 6-12. (A) At four weeks after surgery, the autologous tendon repair group showed organized collagenous tissue and a diminished cell infiltration compared with two weeks after surgery (Masson's Trichrome 20x). (B) GFP expressing marrow-derived cells only in the vicinity of new blood vessels or areas of increased cellularity (FITC 20x).

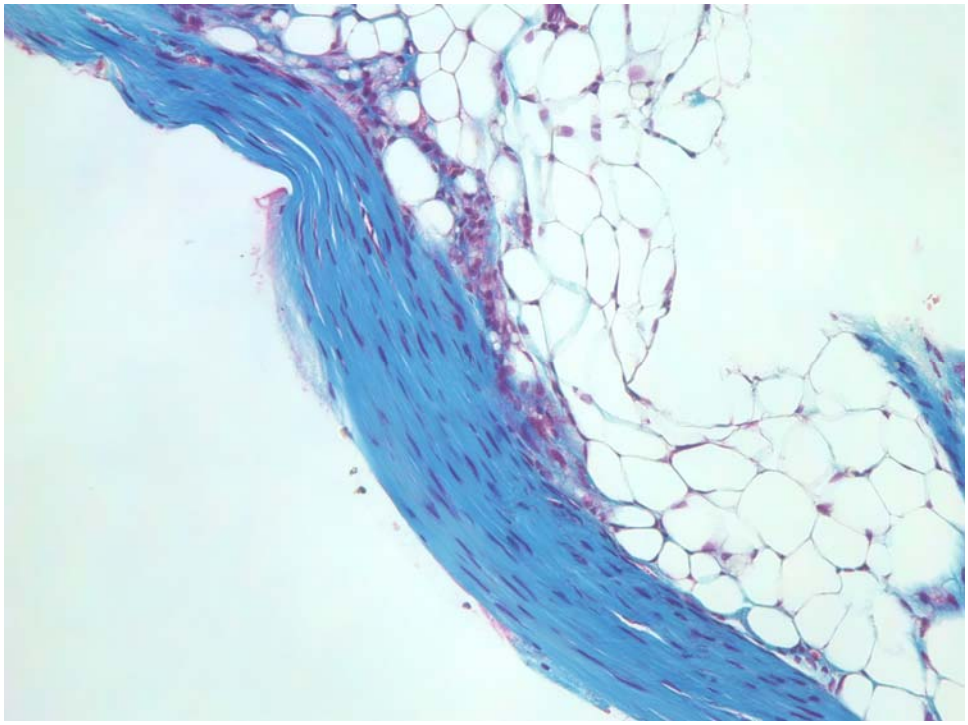

Figure 6-13. At sixteen weeks after surgery, the autologous tendon repair group showed diminished cell infiltration to near normal, and the remodeled tendon was organized collagenous tissue. No GFP cells were observed in the tendon body (Masson's Trichrome 20x).

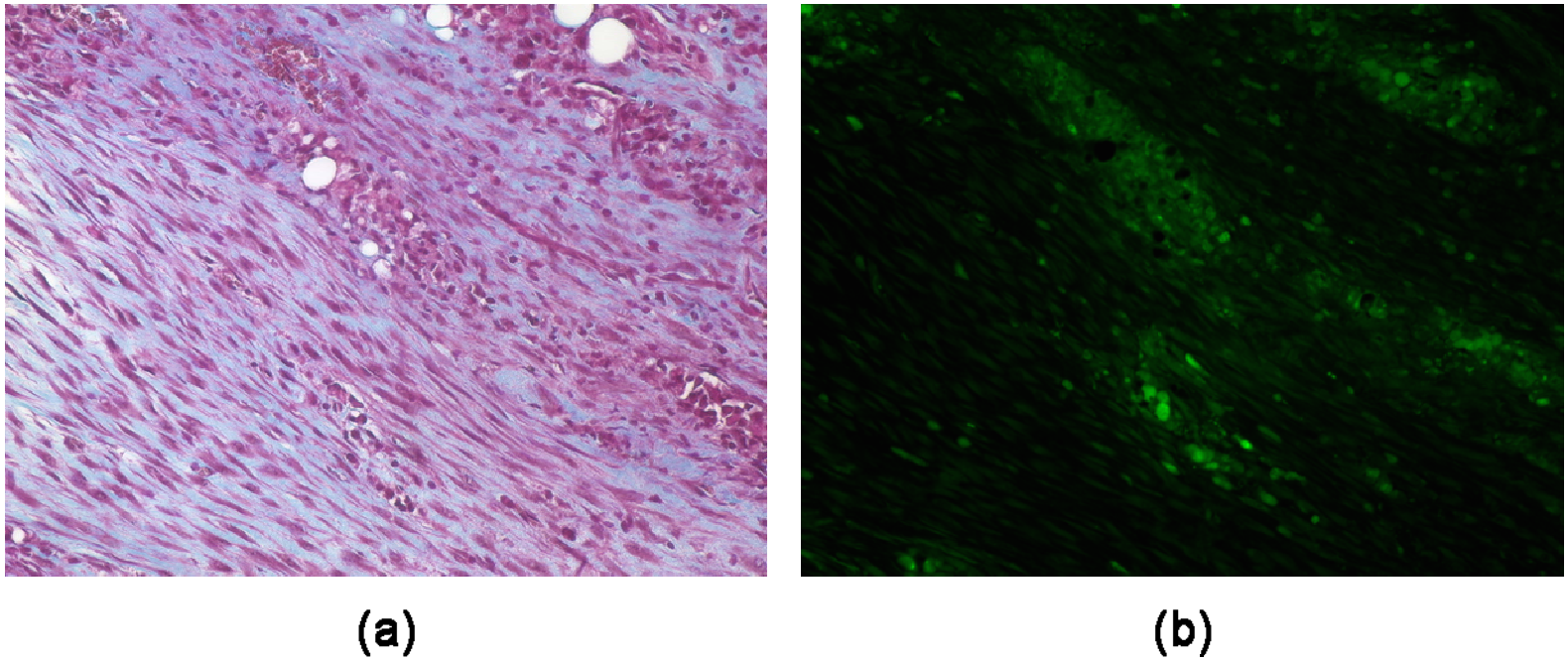

Figure 6-14. (A) At two weeks after surgery, the SIS-ECM repair group showed dense mononuclear cell infiltration, abundant blood vessels, and acute inflammation (Masson's Trichrome 20x). (B) There was a robust accumulation of GFP expressing marrow-derived cells in the vicinity of new blood vessel formation and inflammation, as well as in the tendon body (FITC 20x).

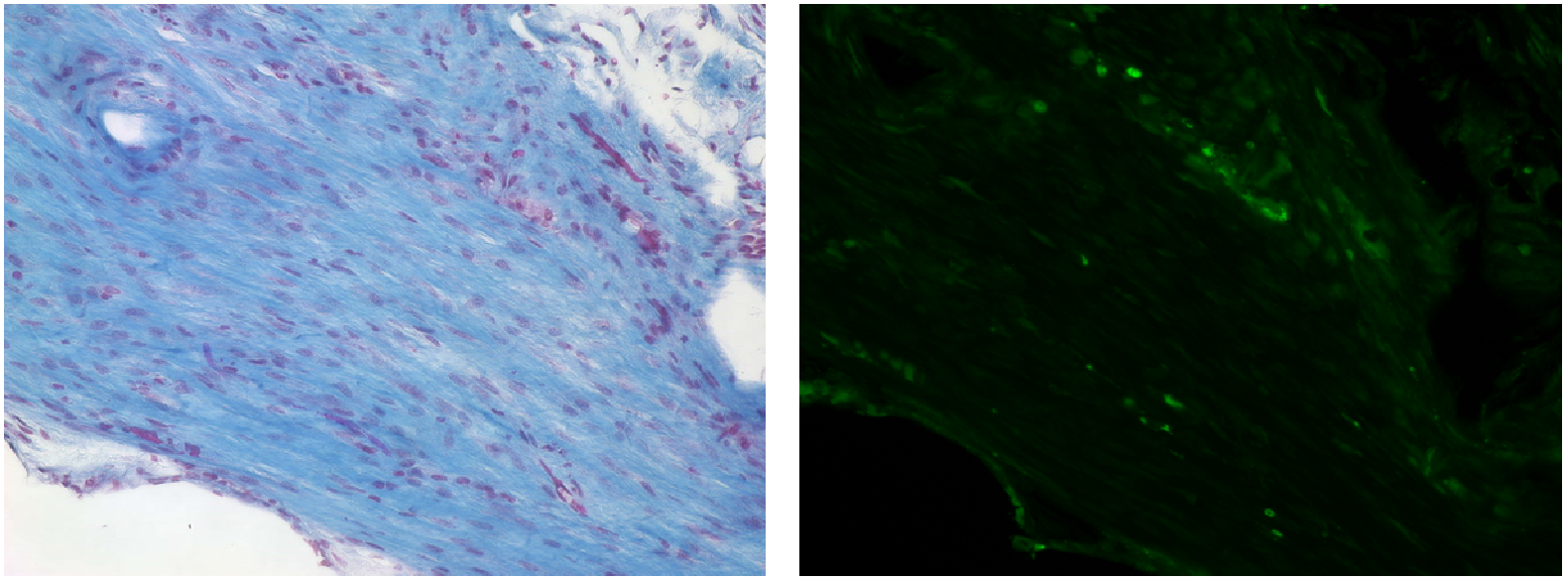

Figure 6-15. (A) At four weeks after surgery, the SIS-ECM repair group showed diminished cellular infiltration compared with 2 weeks after injury, but greater cellularity than normal tendon. The remodeling tendon is organized collagenous tissue (Masson's Trichrome 20x). (B) A robust accumulation of GFP expressing marrow-derived cells in the vicinity of new blood vessel formation and inflammation, as well as in the tendon body (FITC 20x).

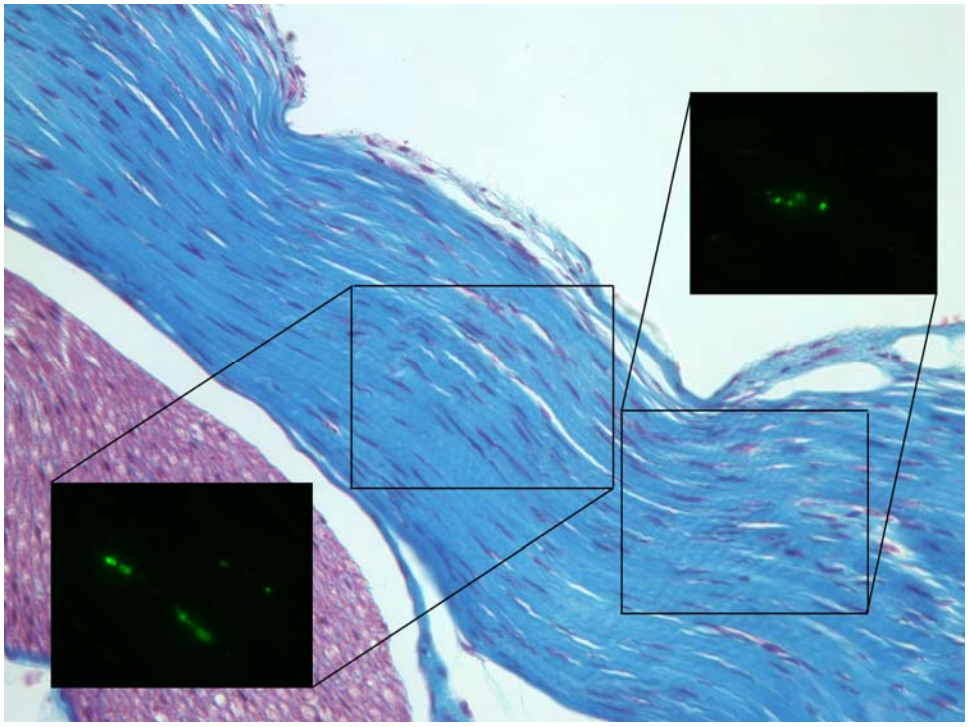

Figure 6-16. At 16 weeks after surgery, the SIS-ECM repair group showed that the cellularity had decreased to near normal, and the tendon consisted primarily of organized collagenous tissue with increased vascularity compared to normal tendon. The inlays show the GFP expressing marrow-derived cells present within organized collagenous tendon tissue (Masson's Trichrome 20x; insets FITC 20x).

6.3 FATE OF BONE MARROW DERIVED CELLS TO THE SITE OF SIS-ECM REMODELING IN A MOUSE ACHILLES TENDON MODEL

An ECM scaffold changes the default mammalian wound healing process in part by recruiting a population of bone marrow derived cells that participates in the long-term remodeling process. To understand the role that these cells play in the remodeling process, it is necessary to examine the change in phenotype of these cells during the course of remodeling. In a subcutaneous implant model,[20] ECM scaffolds were found to recruit bone marrow derived cells that expressed endothelial cell markers 3 months after implantation. It is possible that these cells represented a population of endothelial progenitor cells that originated in the bone marrow. There were also cells that exhibited fibroblastic morphology, but this phenotype was not confirmed by cell surface markers or gene expression patterns. When ECM was used for repair of a mouse Achilles tendon,[296] the morphology and location of the bone marrow derived cells was consistent with a fibroblastic phenotype, but again, this was not verified by phenotypic analysis. Therefore, the mouse Achilles tendon model was repeated to determine whether a portion of the bone marrow derived cells recruited to the site of ECM remodeling differentiate into fibroblasts. In addition, to determine if degradation of the scaffold was important for the recruitment and persistence of the bone marrow derived cells, recruitment of bone marrow derived cells was compared between natural SIS-ECM and SIS-ECM that had been chemically crosslinked with carbodiimide.

Phenotypic analysis to verify that a cell is a fibroblast is challenging because fibroblasts do not have a profile of gene expression or surface markers that is specific only to fibroblasts. A few previous studies have defined fibroblasts based on expression of Col I, Col III, TN-C, and Thy-1.[6, 84, 158, 159] SMA is a marker that can be associated with myofibroblastic cells. All of these genes are expressed by a variety of cells, so the expression of any one of these genes does not guarantee that the cell is a fibroblast, however, for a cell to express several of these genes would certainly suggest that the cells are fibroblast-like. Coupled with the expression of these markers, the loss of expression of a distinct hematopoietic marker (i.e., CD45) by a bone marrow derived cell would strongly suggest differentiation of the cells towards a fibroblastic lineage.

6.3.1 Study Design and Surgical Procedures

All procedures were performed as approved by the *Institutional Animal Care and Use Committee at the University Pittsburgh* (Protocol #0405959) and the animal care complied with the *NIH Guidelines for the Care and Use of Laboratory Animals*.

Fifty-six chimeric mice that expressed GFP in all of their bone marrow-derived cells (Section 7.2.2) were anesthetized with inhalant Isofluorane using a nose cone. The right hind limb of each animal was shaved and prepared for surgery using sterile technique. Under magnification, the Achilles tendon was exposed through an anterolateral skin incision and the surrounding paratenon incised. Two 7-0 Vicryl sutures (Ethicon, Somerville, NJ) were placed proximal and distal in the Achilles tendon. The spacing of the two sutures was 3 mm. A 2 mm segment of the tendon was resected and a 3 x 2 mm 3 layer multilaminate sheet of SIS-ECM was attached to the free ends of the tendon via the two placed sutures (Figure 6-10B). Half of the animals received a natural SIS-ECM device (n = 28), and the other half received a device that had been chemically crosslinked by soaking the material in 10mM of ethyl-3(3-dimethylamino) propyl carbodiimide for 24 hours.[32] So that the rate of ECM degradation could be compared between the natural and chemically crosslinked groups, 12 the devices from each group were made using SIS-ECM that was labeled with ^{14}C. Prior to closing the skin, the graft was rehydrated with sterile saline and the graft was tubularized around the free ends of the tendon (Figure 6-10B). In all animals, the wound was closed in layers using 7-0 Vicryl sutures. Seven animals in each group (n = 4 native, n = 3 radioactive) at time points of 2, 4, 8 and 16 weeks after surgery. During preparation of the specimens for histologic examination, technical difficulty was experienced while try to obtain histologic sections of the tendons treated with chemically crosslinked SIS-ECM, so only data on the native SIS-ECM is reported herein.

6.3.2 Tissue Collection

After sacrifice, the experimental and contralateral Achilles tendons were harvested from each animal and snap frozen. The tissue was then embedded in OCT and 5µm sections were obtained. Unstained sections were mounted onto microdissection slides so that the GFP^+ cells could be visualized and isolated by laser microdissection (mmiCellcut®, Molecular Machines Industries,

Knoxville, TN). Adjacent sections were processed for staining with Masson's Trichrome or immunostaining for GFP and CD45. The Masson's Trichrome stained slides were compared to slides stained for GFP and CD45 to assess the histological appearance of the tissue in the vicinity of positive cells.

6.3.3 Collagen Expression by GFP$^+$ Cells in the SIS-ECM Repair Group

The unstained sections mounted onto microdissection slides for the 16 week animals (non-radioactive) were viewed with FITC to detect the GFP. Fifty regions were laser dissected from the section and transferred to Eppendorf tube with an adhesive cap. The dissected regions were obtained from the midsubstance of the tendon and included cells that were spindle shaped in appearance. Care was taken not to dissect cells that did not express GFP. As a control, fifty regions were also microdissected at random from one native mouse Achilles tendon. RNA isolation and RT-PCR was performed for GAPDH, Col I, Col III, TN-C, and SMA as described in Section 6.2.3.

6.3.4 Immunofluorescent Staining for GFP and CD45

Immunohistochemistry was performed using fluorescent secondary antibodies (AlexaFluor) to visualize GFP and CD45 together. Tissues were frozen in optimal cutting temperature solution (OCT, Tissue Tek) and sectioned on a cryostat at 8 μm and placed on slides. The cryosections were thawed to room temperature, fixed in acetone for 5 min at room temperature, rinsed in PBS and then incubated in 1.5% goat serum (Vector) for 30 min in a 37°C humidified chamber to block nonspecific binding of antibodies. Serum for blocking was goat serum. Following incubation in blocking serum, sections were incubated in a solution with two primary antibodies in a 37°C humidified chamber for 1 hour and then rinsed in PBS. The primary antibodies used were rat anti-mouse CD45 (#550539, BD Pharmingen) at a 1:40 dilution and rabbit anti-GFP (#Ab290, Abcam) at 1:500. Sections were then incubated in a dual secondary antibody solution for 30 min in a humidified 37°C chamber and again rinsed in PBS. The secondary antibodies used were goat anti-rat IgG (#A11081, AlexaFluor) and goat anti-rabbit IgG (#A11008, AlexaFluor). The secondary antibodies were both used at dilutions of

1:500. Following the final PBS rinse the slides were coverslipped with Vectashield containing DAPI (#H1200, Vector) to allow individual cell nuclear material to be visualized. Each PBS rinse in the protocol was for 5 min at room temperature, replacing the PBS 3 times, with occasional agitation.

6.3.5 Immunohistochemical Staining for CD45

Immunohistochemistry was performed using the Vectastain advin-biotin peroxidase method (Elite ABC Kit, # PK-6100, Vector Laboratories). Tissues were frozen in optimal cutting temperature solution (OCT, Tissue Tek) and sectioned on a cryostat at 8 μm. The sections were thawed to room temperature, fixed in acetone for 5 min at room temperature and rinsed in PBS. The sections were then treated with 0.3% hydrogen peroxide in methanol at room temperature for 30 min to quench endogenous peroxidase activity, rinsed in PBS, and incubated in 1.5% rabbit serum (Vector) for 30 min in a 37°C humidified chamber to block nonspecific binding of antibodies. Following incubation in blocking serum, sections were incubated in the primary antibody (rat anti-mouse CD45, 1:20 dilution (#550539, BD Pharmingen)) in a 37°C humidified chamber for 1 hour and rinsed in PBS. Sections were then incubated in the secondary antibody (biotinylated rabbit anti-rat IgG, 1:500 dilution (#BA-4000, Vector)) for 30 min in a humidified 37°C chamber and again rinsed in PBS. Sections were then incubated in Vectastain ABC reagent for 30 min in a humidified 37°C chamber, rinsed 3 times in PBS for a total of five minutes, and incubated in 4% diaminobenzadine substrate solution at room temperature while being viewed on a microscope until slides showed the desired darkness of antigen labeling; finally, slides were rinsed in DI water to stop the development of the diaminobenzadine substrate. Each PBS rinse in the protocol was for 5 min at room temperature, replacing the PBS 3 times, with occasional agitation.

6.3.6 Histologic Findings for the Native Murine Achilles Tendon

Histologically, the native Achilles tendon was composed of a highly organized collagenous matrix. Scattered spindle-shaped fibroblasts could be seen between highly aligned collagen fibers. In the paratendinous tissue, vascular structures were aligned longitudinal to the tendon.

No CD45 or GFP expressing cells were found in the intact Achilles tendon by immunostaining. RNA isolated by microdissection showed expression of Col I, but expressions of Col III and TN-C were undetectable (Figure 6-17).

6.3.7 Findings for the Native SIS-ECM Repair Group

At 16 weeks after implantation, the remodeled tendon repaired with SIS-ECM showed GFP positive marrow-derived cells distributed uniformly throughout the graft segment. Only a small portion of the GFP^+ cells also expressed CD45, indicating that they were not of the hematopoietic cell lineage. The green fluorescent marrow-derived cells within the body of the tendon typically exhibited a spindle-shaped morphology. There were also a large number of GFP positive cells present in the peritenon (Figure 6-18).

The RNA isolated from the GFP^+ cells located within the midsubstance of the tendon were shown to express Col I, Col III (although not in all samples), and SMA. The expression of Col I was generally less than that found in normal tendon fibroblasts, while the expressions of Col III and SMA were greater in the bone marrow derived cells. TN-C was only found in the fibroblasts isolated from the normal tendon fibroblasts. (Figure 6-17)

6.3.8 Findings for the Crosslinked SIS-ECM Repair Group

Due to complications with this group, including self mutilation, low humidity, and early death, the remodeled tendons in this group were not able to be used for histology or microdissection.

6.3.9 Significance of the Differentiation of Bone Marrow Derived Cells

It was shown in previous studies that an ECM scaffold recruits a population of marrow derived cells to the site of remodeling that does not participate in the normal mammalian wound healing response. A small portion of the bone marrow derived cells to express CD45. It is possible that $CD45^-$ bone marrow derived cells are included in the population of cells that were recruited to

the site of ECM remodeling, or that a population $CD45^+$ bone marrow derived cells was recruited to the site and then differentiated into a mesenchymal cell. The specific phenotypic origin of these cells is not clear, but it they may represent a population of mesenchymal progenitor cells.

The gene expression profile of the GFP^+ cells could lead to several interpretations of the results. One interpretation is that the bone marrow derived cells become site specific cells, in particular fibroblastic cells, and participate in the long term remodeling by synthesizing Col I and Col III. Under this interpretation, the expression of SMA by these cells suggests that they exhibit a myofibroblastic phenotype or that they represent the population of circulating fibrocytes. Another interpretation is that these bone marrow derived cells represent remnants of blood vessels that formed in the tissue during the initial phase of remodeling. Col III and SMA are both markers for vascular tissue.

Since these cells constitute a relatively small portion of the total cell population of the remodeled tissue (~30%), the full extent of their role in the remodeling process is not clear. The cells certainly contribute to constructive remodeling by synthesizing new collagen and helping to organize the tissue structure, but they may also guide the behavior of other cells in the remodeling tissue by synthesizing growth factors or by direct cell:cell communication.

It is possible that since the application of interest for the study was the Achilles tendon, mechanical loading played an important role in the differentiation of these cells. It has been shown *in vitro* that the presence of appropriate mechanical loading, as well as the administration of growth factors, can lead to differentiation of bone marrow progenitor cells into fibroblastic cells. As bone marrow derived cells are recruited to the site of ECM remodeling, the local mechanical and biochemical environment causes at least a portion of these cells to become site specific cells. This cell recruitment and differentiation process would explain, at least in part, the constructive remodeling response that has been repeatedly observed when ECM scaffolds are used for tissue reconstruction. Additional work will be necessary to determine the specific bone marrow cell population(s) that are recruited, the specific environmental cues that guide the differentiation in different tissue locations, and the specific peptides that recruit the cells to the site of remodeling.

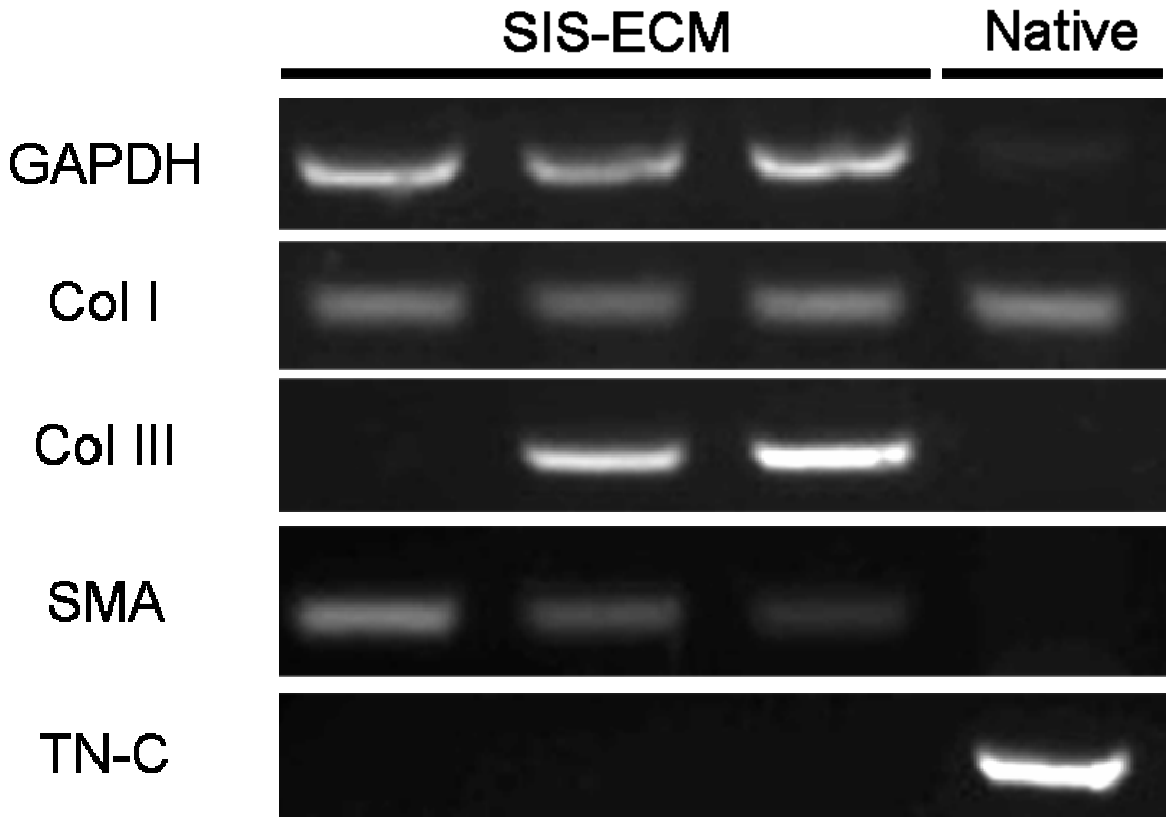

Figure 6-17. Gel electrophoresis of PCR products from RNA isolated from mouse Achilles tendon that was repaired with SIS-ECM (Columms 1-3) and native Achilles tendon. The bone marrow derived cells isolated from the SIS-ECM treated Achilles tendon expressed Col I, Col III (in two of three samples), and SMA. The native fibroblasts expressed Col I and TN-C. This suggests that the bone marrow derived cells become a myofibroblastic cell as opposed to a normal fibroblast.

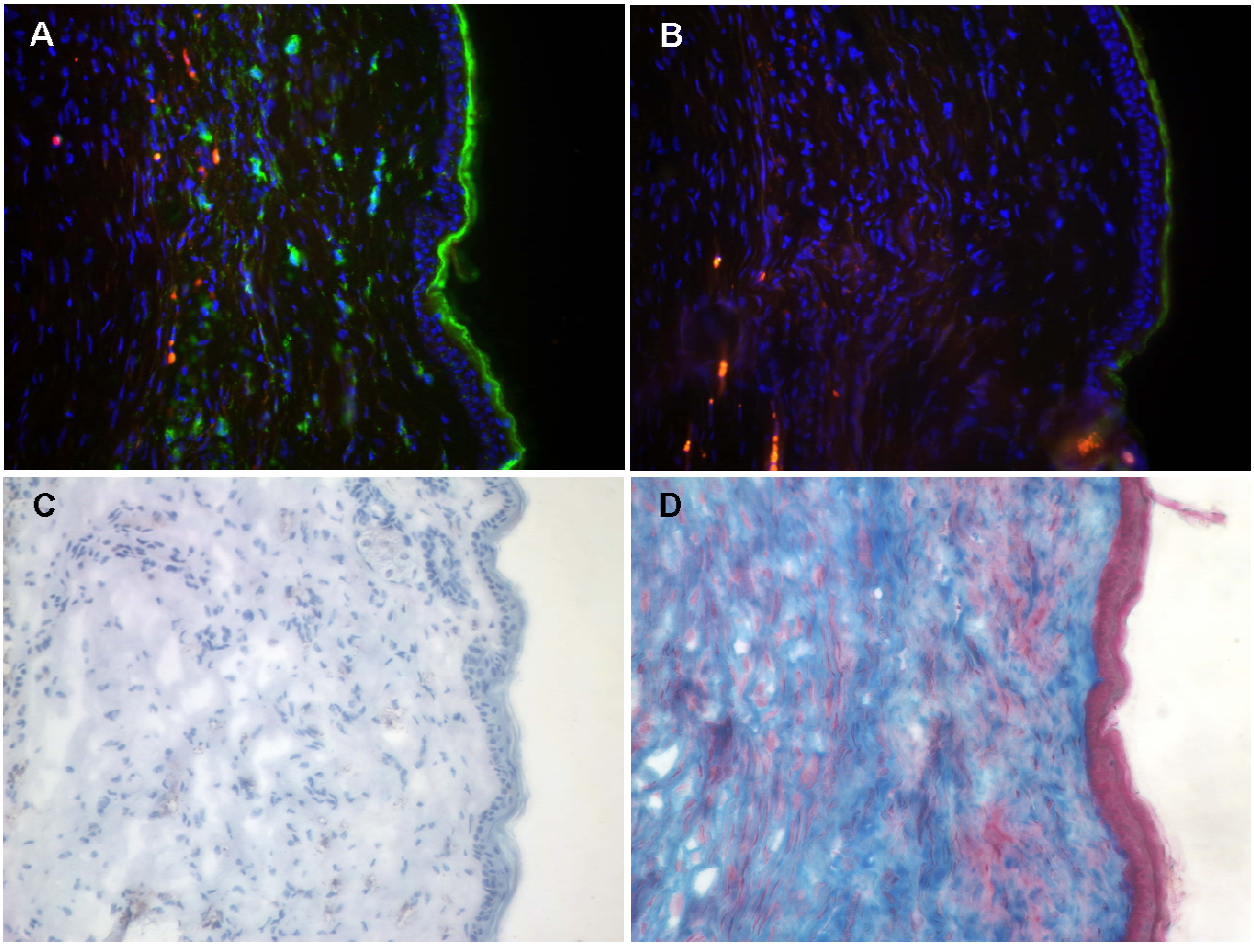

Figure 6-18. Histological sections of the mouse Achilles tendon 16 weeks after repair with SIS-ECM. A) With immunofluorescence, it was shown that GFP^+ bone marrow derived cells were still present in the body of the tendon (Green), but only a few of those cells were double stained for CD45 (Red). The cellularity was increased in the tendon as shown with the DAPI staining (Blue). B) The primary delete verifies that the staining observed was real. C) Immunohistochemical stainingof CD45 was also attempted to verify the results for the immunofluorescence, and again only a few scattered CD45 positive cells were detected. D) The Masson's Trichrome stain show the morphology of the tendon, which is generally organized and with dense collagen aligned along the longitudinal axis of the tendon. The tissue is not a aligned as the native Achilles tendon.

7.0 *IN VITRO* MECHANICAL LOADING OF SIS-ECM

This section describes the experiments that were performed in order to complete Specific Aim 1. Section 7.1 describes a study to determine the fiber kinematics of SIS-ECM under uniaxial and biaxial load.[98] These results were used as a basis to choose the magnitudes of stretch that should be applied to SIS-ECM *in vitro*. Since the collagen fiber architecture of SIS-ECM is specific to the behavior of the small intestine, a better understanding of the fiber kinematics was necessary in order to obtain a sense for the degree of strain that would be transferred from the fibers to the cells seeded on the scaffold. Section 7.2 describes the development of an *in vitro* system that allowed scaffolds seeded with cells to be cyclically stretched. Section 7.2 goes further to describe the effects of a variety of cyclic mechanical loading regimens on the expression of several matrix related genes by fibroblasts seeded on SIS-ECM and the possible implications of these changes for the remodeling of an ECM scaffold.[101]

7.1 FIBER KINEMATICS OF SIS-ECM

Despite extensive use, the pre-clinical and clinical applications of SIS-ECM and other biologically derived collagenous tissue scaffolds have yet to be optimized because of a limited understanding of the mechanical behavior of the native tissue. In addition, cell seeding coupled with *in vitro* mechanical stretching is being considered as a means to modify biologic scaffolds, such as SIS-ECM, to make them more suitable for repair of load bearing tissues such as urethral slings [186, 187] and tendons and ligaments.[7, 206] Ultimately, there is a need for constitutive models to guide the *in vitro* remodeling process and to predict how ECM scaffolds will behave *in vivo* immediately after implantation.

Structural approaches have been utilized to model tissue behavior under multiaxial loading states.[70, 71, 238] Structural constitutive models integrate information on tissue composition and structure to avoid ambiguities in material characterization, and offer insight into the function, structure, and mechanics of tissue components. Moreover, extension of current structural approaches to multi-scale simulations can provide a means to estimate the force and displacement fields surrounding the constituent cell population resulting from tissue deformations. Full realization of structural approaches, however, requires direct quantitative structural information to either validate structural model predictions or for direct implementation into the model. Given the inherent complexity of soft tissues,[69] a detailed knowledge of the fiber kinematics of the scaffold under load is essential for accurate model development.

Several techniques have been developed to investigate the stretch and orientation of collagen fibers in tissue constructs in response to mechanical load, as well as how strain is transmitted from collagen fibers to cells.[80, 154, 155, 247, 266, 275, 297] In general, these techniques incorporate a mechanical loading apparatus with an imaging system (confocal or polarized light microscopy) to visualize the nuclei of the cells [80, 247] or matrix fibers [154, 155, 266, 275, 297] under an applied load. While these systems offer great opportunities for increased understanding of fiber kinematics and cell strain, their utility is limited when it comes to dense collagenous scaffolds such as SIS-ECM due to difficulty visualizing cells and fibers through the thickness of a specimen. More importantly, these methods are not designed to provide angular distributions of large populations of collagen fibers, nor are they able to describe changes in these distributions with applied stress.

Small angle light scattering (SALS) has been demonstrated to be an accurate means to determine fiber distributions in planar collagenous tissues.[234, 237] In the current study, we investigated the fiber kinematics of SIS-ECM using SALS in response to uniaxial and biaxial strain states using a modified version of a biaxial stretching device integrated with the SALS apparatus [33]. An important advance from previous studies was the ability to obtain the angular collagen fiber distributions of SIS-ECM in real-time. Moreover, SIS-ECM collagen fiber kinematics was evaluated under several biaxial stretching protocols to determine path dependency, as well as under uniaxial strain parallel and perpendicular to the preferred fiber direction. Finally, an affine deformation model was applied to the experimental data to determine if the fiber kinematics of SIS-ECM could be predicted for the selected strain paths.

7.1.1 SALS-Biaxial Testing Instrumentation

The testing system was modified from Billiar and Sacks [33] and consisted of a biaxial stretching apparatus (Figure 7-1) positioned such that SALS measurements of the tissue could be obtained while monitoring and controlling the strain level (Figure 7-2). A mirror with a 1 cm diameter hole in the center was placed in front of the specimen at a 45° angle. The hole allowed the laser beam to pass unimpeded to the specimen, while the angled mirror made it possible for a CCD camera to be set-up orthogonal to the path of the laser while allowing tracking of the strain markers. The biaxial stretching device (Figure 7-1) consisted of 4 lead screws coupled via a series of gears to two computer-controlled stepper motors. The test specimens were mounted using sutures that were threaded over pulleys that were free to rotate, thereby insuring that the loads on the specimen were evenly distributed and allowing shear to occur.

A SALS system was used to determine the collagen fiber distribution of the test specimen.[234] Briefly, the system consisted of a 4 MW HeNe (632.8 nm) continuous unpolarized wave laser. As the beam passed through the tissue, it was scattered onto a ground glass screen. The resulting scattering pattern was recorded with a CCD camera system and was analyzed using custom software. The scattering pattern, $I(\theta)$, represented the angular distribution of collagen fibers within the light beam envelope.[234] For these experiments, a beam diameter of 1 mm was used to reduce variability that may have resulted from local differences in the collagen fiber distribution, which may have been detected during movement of the specimen.

From the scattering pattern the preferred fiber orientation and an orientation index (OI) were calculated. The OI has been defined as an angle about the preferred fiber direction that contained 50% of all fibers.[234] In the present study, the OI was normalized to simplify comparisons between strain states. The normalized orientation index (NOI) was defined as NOI = (90° - OI)/90° x 100%. An NOI of 100% indicated that the collagen fibers in the tissue were perfectly aligned and an NOI of 0% indicated random fiber alignment.

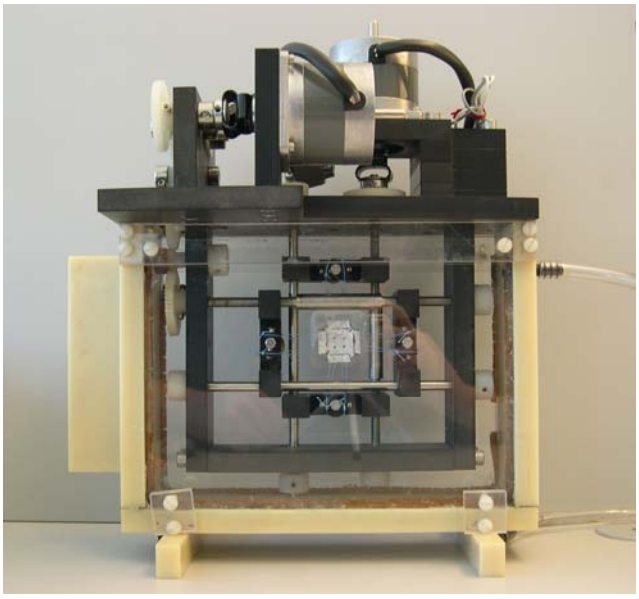

Figure 7-1. Photograph of the Biaxial Mechanical Stretching Device (28cm x 33cm x 10cm). The biaxial stretching device consisted of 4 lead screws coupled via a series of gears to two computer-controlled stepper motors. The specimens were mounted using sutures that were threaded over pulleys that were free to rotate. The geometry of the specimens is also shown. The extensions of the specimen were folded to increase the suture retention strength, and four graphite markers were fixed to the specimen for strain tracking.

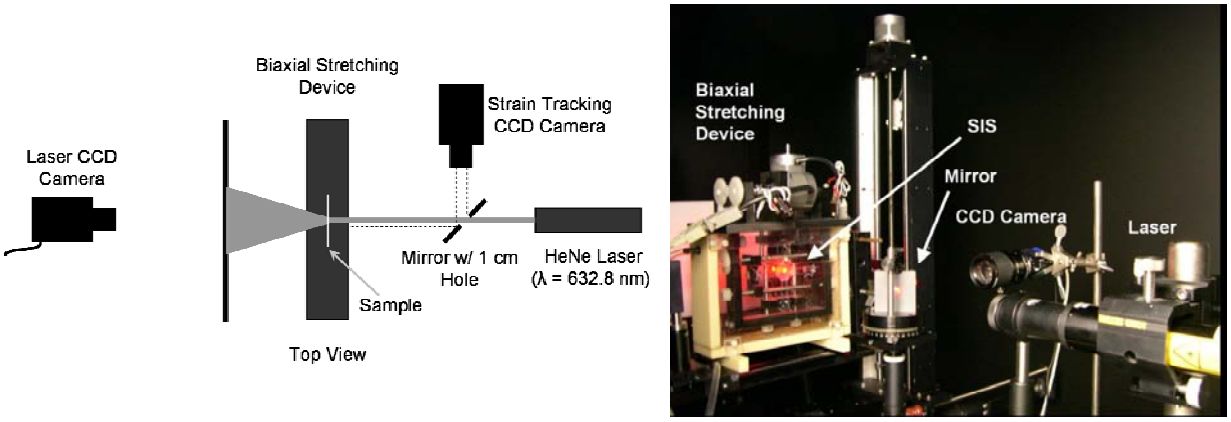

Figure 7-2. A) Schematic and B) photograph of the SALS – Biaxial Fiber Kinematics Testing System. The biaxial stretching device is mounted on the SALS device in a reservoir for holding PBS or other media. The laser passes through a 1 cm hole in the mirror to impact the specimen. The mirror is mounted at 45° to the specimen to reflect the image to a CCD camera which is set-up orthogonal to the path of the laser to allow simultaneous fiber architecture measurement and tracking of the strain markers. This allows the user to obtain real-time measurements of the collagen fiber distribution under load.

7.1.2 SIS-ECM Specimen Preparation

Briefly, the small intestine was mechanically delaminated to remove the tunica muscularis externa and the tunica mucosa. The remaining tunica submucosa and basilar portion of the tunica mucosa consisted of extracellular matrix and the constituent cells. The SIS-ECM was then disinfected and decellularized in a 0.1% peracetic acid (PAA)/4% ethanol solution followed by two rinses each in phosphate buffered saline (PBS) and deionized water. This process yielded an acellular material, which was lyophilized and terminally sterilized with ethylene oxide (EtO). The thickness of the specimens was approximately 100 μm.

The specimens for biaxial testing were prepared by cutting the SIS-ECM into 35 mm square crosses with extensions that were 15 mm wide and 10 mm long (Figure 7-1). Fifteen specimens were cut such that the principal axes of the specimen was aligned with the longitudinal axis of the small intestine, which has been shown to correspond to the preferred collagen fiber direction (PD).[215, 216, 237] The geometry of the specimen was chosen to reduce the stress concentrations at the corners of the specimen and obtain more uniform strain at the interior of the specimen, based on the results of finite element modeling.[261] For uniaxial testing, the SIS-ECM was cut into a dog bone shaped specimen with an 8 mm x 40 mm midsubstance. A total of ten specimens were tested, with five samples cut such that the long axis of the specimen was parallel to the PD. The other five specimens were cut such that the long axis was perpendicular to the PD, in other words, corresponding to the cross preferred fiber direction (XD). For both the uniaxial and biaxial samples, the portion of the tissue used to mount the specimen to the testing device was folded to increase suture retention strength. For strain tracking, four graphite markers (0.5 mm diameter) were fixed to the tissue in a 5 mm square pattern using cyanoacrylate adhesive.

7.1.3 Fiber Kinematics Analysis Methodology

The lyophilized SIS-ECM was mounted in the mechanical testing device with the strain axes aligned to the PD and XD directions. The specimen was allowed to hydrate for 15 minutes in PBS prior to obtaining the initial reference dimensions.[286] Unlike previous studies, it is was not necessary to clear the material to obtain SALS measurements, which eliminated the need for

repeated dehydration/rehydration cycles used in the previous study.[33] The magnitude of stretch applied was monitored for each specimen, with accuracy within ±0.001. For biaxial specimens, one of three loading paths was used to obtain an equibiaxial strain state (β_{EB} in Figure 7-3). These paths included 1) stretching first in the PD to a stretch of 1.10 while maintaining the XD at a stretch of 1.00 (strip biaxial stretch to β_{PD}), then stretching in the XD to a stretch of 1.10 while maintaining the PD at 1.10 (equibiaxial stretch at β_{EB}), 2) stretching in the XD to 1.10 while maintaining the PD at a stretch of 1.00 (strip biaxial stretch to β_{XD}), then stretching in the PD to a stretch of 1.10 while maintaining the stretch in the XD at 1.10 (equibiaxial stretch at β_{EB}), and 3) stretching simultaneously in both directions equally to equibiaxial stretch of 1.10 (equibiaxial stretch at β_{EB}). The loading paths were repeated five times, and the strain and collagen fiber distribution was obtained for the unloaded state, the strip biaxial state (if applicable), and the equibiaxial state of each cycle.

For uniaxial fiber kinematics testing, all specimens were subjected to a stretch of 1.25 in intervals of 0.05 stretch. The stretch states are referred to as β_i where the subscript **i** indicates the percent strain. Each loading path was performed once, and the collagen fiber distribution was obtained for the unloaded state and at each stretch interval. The transverse axis of the specimens was unconfined and the specimens were permitted to contract laterally. Each stretch state was maintained for one to two minutes prior to obtaining the collagen fiber distribution.

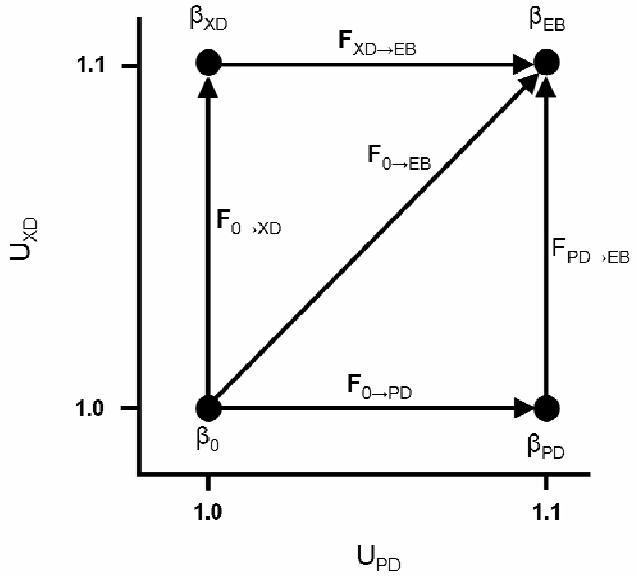

Figure 7-3. Graphical representation of the biaxial stretching protocols utilized. Angular fiber distributions were obtained at β_0 and β_{EB} for each test of each specimen, and at β_{XD} and β_{PD} when strip biaxial stretch was applied.

7.1.4 Strain Analysis

Using the strain tracking data, the in-plane Green's strain tensor **E** was computed as described previously.[235, 236] Briefly, the in-plane deformation gradient tensor **F** was first computed in real time from the marker positions. The Green's strain tensor **E** was then calculated using $\mathbf{E}=\frac{1}{2}(\mathbf{F}^T\mathbf{F} - \mathbf{I})$, where **I** is the identity tensor. The shear angle α was computed from **E** to an accuracy of ±0.1° using

$$\alpha = \sin^{-1}\frac{2E_{12}}{\sqrt{1 + 2E_{11}}\sqrt{1 + 2E_{22}}} \qquad (6\text{-}1).$$

Polar decomposition of the deformation gradient tensor was performed in order to remove small rigid body rotations that occurred during experimentation. The deformation gradient tensor is the product of the right stretch tensor **U** and the rotation matrix **R** as:

$$\mathbf{F} = \mathbf{R}\cdot\mathbf{U} \qquad (6\text{-}2).$$

For ease of comparison, the rotation is presented as the angle of rigid body rotation Θ, which was also calculated from components of **F** using:

$$\Theta = \tan^{-1}\frac{F_{21} - F_{12}}{F_{11} + F_{22}} \qquad (6\text{-}3).$$

Note that the resulting experimentally obtained statistical fiber distributions were shifted back to their actual orientations by the angle Θ. The components of **U** were then used as input for the affine deformation model. The term U_{PD} represents stretch in the preferred fiber direction and U_{XD} represents stretch in the cross-preferred fiber direction. Note that the use of **U** instead of **F** greatly simplified the following formulations with no loss of accuracy, since the rigid body rotations can easily be added back to get actual fiber angles in the deformed state, as done here.

7.1.5 Approach for Modeling Fiber Kinematics

For comparisons between the various loading conditions, it was necessary to determine the statistical distribution function of the angular distribution of collagen fibers, $R(\theta)$, as described previously.[238] $R(\theta)d\theta$ is defined as the fraction of collagen fibers oriented between θ and $\theta + d\theta$ and subjected to the normalization constraint. $R(\theta)$ was determined directly from the mean scattered light distribution $I(\theta)$ for each loading condition for each specimen using

$$R(\theta) = \frac{I(\theta)}{\sum_{i=1}^{180} (I_i(\theta)\Delta\theta)} \qquad (6\text{-}4),$$

where $\Delta\theta = \pi/180$ since $I(\theta)$ is measured in discrete 1° increments.[234] The statistical fiber distribution for the initial unloaded state, $R_0(\theta)$ was then used as input to the affine deformation model.

From the work of Billiar and Sacks,[33] assuming a homogeneous affine deformation with stretch tensor $\mathbf{U}$, the rotation of fibers at an angle θ in the reference (unloaded) state to the angle β in the deformed state is given by [Eq. (20) and (21) from [169]]

$$\cot(\beta) = \frac{U_{11}}{U_{22}}\cot(\theta) + U_{12}\,. \qquad (6\text{-}5)$$

Further assuming that the number of fibers within a differential angular element does not change from the reference state, $d\theta$, to the deformed state, $d\beta$, then $NR(\theta)\, d\theta = NR(\beta)\, d\beta$ where $R_0(\theta)$ is the angular fiber distribution in the reference state and N is the total number of fibers in the region of interest. This gives

$$R'(\beta) = R_0(\theta)\frac{d\theta}{d\beta} \qquad (6\text{-}6).$$

Taking the derivative of Eq. (6-5) and utilizing the general form of the relationships from [Eq. (18) and (21), [169]],

$$U_{11}^2\cos^2\theta + 2U_{11}U_{12}U_{22}\sin\theta\cos\theta + U_{22}^2\left(U_{12}+1\right)\sin^2\theta = U_{22}^2\frac{\sin^2\theta}{\sin^2\beta} \qquad (6\text{-}7),$$

we obtain a function for $\frac{d\theta}{d\beta}$, which can then be substituted in Eq. (6) to obtain a transformation between the initial and the deformed angular fiber distributions that includes the shear term U_{12},

$$R'(\beta) = R_0(\theta)\frac{1}{U_{11}U_{22}}\left(U_{11}^2\cos^2\theta + U_{22}^2\sin^2\theta\right) + \frac{U_{22}U_{12}^2}{U_{11}}\sin^2\theta + U_{12}\sin(2\theta) \qquad (6\text{-}8),$$

where $R'(\beta)$ is the angular fiber distribution in the deformed state as a function of the deformed state angle β. In the case that U_{12} is small (as was the case in the present study), Eq. (6-8) can be reduced to the simplified form

$$R'(\beta) = \frac{R_0(\theta)}{U_{PD}U_{XD}}\cdot\left(U_{PD}^2\cos^2(\theta) + U_{XD}^2\sin^2(\theta)\right) \qquad (6\text{-}9),$$

in which PD of the specimen corresponded to the 11 direction of the specimen, and XD of the specimen corresponded to the 22 direction. β represents the direction θ after deformation and is calculated by [169]

$$\beta = \cot\left(\frac{U_{XD}}{U_{PD}}\tan(\theta)\right) \qquad (6\text{-}10).$$

7.1.6 Statistics

The correlation, r^2, of the predicted angular fiber distribution from the affine model compared to the experimental data was assessed by calculating the ratio of the mean square error (MSE) to the variance of the experimental data. To determine the MSE, $R'(\beta)$ was first interpolated to obtain the affine transformation in terms of θ and is referred to as $R'(\theta)$. The MSE was obtained by dividing the total sum of squares of the normalized intensity residuals between the experimentally determined deformed statistical fiber distribution, $R_D(\theta)$, and the interpolated affine transformation, $R'(\theta)$, by the number of measurements, n, where n = 180 for the current experiments:

$$MSE = \frac{\sum_{i=1}^{180}(R_D(\theta_i)-R'(\theta_i))^2}{n} \qquad (6\text{-}11).$$

The correlation, r^2, was then calculated as

$$r^2 = 1 - \frac{MSE}{Var\, R_D(\theta)} \qquad (6\text{-}12).$$

To evaluate statistical significance of changes in the NOI, shear angle, and rigid body rotation, the one-way ANOVA with multiple comparisons was used at significance level of p = 0.05. For the comparison of NOI, a one-tail test was used for uniaxial and strip biaxial stretch, and a two-tail test was used for equibiaxial stretch.

7.1.7 Biaxial Fiber Kinematics Results

The experimental test system was able to precisely apply biaxial stretch regimens to β_{PD}, β_{XD}, and β_{EB}, and uniaxial stretches to β_i (Table 7-1). The average NOI for all specimens in the

unloaded configuration was found to be 49.1% ± 3.1%, suggesting that the samples had a moderate degree of alignment. For all biaxial loading conditions, no difference in the collagen fiber distributions was observed with successive cycles of stretch, so all data presented is for the fifth and final application of stretch. It was observed that strip biaxial stretch to $\boldsymbol{\beta_{XD}}$ led to a decrease in the intensity of the angular fiber distribution, which indicates a decrease in collagen fiber alignment (Figure 7-4A). The NOI of 45.6% ± 3.7%, was significantly less than that for the unloaded condition ($p<0.05$), with a ΔNOI between the unloaded condition and that for strip biaxial load in the XD of -2.9% ± 1.0% (Table 7-2). In contrast, it was found that 10% strip biaxial stretch to $\boldsymbol{\beta_{PD}}$ led to an increase in fiber alignment in the preferred fiber direction as indicated by an increase in the maximum intensity for $R_{PD}(\theta)$ (Figure 7-5A). The NOI for specimens subjected to strip biaxial stretch in the PD was 51.2% ± 3.1%, which is statistically greater than the NOI obtained for the unloaded specimens ($p<0.05$). The ΔNOI for specimens under this loading condition was 2.7% ± 1.8% (Table 7-2). Due to variability in the PD from specimen to specimen, the preferred collagen fiber direction of the specimen did not always coincide with the direction of stretch. However, it was observed that the PD of the specimen shifted toward the direction of stretch by 7.2° ± 5.7°. For strip biaxial stretch in either PD or XD, the affine deformation model yielded predictions with high correlation to the experimentally derived angular fiber distributions. The average r^2 value for strip biaxial stretch in the PD and XD were found to be 0.984 ± 0.016 and 0.987 ± 0.009, respectively (Table 7-3). The affine prediction, $R'(\beta_{XD})$, for strip biaxial stretch in the XD (Figure 7-4A) showed a decrease in the intensity of the distribution that had a similar shape to the experimental data. Likewise, the affine prediction for strip biaxial stretch along the PD, $R'(\beta_{PD})$, showed a distribution that compared well to the shape of the experimentally determined collagen fiber distribution (Figure 7-5A).

When the specimens were stretched to $\boldsymbol{\beta_{EB}}$ under equibiaxial stretch, no statistical difference was observed between the angular fiber distributions for equibiaxial stretch condition and the initial unloaded condition ($p=0.31$). The NOI for 10% equibiaxial stretch was found to be 49.2% ± 5.3% with a ΔNOI of 0.3% ± 1.8% (Table 7-2). Fig. 6-6 shows a set of typical statistical distribution functions for one specimen loaded to β_{EB} under 10% equibiaxial stretch. Similarly, no statistical differences were detected between the NOI for unloaded specimens and specimens subjected to 10% equibiaxial stretch subsequent to a 10% strip biaxial stretch in either

the XD or PD (48.3% ± 3.6% and 49.7% ± 3.6%, respectively) (Table 7-2). The angular fiber distributions for these loading conditions are shown in Figure 7-4B and Figure 7-5B, respectively. Affine deformation fiber kinematics predicted the changes in the collagen fiber distribution with high correlation for 10% equibiaxial stretch. The average r^2 value was found to be 0.982 ± 0.020 (Table 7-3). Representative predictions for each condition (shown in Figure 7-4, Figure 7-5, and Figure 7-6) show that the affine predictions match the shape and intensity of the experimental data well.

7.1.8 Uniaxial Fiber Kinematics Results

For the uniaxially tested specimens, the initial NOI for all samples was found to be 51.3% ± 3.8% in the initial unloaded configuration. For samples stretched along the PD, the NOI tended to increase, and became significantly greater than the initial NOI at a stretch of 1.15 ($p<0.05$) (Table 7-2). The maximum NOI was found to be 58.3% ± 2.3% at a stretch level of $\lambda = 1.25$, with a ΔNOI of 7.8% ± 2.7%. The NOI and ΔNOI for each stretch interval is presented in Table 2. Due to the variability of the specimens, it was found that the PD deviated from the stretch direction by up to 12°. The PD tended to shift and was found to be aligned with the direction of stretch after the sample had been subjected to 10% stretch (Figure 7-7A).

When the samples were stretched along the XD, the fiber kinematics differed substantially. At a stretch up to 1.15, the NOI was found to be significantly less than that observed for the unloaded condition ($p<0.05$). However, when subjected to stretches of 1.20 or greater, no significant differences were found between the NOI for the unloaded and loaded conditions (Table 7-2). In addition, a dramatic shift in the PD was observed. Since the sample was prepared such that the long axis of the sample corresponded to the XD, the initial deviation of the PD from the stretch direction was large (70° ± 8.9°). However, it was observed that the PD of the specimens had shifted towards the stretch direction by a stretch of 1.15 (Figure 7-8A).

The affine deformation model did not provide a good prediction of the change in the collagen fiber orientation when the samples were subjected to uniaxial stretch in either the PD or XD (Table 7-3). The predictions for stretch in the PD were good for low strain with an $r^2 = 0.985 \pm 0.011$ for a stretch of 1.05, but the predictions became progressively worse with increased stretch to an $r^2 = 0.667 \pm 0.100$ for a stretch of 1.25. The r^2 value for stretch in the XD

was 0.880 ± 0.180 for a stretch of 1.05 and progressively decreased to 0.309 ± 0.230 for a stretch of 1.25. Representative predictions for stretch in the PD and XD at a stretch of 1.25 are shown in Figure 7-7B and Figure 7-8B, respectively.

7.1.9 Shear and Rigid Body Rotations

The shear angle α was found to be 2.3° ± 1.7° for the 10% equibiaxial stretch of the specimens oriented with the preferred fiber alignment. The shear angle was quite small regardless of the orientation of the specimens, which indicated that the assumption for the affine deformation model of negligible shear was appropriate for this study. The shear angle was also found to be small for both uniaxial stretching conditions with values of α = 3.8° ± 2.6° for stretch in the PD and 1.9° ± 1.6° for stretch in XD. The rigid body rotations Θ were found to be 2.4° ± 1.2°, 2.3° ± 1.0°, and 1.8° ± 0.9° for equibiaxial stretch, strip biaxial stretch in the PD, and strip biaxial in the XD, respectively. None of these values were statistically different from zero ($p>0.05$). Uniaxial stretch likewise caused only small rigid body rotations with Θ = 1.7° ± 0.8° for stretch in the PD and 0.5° ± 0.4° for stretch in the XD. None of the values for α or Θ were found to be statistically different from zero ($p >0.05$).

7.1.10 Summary of Current Experimental Approach and Findings

The current study used a testing system which incorporated SALS measurements and strain tracking to obtain fiber kinematics of SIS-ECM under a number of uniaxial and biaxial strain paths. A novel aspect of this experimental design was the ability to obtain real-time fiber kinematics by taking advantage of the natural translucency of SIS-ECM that has been lyophilized and then rehydrated in PBS. To limit the complexity of the hardware, the system was designed to operate such that stretch-scan steps were required, however it can be envisioned that the entire system could be automated.

The results of this study demonstrated that strip biaxial stretch in the preferred fiber direction (U_{PD}:U_{XD} = 1.10:1.00) led to an increase in the collagen fiber alignment, while strip biaxial stretch in the cross-preferred fiber direction (U_{PD}:U_{XD} = 1.00:1.10) yielded a decrease in

collagen fiber alignment. Equibiaxial stretch (U_{PD}:U_{XD} =1.10:1.10) did not substantially change the fiber distribution compared to the initial unloaded configuration. Moreover, all three paths to β_{EB} resulted in collagen fiber distributions that were not statistically different from the initial unloaded distribution for that specimen. Differences in the collagen fiber distribution in response to different strain paths to the same deformation state would imply path dependency due to reorientation of the collagen fibers, a hypoelastic response. Therefore, SIS-ECM exhibits hyperelastic behavior.[70, 71, 92] For all biaxial strain paths, the change in the fiber distribution was able to be modeled with an affine deformation model with high correlation ($r^2 > 0.98$).

Under uniaxial stretch in the PD, the collagen fiber distributions initially rotated towards the direction of stretch with a progressive increase in the collagen fiber alignment. The affine deformation model tended to predict distributions that were much more aligned than those obtained experimentally. This lack of correlation may have been due to interconnectivity between the fibers. Stretch in the XD led to an initial decrease in collagen fiber alignment followed by a subsequent increase in alignment to that observed in the unloaded condition, and the preferred fiber direction changed by up to 70° to align with the direction of stretch. Similar large "ensemble" rotations of a collagen fiber population have been observed in bovine pericardium under strip biaxial stretch levels of 1.00:1.30.[33] The changes in the collagen fiber distribution under uniaxial stretch in the XD could not be modeled using an affine deformation model due to the large apparent fiber rotations observed.

7.1.11 Comparison to Previous Studies

In a previous study,[103] the affine deformation model corresponded well to the fiber kinematics for native SIS under equibiaxial stretch of U_{PD}:U_{XD} = 1.12:1.12 and strip biaxial stretch of U_{PD}:U_{XD} = 1.30:1.00. However, strip biaxial stretch levels of U_{PD}:U_{XD} = 1.00:1.30 led to separation of the population into a dual-fiber distribution due to the presence of two subpopulations of collagen fibers which are oriented at approximately ± 30° from the PD,[237] and could not be modeled with the affine deformation theory. The differences in fiber kinematics and attainable strains are likely attributable to the preparation of the specimens. In the earlier study, native untreated SIS-ECM was analyzed while in the current study, the SIS-ECM was treated with 0.1% PAA to disinfect and decellularize the material, lyophilized for storage, and

terminally sterilized with EtO. The additional processing was done to mimic the methods used to manufacture a device composed of SIS-ECM that is clinically available (i.e. Oasis®, Cook Biotech). PAA treatment has been associated with the formation of dityrosine and disulfide crosslinks due to its reactivity with oxygen-free radicals,[45, 200, 283] which may alter collagen fiber motility. Furthermore, in response to uniaxial tensile testing of ECM scaffolds, material that had been lyophilized and rehydrated tended to have an ultimate strain that was ~2/3 of that measured for hydrated material.[91]

7.1.12 Limitations

A limitation of the current study is that the maximum biaxial stretch that could be consistently applied was only 10% equibiaxial stretch, which was a consideration in the investigation of larger uniaxial strains. However, this range of stretch represents the most likely level of stretch that the material will be subjected to *in vivo*. The strains observed during normal motion for the rotator cuff and Achilles tendon, which are two of the most common sites treated with SIS clinically, are reported to be in the range of 1-5%,[31, 85, 188, 230] with failure strain of the Achilles tendon midsubstance reported to be approximately 10%.[291] Furthermore, early after surgical implantation, the patient is generally limited only to passive range of motion exercises or controlled loading conditions.

An additional limitation was the single application of stretch for the uniaxial stretch experiments. The choice not to precondition the specimen was based on the inability to repeatedly apply high magnitudes of stretch to the scaffold without causing damage to the scaffold. Furthermore, over five cycles of 10% equibiaxial stretch, no differences were observed in the deformed collagen fiber distributions. However, it is possible that the lack of preconditioning may have lead to a lack of reproducibility of the results.

7.1.13 Applications

The results of this study may prove useful in designing mechanical conditioning protocols to guide remodeling of SIS-ECM *in vitro* to develop scaffolds that are better suited for tissue specific repairs, such as tendons and ligaments. These protocols must be designed with

appropriate magnitudes of stretch for specific types of ECM scaffolds as the fiber architectures and kinematics can vary greatly. Based on this study, it is evident that stretch along the PD could lead to remodeling of the scaffold such that the collagen fibers could become more aligned. It is still unknown how strain applied to collagen fibers within a naturally derived ECM scaffold is transferred to cells, which will ultimately determine the cellular response with regard to cell differentiation and tissue remodeling.[217, 296] For *in vivo* applications it has been demonstrated that SIS-ECM is completely resorbed by 3 months after implantation in a dog model,[229] with up to 40% of the mass loss occurring in the first two weeks. Thus, fiber kinematics of an implant is likely to change very quickly after surgery. However, the initial fiber kinematics is an important consideration for designing the initial strength of the material. By applying a prescribed stretch to SIS-ECM during the manufacturing of lyophilized or multilaminate devices, the mechanical behavior of the device could be modified.

A primary goal of the present study was to verify that the affine fiber kinematics model was valid for SIS-ECM under all relevant strain paths, so that fiber orientation data can be used to develop a structural model of SIS-ECM.[238] Such a model could be used to predict the loading environment to which cells are exposed in the initial phase of migration into the scaffold for a variety of implantation sites. A structural constitutive model would also be beneficial in the design of devices made from SIS-ECM for site specific tissue repair. Results of the present study suggest that the affine model is appropriate for biaxial deformations within the strains applied. However, based on the current results for uniaxial deformations, a non-affine approach that incorporates collagen fiber bending or variations in crosslinking density may have to be utilized to obtain a complete prediction of SIS-ECM fiber kinematics under large strains.[4, 27, 56, 73, 113, 114]

Table 7-1. Components of the stretch tensor obtained for each biaxial and uniaxial stretch conditions.

		PD		XD		EB	
		U_{PD}	U_{XD}	U_{PD}	U_{XD}	U_{PD}	U_{XD}
Biaxial	β_0	1.001	1.002	1.001	1.001	1.000	1.000
	β_{PD}	1.100	1.002				
	β_{XD}			1.004	1.103		
	β_{EB}	1.103	1.102	1.102	1.102	1.102	1.101
Uniaxial	β_0	1.000	1.002	1.000	1.000		
	β_5	1.053	0.948	0.936	1.052		
	β_{10}	1.105	0.856	0.841	1.103		
	β_{15}	1.152	0.768	0.761	1.151		
	β_{20}	1.203	0.667	0.692	1.200		
	β_{25}	1.253	0.604	0.651	1.248		

Table 7-2. Normalized Orientation Index (NOI) for biaxial and uniaxial stretch conditions and the ΔNOI relative to the initial unloaded condition. Statistical significance relative to the unloaded NOI. († $p < 0.05$)

		PD		XD		EB	
		NOI	**ΔNOI**	**NOI**	**ΔNOI**	**NOI**	**ΔNOI**
Biaxial	β_{PD}	51.2% ± 3.1% †	2.7% ± 1.8%			49.7% ± 3.4%	0.0% ± 1.9%
	β_{XD}			45.6% ± 3.7% †	-2.9% ± 1.0%	48.3% ± 3.6%	-0.4% ± 1.3%
	β_{EB}					49.2% ± 5.3%	0.3% ± 1.8%
Uniaxial	β_{0}	49.8% ± 4.0%		53.1% ± 2.1%			
	β_{5}	52.0% ± 4.0%	2.2% ± 4.2%	45.8% ± 4.3% †	-6.9% ± 3.2%		
	β_{10}	54.7% ± 3.1%	4.9% ± 3.8%	48.0% ± 4.8% †	-5.1% ± 3.2%		
	β_{15}	57.1% ± 3.7% †	7.3% ± 3.2%	46.7% ± 6.7% †	-6.4% ± 4.9%		
	β_{20}	57.6% ± 2.5% †	7.8% ± 1.8%	48.2% ± 6.5%	-4.9% ± 5.2%		
	β_{25}	58.3% ± 2.3% †	7.8% ± 2.7%	48.6% ± 9.4%	-4.7% ± 10.8%		

Table 7-3. Correlation coefficients for the affine transformation predictions of collagen fiber distributions for uniaxial, strip biaxial, and equibiaxial stretch.

		PD	XD	EB
Biaxial	β_{PD}	0.984 ± 0.016		0.981 ± 0.022
	β_{XD}		0.987 ± 0.009	0.989 ± 0.007
	β_{EB}			0.983 ± 0.018
Uniaxial	β_{5}	0.985 ± 0.011	0.880 ± 0.180	
	β_{10}	0.964 ± 0.018	0.750 ± 0.225	
	β_{15}	0.908 ± 0.036	0.692 ± 0.207	
	β_{20}	0.717 ± 0.144	0.520 ± 0.289	
	β_{25}	0.667 ± 0.100	0.309 ± 0.230	

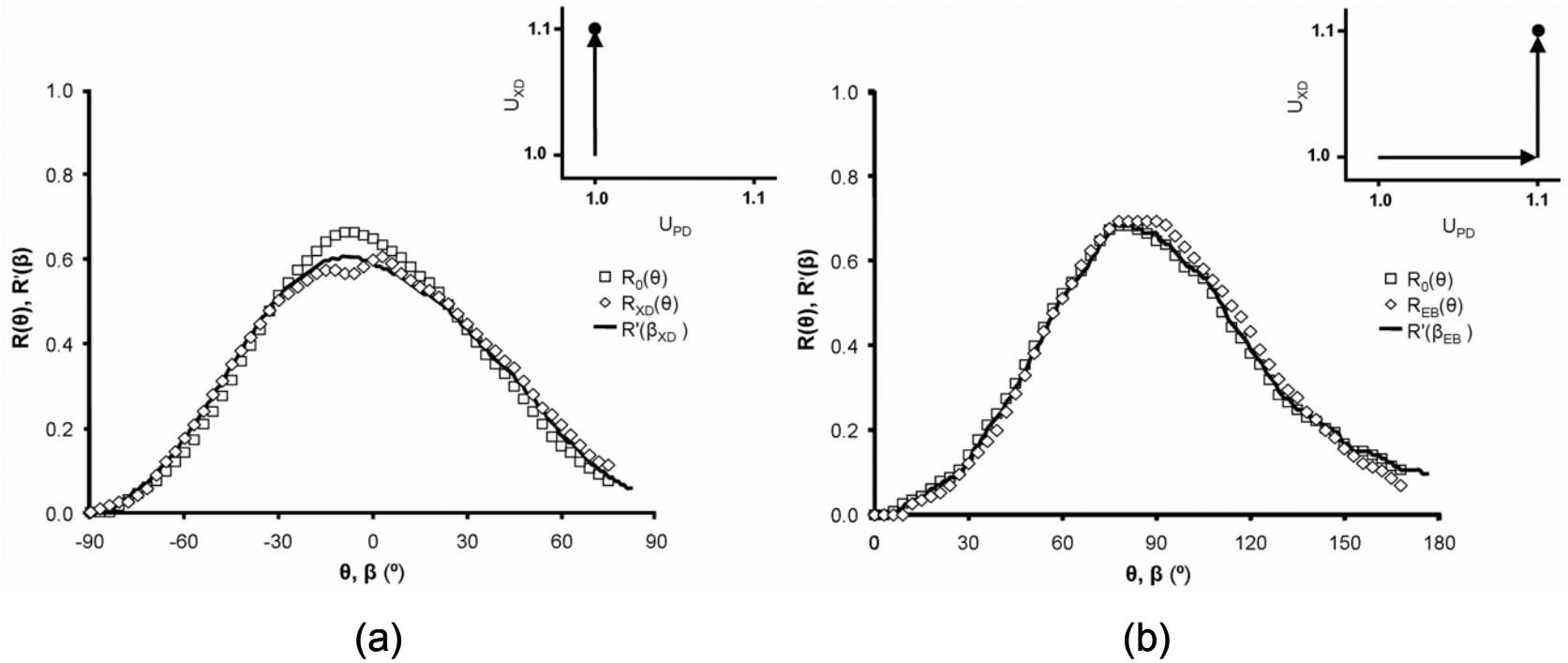

Figure 7-4. Representative statistical distribution functions of the angular distribution of collagen fibers for specimens subjected to A) 10% strip biaxial stretch along the XD and then to B) 10% equibiaxial stretch. The initial collagen fiber distribution is represented as $R(\theta)$, the collagen fiber distribution for strip biaxial stretch in the XD is represented as $R_{XD}(\theta)$, and the collagen fiber distribution for equibiaxial stretch is represented as $R_{EB}(\theta)$. Strip biaxial stretch along the XD led to a widening of the collagen fiber distribution as indicated by the decrease in normalized intensity. The average change in normalized orientation index was -2.9% ± 1.0%. The prediction of the deformed statistical fiber distributions, $R'(\beta_{XD})$ and $R'(\beta_{EB})$, are also shown in each graph. The predicted distribution accurately predicted the results observed experimentally.

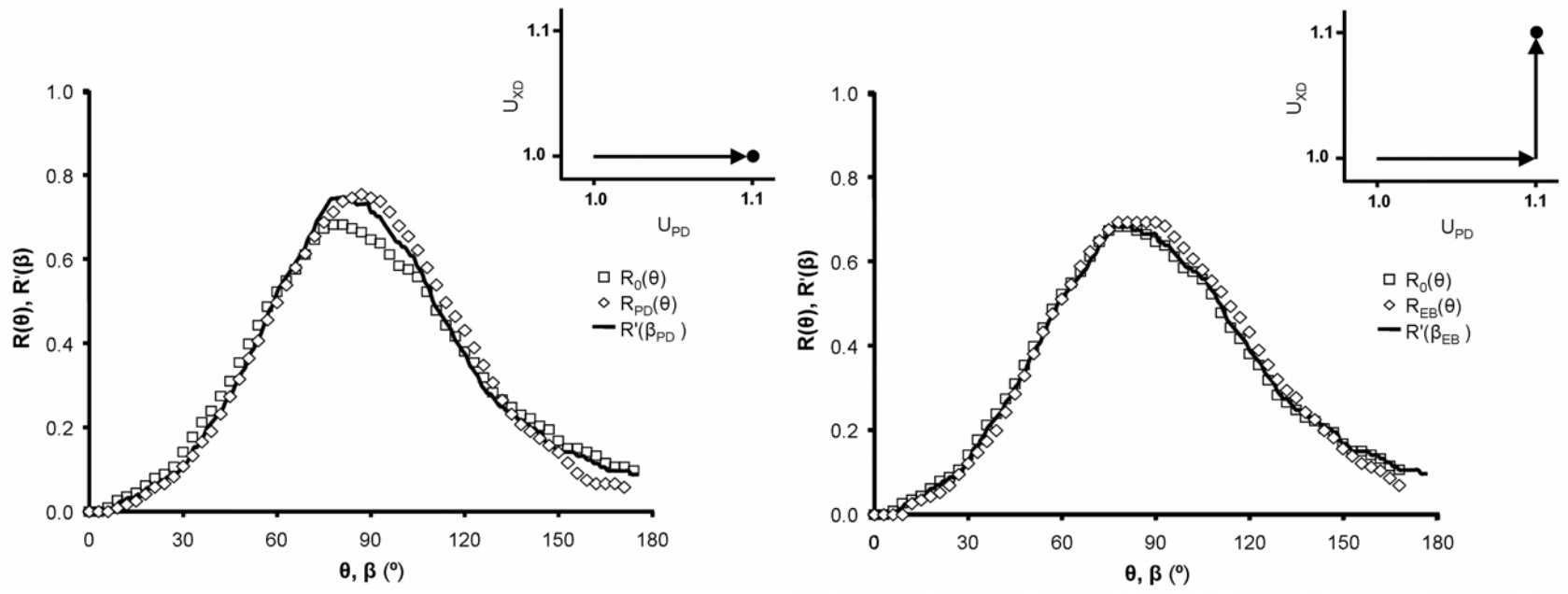

Figure 7-5. Representative statistical distribution functions of the angular distribution of collagen fibers for specimens subjected to A) 10% strip biaxial stretch along the preferred fiber direction and then to B) 10% equibiaxial stretch. The initial collagen fiber distribution is represented as $R(\theta)$, the collagen fiber distribution for strip biaxial stretch in the PD is represented as $R_{PD}(\theta)$, and the collagen fiber distribution for equibiaxial stretch is represented as $R_{EB}(\theta)$. Strip biaxial stretch of 10% in the PD led to an increase in the collagen fiber alignment as indicated by the increase in normalized intensity. The average change in normalized orientation index was 2.7% ± 1.8%. The prediction of the deformed statistical fiber distributions, $R'(\beta_{PD})$ and $R'(\beta_{EB})$, are also shown in each graph. The predicted distribution accurately predicted the results observed experimentally.

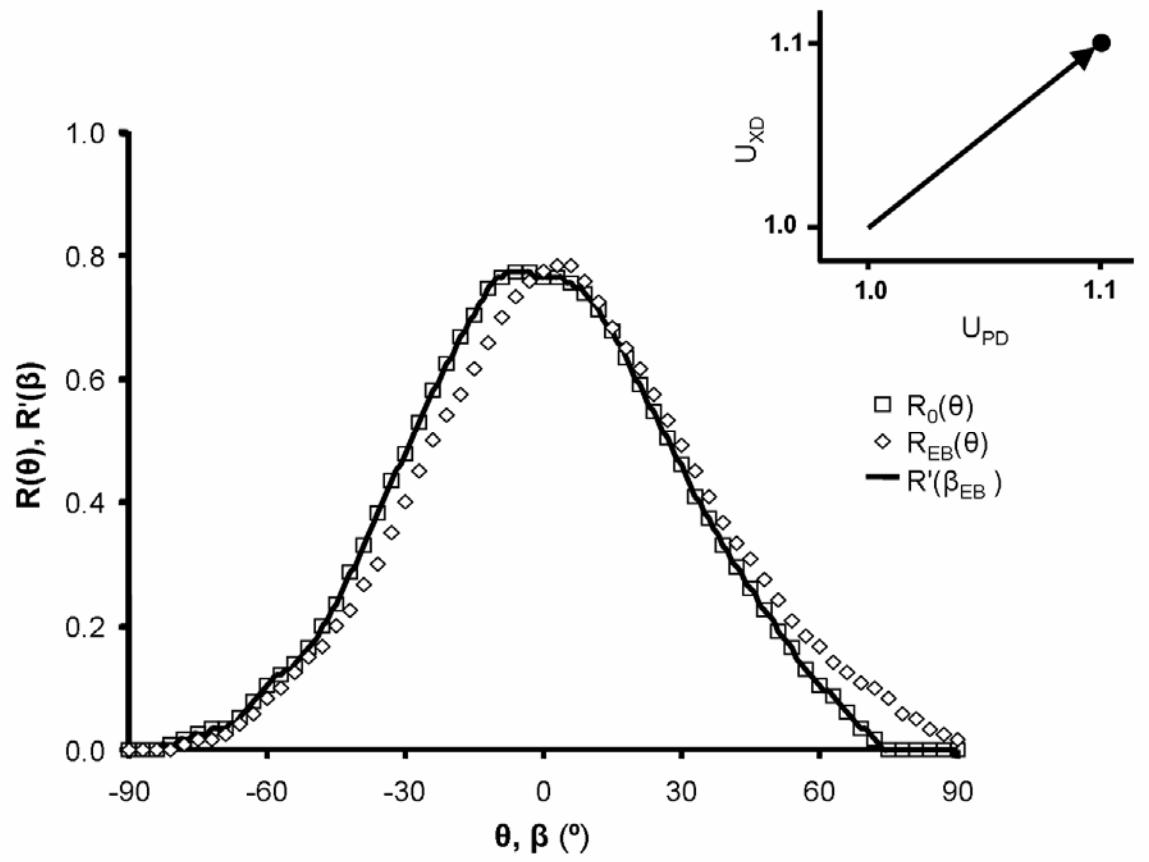

Figure 7-6. Representative statistical distribution functions of the angular distribution of collagen fibers for specimens subjected to 10% equbiaxial stretch. The initial collagen fiber distribution is represented as $R(\theta)$ and the collagen fiber distribution for equibiaxial stretch is represented as $R_{EB}(\theta)$. No detectable change in the collagen fiber distribution was observed. The average change in normalized orientation index was 0.3% ± 1.8%. %. The prediction of the deformed statistical fiber distribution, $R'(\beta_{EB})$, is also shown in the graph. The predicted distribution accurately predicted the results observed experimentally.

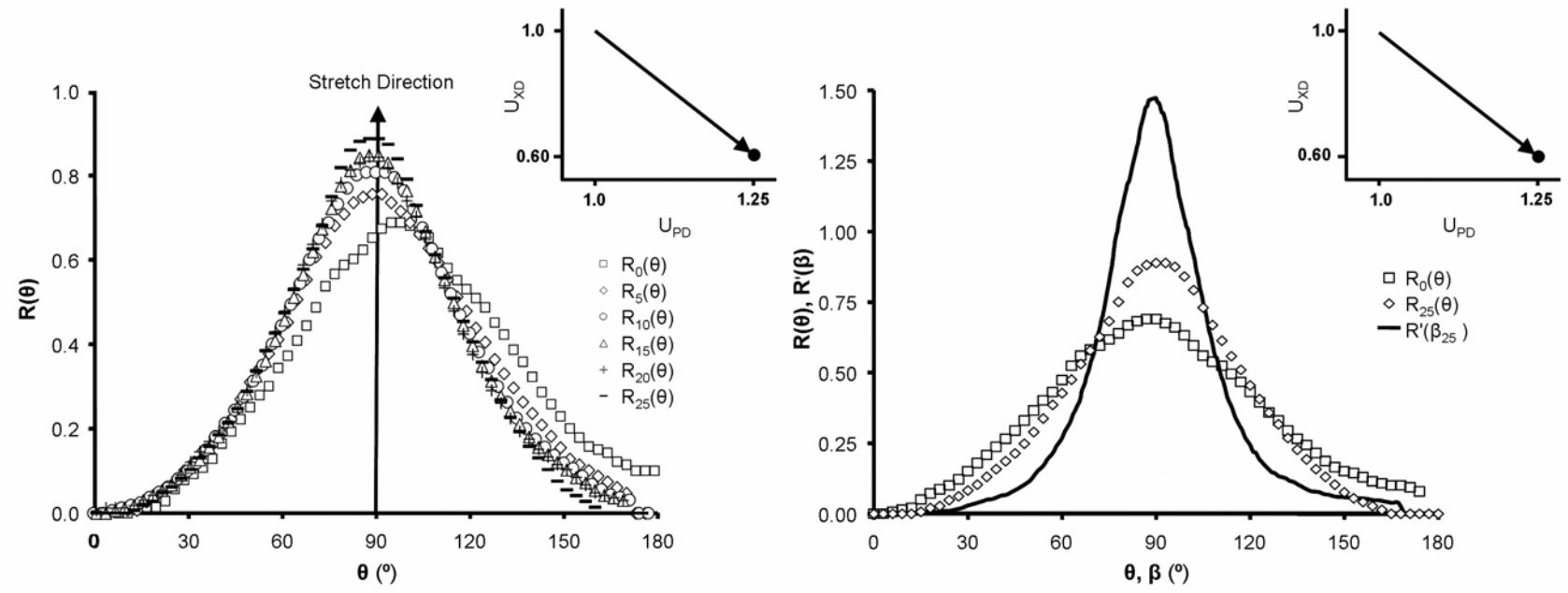

Figure 7-7. Representative statistical distribution functions of the angular distribution of collagen fibers for specimens subjected to increasing magnitudes of uniaxial stretch up to 25% the PD. The initial collagen fiber distribution is represented as $R(\theta)$ and the deformed collagen fiber distributions are represented as $R_5(\theta)$, $R_{10}(\theta)$, $R_{15}(\theta)$, $R_{20}(\theta)$, and $R_{25}(\theta)$, where the subscript indicates the percentage of uniaxial stretch. A) The distribution tends to become more aligned and shifts toward the direction of stretch. B) The prediction of the deformed statistical fiber distribution at 25% stretch, $R'(\beta_{25})$, is also shown. The predicted distribution predicted a degree of alignment much greater than that observed experimentally.

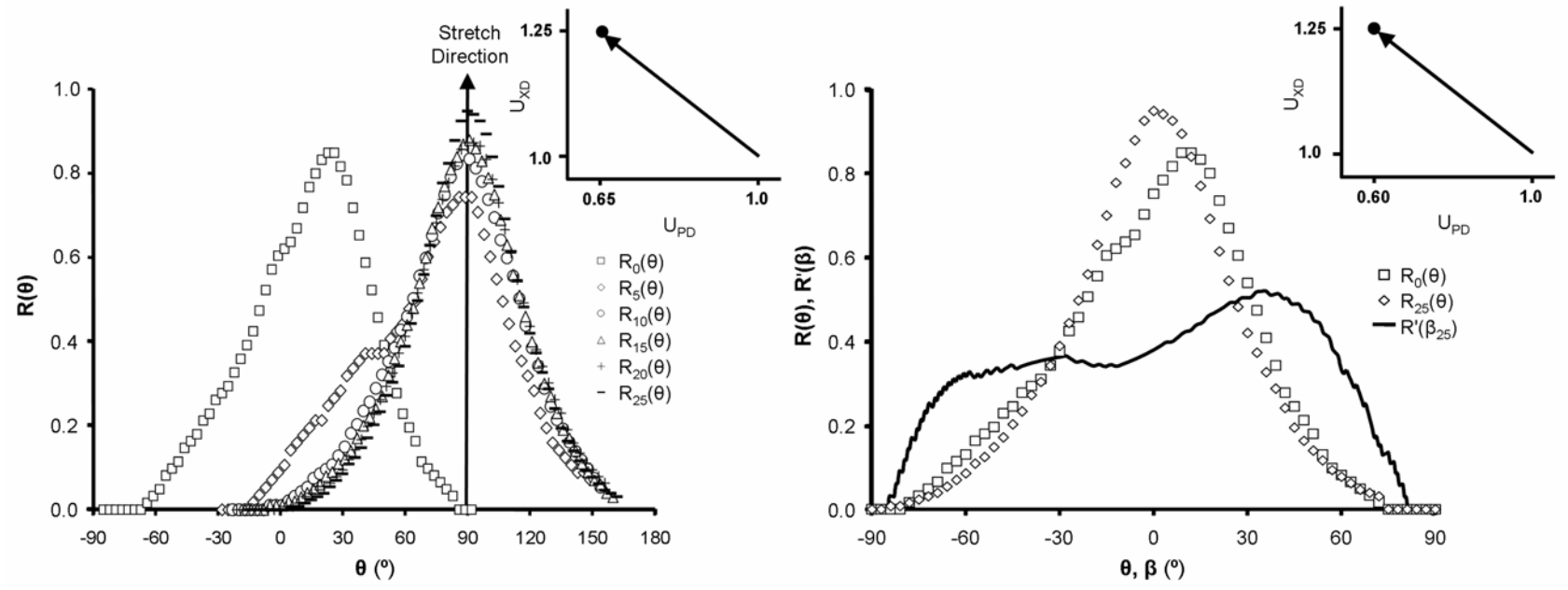

Figure 7-8. Representative statistical distribution functions of the angular distribution of collagen fibers for specimens subjected to increasing magnitudes of uniaxial stretch up to 25% the XD. The initial collagen fiber distribution is represented as $R(\theta)$ and the deformed collagen fiber distributions are represented as $R_5(\theta)$, $R_{10}(\theta)$, $R_{15}(\theta)$, $R_{20}(\theta)$, and $R_{25}(\theta)$, where the subscript indicates the percentage of uniaxial stretch. A) A dramatic shift in the preferred fiber orientation towards the stretching direction was observed, while the degree of orientation initially decreased and then tended to approach the NOI for the unloaded condition. B) The prediction of the deformed statistical fiber distribution at 25% stretch, $R'(\beta_{25})$, is also shown. The predicted distribution did not accurately predict the rotation or degree of alignment observed experimentally.

7.2 GENE EXPRESSION BY FIBROBLASTS SEEDED ON SIS-ECM SUBJECTED TO CYCLIC STRETCHING

A number of *in vitro* models have been developed to study the basic interactions between cells and ECM in response to mechanical loading have shown that static and dynamic uniaxial tensile loading leads to regulation of matrix synthesis by cells,[127, 166, 220, 221] increased alignment of fibroblasts and collagen fibers in the direction of stretch,[80, 127] and enhanced mechanical properties of the scaffold.[127, 147] The response of cells seeded on SIS-ECM to mechanical loading may more closely mimic the *in vivo* condition as compared to cells seeded on a purified collagen matrix because SIS-ECM retains its native 3-D tissue architecture[98, 103, 237] and has a diverse biochemical composition including active growth factors, glycosaminoglycans, and fibronectin. [118, 120, 122, 274] Therefore, the research question was whether the response of fibroblasts seeded on SIS-ECM to mechanical loading *in vitro* alters the expression of various matrix related genes in such a way that would be predictive of the constructive remodeling response observed *in vivo*.

The first objective of the present study was to investigate the changes in the gene expression of fibroblasts seeded on an SIS-ECM scaffold and subjected to cyclic mechanical loading regimens (5%, 10%, and 15% @ 0.1 Hz, 0.3 Hz, and 0.5 Hz). The matrix related genes of interest were Col I, collagen III (Col III), SMA, TN-C, matrix metalloprotease-2 (MMP-2), MMP-9, TGF-β_1, and TGF-β_3. It was hypothesized that the changes in expression of these genes will be consistent with a constructive remodeling response, specifically increased collagen expression, increased expression of TN-C and SMA, moderated expression of MMP-2 and MMP-9, and increased expression of TGF-β_1 and TGF-β_3.

The second objective of the present study was to determine the changes in the mechanical behavior of the SIS-ECM scaffold during the course of the stretching experiment and attempt to correlate these changes with the gene expression patterns noted above. The combined objectives of characterizing changes in the gene expression of cells on a scaffold and changes in the mechanical behavior of the scaffold required the development of a Cyclic Stretching Tissue Culture (CSTC) System with the capabilities of **1)** operation in a cell culture environment (i.e.,

maintaining cell viability without contamination) for extended periods of time, **2)** application of precise displacement waveforms to the scaffold, and **3)** continuous measurement of the load within the scaffold. Development of the CSTC System was necessary so that load in each scaffold could be monitored independently. This allowed for the application of identical preloads to each scaffold to reduce the effects of scaffold to scaffold variability. Furthermore, it allowed for application of different magnitudes and frequencies of stretch to different scaffold simultaneously, thereby reducing the effects of cell preparation on separate experiments.

7.2.1 Development of the Cyclic Stretching Tissue Culture System

The CSTC system specifically developed for this study consisted of eight independently operating stations. (Figure 7-9) Each station consisted of a culture chamber, tissue clamps, a linear actuator, and a load cell. Components were made from stainless steel and polycarbonate to allow sterilization and operation in a standard cell culture incubator for extended periods of time (days to weeks) without corrosion. The bottleneck of a vented culture flask was fixed to the culture chamber to allow for gas exchange and aspiration of media.[168] Tissue clamps with sinusoidal grips to limit slippage were connected to shafts that passed through the culture chamber walls to attach to the linear actuator and the load cell. Self aligning connectors allowed for removal of the chamber from the incubator.

The linear actuator (HSI, Inc., Waterbury, CT, Series 43000, Captive, Size 17) had a travel of 25.4 mm. A miniature submersible load cell (Sensotec, Columbus, OH, Model 31, range 0-10 lb.) was chosen to monitor loads in the humidified environment. To control the motors and monitor loads, custom LabVIEW virtual instruments (VIs) were created to work in concert with a four axis stepper motor drive (National Instruments (NI), Austin, TX, MID-7604) that received signals from a motion control card (NI, PCI-7334), and an analog to digital data acquisition card (NI, PCI-6023E).[218] These programs allowed the user to apply a preload to each sample independently, define the displacement profile, temporarily suspend operation for aspiration of the media, and process the data.

The CSTC system has been in operation in a standard culture environment for a period of 24 months without corrosion. Stretching experiments have been conducted for up to 4 weeks with media changes every three days and no evidence of bacterial or fungal contamination. The

testing system was shown to accurately control linear displacement and monitor load. Displacements were found to be accurate and repeatable within 0.02 mm. With the overall displacements to be in a range of 2-6 mm, the repeatability has been within 1%. Using a spring with a known spring constant of 0.42 ± 0.04 N/mm, the system yielded a calculated spring constant of 0.41 ± 0.01 N/mm ($R^2 > 0.99$) following cyclic stretching for 72 hours.

7.2.2 Methodology for Cyclic Stretching Experiments

Porcine small intestine was harvested from market weight pigs (~110-130kg) immediately after euthanasia. After rinsing, the tunica muscularis externa and the majority of the tunica mucosa were removed. The remaining tunica submucosa and basilar portion of the tunica mucosa consisted of extracellular matrix and the constituent cells. The SIS-ECM was then disinfected and decellularized in a 0.1% PAA/4% ethanol solution followed by two rinses each in phosphate buffered saline and deionized water. This process yielded an acellular material, which was then lyophilized and terminally sterilized with EtO.

Thirty SIS-ECM scaffolds were rehydrated in Dulbecco's Modified Eagle Medium (Invitrogen, Life Technologies, Carlsbad, CA) supplemented with 10% bovine calf serum (HyClone, Logan, UT) and 1% penicillin/streptomycin (Invitrogen, Life Technologies) (DMEM-CS) and cut into dog bone shaped specimens (Length: Width; 4.0 cm:0.8 cm). The long axis of the specimen corresponded to the longitudinal axis of the small intestine, which has been shown to be the direction of preferred collagen fiber alignment.[237]

All cell culture was performed at 37°C in a humidified incubator with 5% CO_2. Each specimen was seeded with $1.6x10^6$ NIH 3T3 fibroblasts ($0.5x10^6$ cells/cm^2) (ATCC, Manassas, VA) and 8 hours were allowed for cell attachment. NIH 3T3 fibroblasts as opposed to a primary cell line because it was expected that an immortalized cell line would yield more repeatable results, minimizing the variability of the experiments. The cell seeded scaffolds were transferred to the individual stations of the CSTC system, where they were allowed to acclimate in DMEM-CS plus 50μg/ml ascorbic acid (Sigma-Aldrich, Inc., St. Louis, MO) (DMEM-AA) for 36-40 hours prior to stretching. After the acclimation period, the media was aspirated and fresh DMEM-AA was added to the specimens. For all specimens, a 0.05N preload was applied to establish the zero position. The scaffolds to be subjected to cyclic stretch were elongated to

baseline stretch of 2.5%. Cyclic stretching regimens were then applied to 5%, 10%, or 15% stretch at 0.1 Hz, 0.3 Hz, and 0.5 Hz for 20 minutes, 3 times daily at 8 hour intervals for 3 days. The frequency of stretch generally mimicked the frequency of stretch during normal walking,[202] and the magnitude of stretch was based on a study of the fiber kinematics of SIS-ECM in which 5% uniaxial stretch caused rotation of collagen fiber towards the direction of stretch while 10% and 15% stretch increased the degree of alignment.[98] Three SIS-ECM/cell constructs were subjected to each stretch regimen. The cyclic load elongation data was obtained throughout the stretching period at a frequency of 10 Hz. Elongation of the scaffold occurred as a result of cyclic stretching; therefore the specimens were returned to their zero configurations and the 0.05N preload was reapplied at the end of each 24 hour period. The displacement required to reach the preload was recorded. The stiffness for the last 1 mm of elongation was calculated for the 10th cycle during each 20 minute interval. Intermittent stretching and reapplication of the preload was performed based on preliminary studies which showed that continuous cyclic stretching of SIS-ECM led to a load relaxation of approximately 50% within 24 hours.

7.2.3 RNA Isolation and RT-PCR

The cell/scaffold complexes were snap frozen in 350µl of RLT solution from an RNeasy kit (Qiagen, Valencia, CA) and stored at -80°C until needed for further analysis (maximum of two days). After thawing, an additional 350µl of RLT solution was added to the cell/scaffold complex and the suspension was vortexes. The RLT solution was then removed, placed into two QIAshredder spin columns (Qiagen), and centrifuged at >8000 rpm for 2 minutes. RNA was isolated from the flow through from the QIAshredder using an RNeasy kit (Qiagen) per the manufacturer's instructions. The concentrations of the resulting RNA solutions were measured using a spectrophotometer (BioMate 3, Thermo Spectronic, Rochester, NY) at 260nm.

cDNA was synthesized from 1µg total RNA using the Superscript™ First-Strand Synthesis System for RT-PCR (Invitrogen, Life Technologies) per the manufacturer's protocol. Semi-quantitative PCR was performed using the synthesized cDNA and gene primers specific for murine Col I, Col III, SMA, TN-C, MMP-2, MMP-9, TGF-β_1, TGF-β_3 and GAPDH (Table 1) in EasyStart™ Micro100 tubes (Molecular BioProducts, Inc., San Diego, CA). The PCR reactions were performed in an Eppendorf Mastercycler with a typical reaction having the

following parameters: initial five minute denaturation 95°C, a gene specific number of cycles (Table 7-4) consisting of 30 seconds denaturation at 95°C, primer specific annealing temperature (Table 7-4) for 30 seconds, and elongation at 72°C for 1 minute.

The PCR products were separated on a 2% agarose gel, stained with ethidium bromide, visualized on a Kodak Image Station (Kodak, Rochester, NY) equipped with an ultraviolet light and digitally photographed using a 600WB35 filter. Densitometry was performed using the Kodak 1D software. Relative values were determined for each band and analyzed using GAPDH as the internal standard. Examples of the bands obtained for Col I and Col III are shown in Figure 7-11.

7.2.4 Actin Staining

Six additional SIS-ECM scaffolds were seeded with NIH-3T3 fibroblasts and subjected to cyclic mechanical stretching as described above. At the end of the stretching regimen, the specimens were fixed in 2% paraformaldehyde and cell membranes were permeablized with 0.1% Triton X-100 (Spectrum Chemical, Gardena, CA) for 30 minutes. The specimens were then washed with 0.5% bovine serum albumin (BSA) (Sigma-Aldrich, Inc.), and incubated with Phalloidin Alexa 488 (Sigma-Aldrich, Inc.) for 1 hour. The specimens were washed again with 0.5% BSA and stained with Hoechst for 1 minute. The specimens were then viewed with a confocal microscope (FluoView 1000, Olympus, Melville, NY). Stacked digital micrographs were obtained at 40X and 100X and three-dimensional reconstructions were created using MetaMorph software (Molecular Devices, Sunnyvale, CA).

7.2.5 Statistics

Comparisons between the relative expression of each gene for fibroblasts were seeded on SIS without stretch and on TCP were made using a Student t-test with significance set at $p < 0.05$. For determination of the effects of magnitude and frequency of stretch on the gene expression of fibroblasts seeded on SIS and on the stiffness and elongation of the scaffold, a two-way ANOVA was performed with the Tukey *post hoc* analysis using the SAS® statistical software package (SAS Institute Inc., Cary, NC). Again, statistical significance was set at $p < 0.05$.

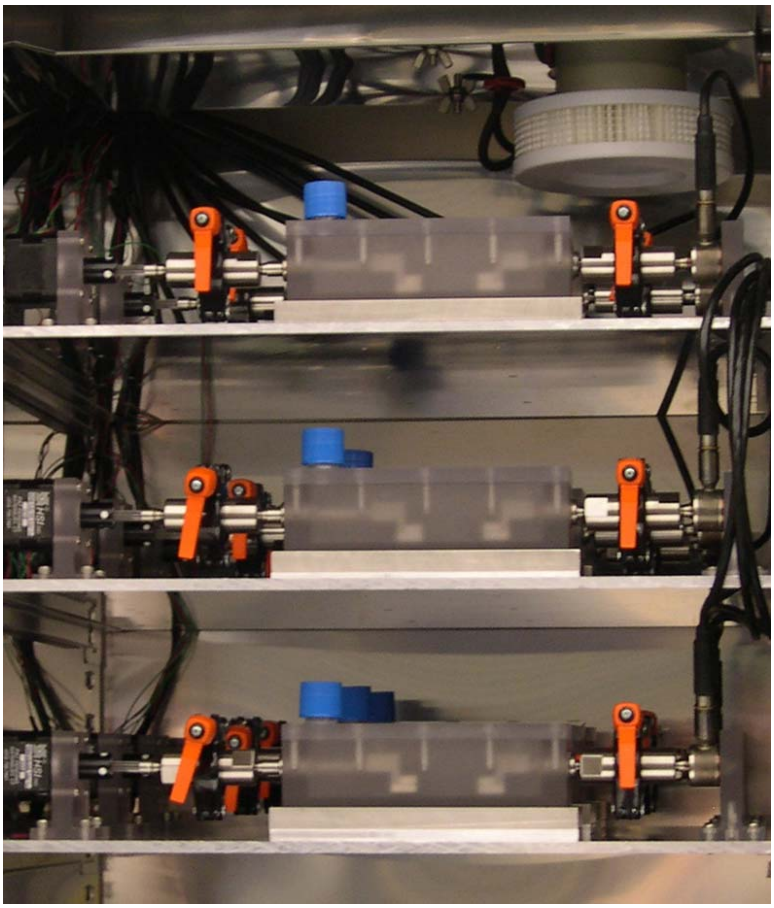

Figure 7-9. Photograph of the 8 station Cyclic Stretching Tissue Culture System. From left to right, each station consists of a linear actuator, sterile stretching chamber with tissue clamps to submerge the scaffold, and a submersible load cell to monitor the load generated by the scaffold. The tissue clamps are connected to the linear actuator and load cell with stainless steel shafts that pass through the wall of the stretching chamber and link to self aligning connectors.

Table 7-4. Sequences for murine specific primer sets and conditions for PCR reaction.

Primer	Sequence (5'-3')	Amplimer Size	Annealing Temperature	Number of Cycles	Reference
GAPDH S GAPDH AS	CGCAACGACCCCTTCATTGACC CGATGAGCCCTTCCACAATGCC	432bp	55°C	35	[174]
Col IA S Col IA AS	CGGGATCCGCCAAGAAGACATCCCTGAAG CGCAAGCTTTCATTGCATTGCACGTCAT	142bp	56°C	40	[174]
Col III S Col III AS	CGCAAGCTTATGCAGCCACCTTGGTCAGTC CGGGATCCAGGCCAGGGTCACCATTTCTC	284bp	60°C	40	[246]
SMA S SMA AS	CGGGATCCAAACAGGAATACGACGAAG CGCAAGCTTCAGGAATGATTTGGAAAGGA	135bp	56°C	40	[246]
TN-C S TN-C AS	CGGATCCGTTTGGAGACCGCAGAGAAGAA CGCAAGCTTTGTCCCCATATCTGCCCATCA	365bp	56°C	40	[211]
MMP-2 S MMP-2 AS	CGCAAGCTTCCTTTTTATGGCTTTCAGCA CGGGATCCCACAGAGTGAGGAGGGGAAC	322bp	64°C	40	[105]
MMP-9 S MMP-9 AS	CGCAAGCTTGCAGACCAAGAGGGTTTTCT CGGGATCCCTGGAAGATGTCGTGTGAGTT	279bp	68°C	55	[105]
TGF-β_1 S TGF-β_1 AS	CGCAAGCTTCTTCAGCTCCACACAGAGAAGAACTG CGGGATCCCACAATCATGTTGGACAACTGGTCC	391bp	68°C	45	[246]
TGF-β_3 S TGF-β_3 AS	GCTCTTCCAGATACTTCGAC AGCAGTTCTCCTCCAGGTTG	439bp	48°C	45	[178]

7.2.6 Fibroblast Survival and Alignment

Cells survived well after seeding on SIS-ECM and exposure to cyclic mechanical loading regimens. A Live/Dead Assay showed that >95% of the cells on the scaffold were alive. Actin staining showed that the fibroblasts responded to the cyclic stretching regimens by aligning along the direction of stretch. It can be seen that the fibroblasts were elongated in the direction of stretch and contained prominent aligned actin filaments (Figure 7-10).

7.2.7 Gene Expression in Response to Cyclic Stretching

Changes in the Col I expression were found to be more dependent on the frequency of stretch than the magnitude. Even though no difference were detected between the expression of Col I at a frequency of 0.1Hz stretch for all magnitudes compared to 0% stretch, the expression was significantly greater in response to cyclic stretch at 0.3 Hz and 0.5 Hz for all magnitudes of stretch. There was a five fold increase in Col I expression at 0.5 Hz and 10% stretch. At each magnitude of stretch, the Col I expression increased in a frequency dependent manner, except for the 15% stretch for which there was no statistical difference between 0.3 Hz and 0.5 Hz (Figure 7-11A & B) (Table 7-5).

The expression of Col III was also found to be primarily dependent on the frequency of stretch, although the expression tended to decrease with increasing frequency and the extent of change was less dramatic. The maximum change observed was approximately a 25% decrease between fibroblasts seeded on SIS-ECM stretched at 0.3Hz compared with no stretch. The only statistically significant differences were between stretching 0.3 Hz compared to both the no stretch condition on SIS-ECM and to stretch at 0.1 Hz (Figure 7-11C & D) (Table 7-5).

SMA expression by fibroblasts seeded on SIS-ECM subjected to stretch at 0.3 Hz and 0.5 Hz approximately doubled as compared to fibroblasts on SIS-ECM without stretch. Statistical significance between the frequency groups were found for every comparison except for no stretch and stretch at 0.1 Hz, although the degree of change between 0.3 Hz and 0.5 Hz was small. Furthermore, all magnitudes of stretch were found to significantly increase the expression of SMA by fibroblasts seeded on SIS (Figure 7-12A) (Table 7-5).

Tn-C expression was significantly decreased in response to cyclic stretching at 0.1 Hz as compared to TN-C expression by cells seeded on SIS-ECM without stretch. Increased frequency then led to increased TN-C expression in a frequency dependent manner. The differences between each frequency of stretch were statistically significant, but the expression at 0.3 Hz and 0.5 Hz stretching were not significantly different from the 0% stretch condition. No significant effects were detected with respect to the magnitude of stretch (Figure 7-12B) (Table 7-5).

The expression of MMP-2 followed a similar pattern to that observed for Col III expression. The decrease in expression was primarily a result of changes in the frequency of stretch. The only significant differences that were detected were between 0.3 Hz and both the 0% stretch condition and 0.1 Hz. A 50% decrease in MMP-2 expression was observed for stretch of fibroblasts at 15% stretch at 0.3 Hz compared to fibroblasts seeded on SIS-ECM with no stretch (Figure 7-13A) (Table 7-5).

MMP-9 tended to change in response to both magnitude and frequency of stretch. No statistical differences were found between the stretch and no stretch conditions, but expression of MMP-9 stretch at 0.1Hz was found to be significantly less than expression at 0.3 Hz and 0.5 Hz. The difference was approximately 30%. Although statistical significance was not detected, the expression of MMP-9 tended to increase in a magnitude dependent manner at frequencies of 0.3 Hz and 0.5 Hz (Figure 7-13B) (Table 7-5).

The changes in TGF-β_1 expression were dependent on the frequency of stretch ($p < 0.05$) and approached dependence on the magnitude of stretch ($p = 0.068$). In comparing the effects of frequency, the only comparison that did not show significant differences was between fibroblasts on SIS without stretch and fibroblasts on SIS subjected to 0.1 Hz stretch. TGF-β_1 expression increased in a frequency dependent manner. With regard to the effects of the magnitude of stretch, TGF-β_1 expression was significantly greater in response to 10% stretch and 15% stretch as compared to 0% stretch (Figure 7-14A) (Table 7-5).

There significant increases in TGF-β_3 expression at 0.5 Hz as compared to 0.1 Hz and 0.3 Hz, and in response to 10% stretch as compared to 5% stretch. Although no statistical significance was shown, TGF-β_3 expression tended to increase in a frequency dependent manner at 10% and 15% stretch (Figure 7-14B) (Table 7-5).

No differences were observed between the gene expression NIH-3T3 fibroblasts seeded on SIS-ECM with 0% stretch and fibroblasts seeded on standard TCP, except for SMA.

However, in the case of SMA, significance was due to the small standard deviation. The real difference was less than 10% (Table 7-5).

7.2.8 Changes in Stiffness of SIS-ECM Scaffolds

In terms of the mechanical behavior of the fibroblasts seeded SIS-ECM, the stiffness and maximum load decreased during each 24 hour period (i.e., Initial to Interval 3, Interval 4 to Interval 6, Interval 7 to Interval 10) (Figure 7-15). Upon reapplying the preload to the specimen, an increase in the stiffness and maximum load was observed, along with an increase in the initial elongation required to reach a preload of 0.05N (ranging from 1.7% ± 0.9% for 15% stretch at 0.5Hz to 11.4% ± 3.4% for 10 % stretch at 0.3 Hz) (Table 7-6). This finding indicates that the specimens were experiencing permanent creep as a result of cyclic stretching. In addition, the stiffness of the SIS-ECM scaffolds varied considerably (Table 7-6). The stiffness increased for all specimens over the course of the experiments, but no dependence was shown between the percentage increase in stiffness and either the frequency or magnitude of stretch.

A new CSTC System has been developed to study the effect of cyclic mechanical loading on cells seeded on a scaffold of interest. The system is capable of independently applying cyclic load to eight cell-seeded scaffolds for periods lasting several weeks (preliminary studies have been performed for up to 4 weeks). A major advantage of the new testing system is its ability to independently apply precise displacement waveforms to each specimen while accurately and continuously monitoring the loads. This functionality provides real-time feedback about changes in the mechanical behavior of cell-seeded biologic scaffolds in response to cyclic stretching.

7.2.9 Relevance of Changes in Gene Expression to *In Vivo* Remodeling

The present study used the new CSTC system to investigate the expression of matrix-related proteins by fibroblasts seeded on SIS-ECM after the application of cyclic mechanical stretch as a basis for developing a better understanding of the role of mechanical loading in the constructive remodeling response observed with ECM scaffolds *in vivo*. The expression of Col I showed the most substantial increase in response to cyclic stretching in a frequency dependent manner, while the expression of Col III decreased slightly. Most *in vitro* studies that have investigated the

expression of Col I and Col III have shown that both genes are increased in response to a mechanical stimuli.[149, 184, 292] If the SIS-ECM environment in the presence of mechanical loading encourages a more normal Col III to Col I ratio[210] and a more normal distribution of collagen fibril diameters in the healing tissue,[35, 170] then this could partially explain the improved mechanical properties that have been reported in *in vivo* studies.[180, 206]

The increased expression of SMA and TN-C, along with increased expression of TGF-β_1, suggests that the fibroblasts seeded on SIS-ECM became more contractile with increasing frequency of stretch.[61, 86, 298] If the fibroblasts exhibit a contractile phenotype, then the cells will tend to align along the direction of stretch,[80, 127] and this alignment was confirmed in the present study. It has been shown previously that alignment of fibroblasts leads to alignment of newly synthesized and existing collagen in the same direction.[80, 192, 279] The results for TGF-β_3 are difficult to explain since it is thought to play a role in scarless fetal wound healing and has been shown to reduce the contractility of cells.[51, 204] The increased expression of TGF-β_3 may moderate the contractile behavior.

It has been suggested that MMP-9 is involved in collagen degradation, while MMP-2 is involved in collagen degradation and remodeling.[250, 281] The present finding of increased expression of MMP-9 suggests that the collagen present within a SIS-ECM scaffold will be degraded and removed from the scaffold as opposed to being incorporated into the new host tissue. Several studies that have investigated the degradation and fate of an ECM scaffold implanted *in vivo* have shown complete removal of the scaffold from the remodeling site within 60-90 days after implantation accompanied by complete replacement with host tissue.[100, 229] Further study is necessary to understand and confirm this phenomenon.

7.2.10 Significance of Changes in the Stiffness of the SIS-ECM Scaffolds

The stiffness varied considerably from scaffold to scaffold, which is likely due to the natural variability of SIS-ECM.[227] This study showed that the stiffness of each scaffold increased moderately over the course of each mechanical conditioning regimen, although there was no correlation between the magnitude and frequency of stretch to the magnitude of the increase in stiffness. It was also shown that each scaffold became slack during the stretching regimen such that it was necessary to elongate the specimen in order to reapply the preload. It is likely that

this elongation was solely responsible for the increase in stiffness that was measured, effectively leading to stiffness measurements further into the linear region of the load-elongation curve after fiber reorientation had taken place.[7]

7.2.11 Limitations

The present study was intended to evaluate the response of fibroblasts seeded on SIS-ECM to a range magnitudes of stretch are that structurally relevant to SIS-ECM based on the fiber kinematics results presented in Section 6.1 and a range of frequencies that are physiologically relevant.[202] There may be other stretching regimens that would add to our knowledge of how fibroblasts seeded on SIS-ECM contribute to a constructive remodeling response. In particular, the effects of strain rate on fibroblast gene expression may be important. Furthermore, the CSTC system is capable of performing load control experiments and could also be easily modified to allow the application of more complex loading regimens to simulate *in vivo* conditions.[139]

7.2.12 Application of Model to Other Cell Types

The present study shows that cyclic stretching of fibroblasts seeded on SIS-ECM leads to changes in the gene expression that are suggestive of tissue remodeling towards a tendon or a ligament. It has been shown that a wide variety of cells participate in the remodeling of SIS-ECM scaffolds, beginning with neutrophils and macrophages in the immediate post-implantation period with a transition to tissue specific cell lineages (i.e., fibroblasts, smooth muscle cells, epithelial cells) within 4 to 8 weeks.[21, 100] SIS-ECM also recruits bone marrow derived cells to the site of remodeling, and these cells participate in the long-term remodeling process.[20, 296] This population of bone marrow derived cells may include mesenchymal progenitor cells that differentiate into site appropriate cells in response to the local mechanical environment.[84, 161, 224] Previous *in vitro* studies have shown that cyclic mechanical loading promotes differentiation of bone marrow cells into fibroblastic cells, smooth muscle cells, and osteoblastic cells.[6, 109, 195] In future studies, a variety of different cell types will be tested using the new CSTC system expand our understanding of the role of mechanical environment on the remodeling of ECM scaffolds *in vivo*.

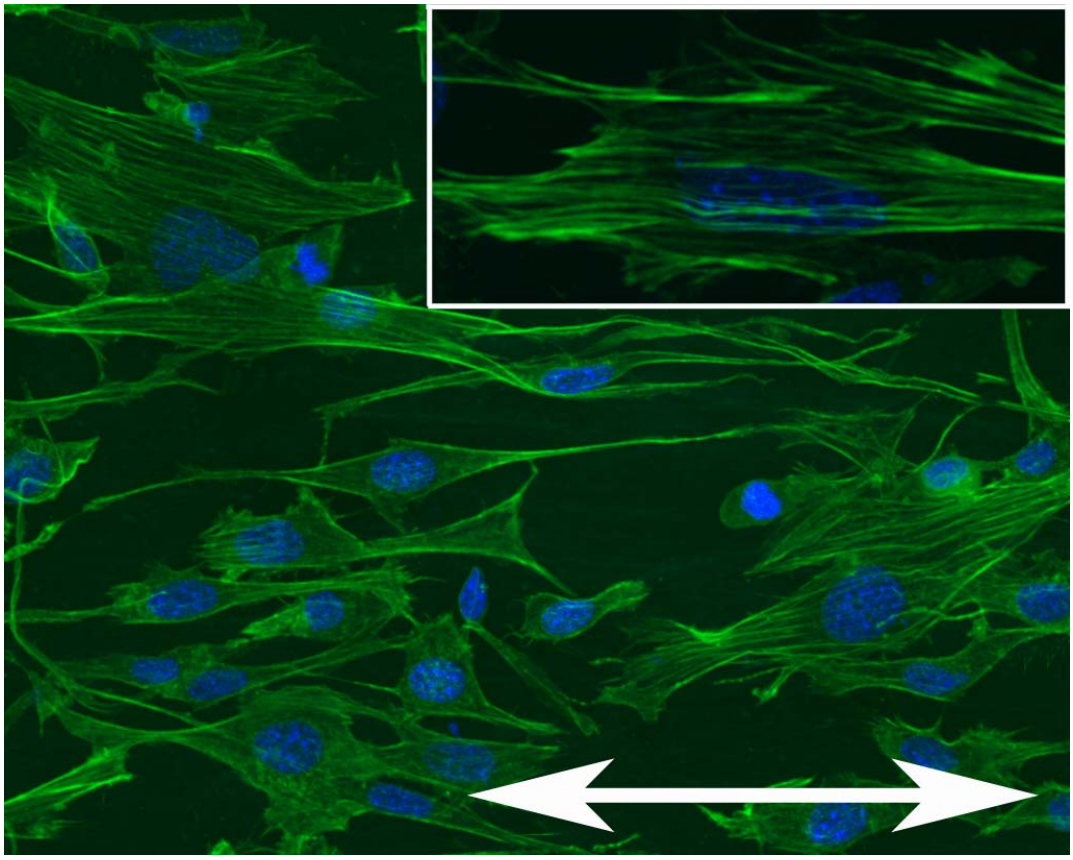

Figure 7-10. 3-D reconstruction of actin and Hoechst staining of NIH-3T3 fibroblasts cells seeded on SIS-ECM and subjected to cyclic stretch of 10% at a frequency of 0.1Hz. The cells generally align with the direction of stretch which is indicated by the white arrow. (Background: 40X, Insert: 100X)

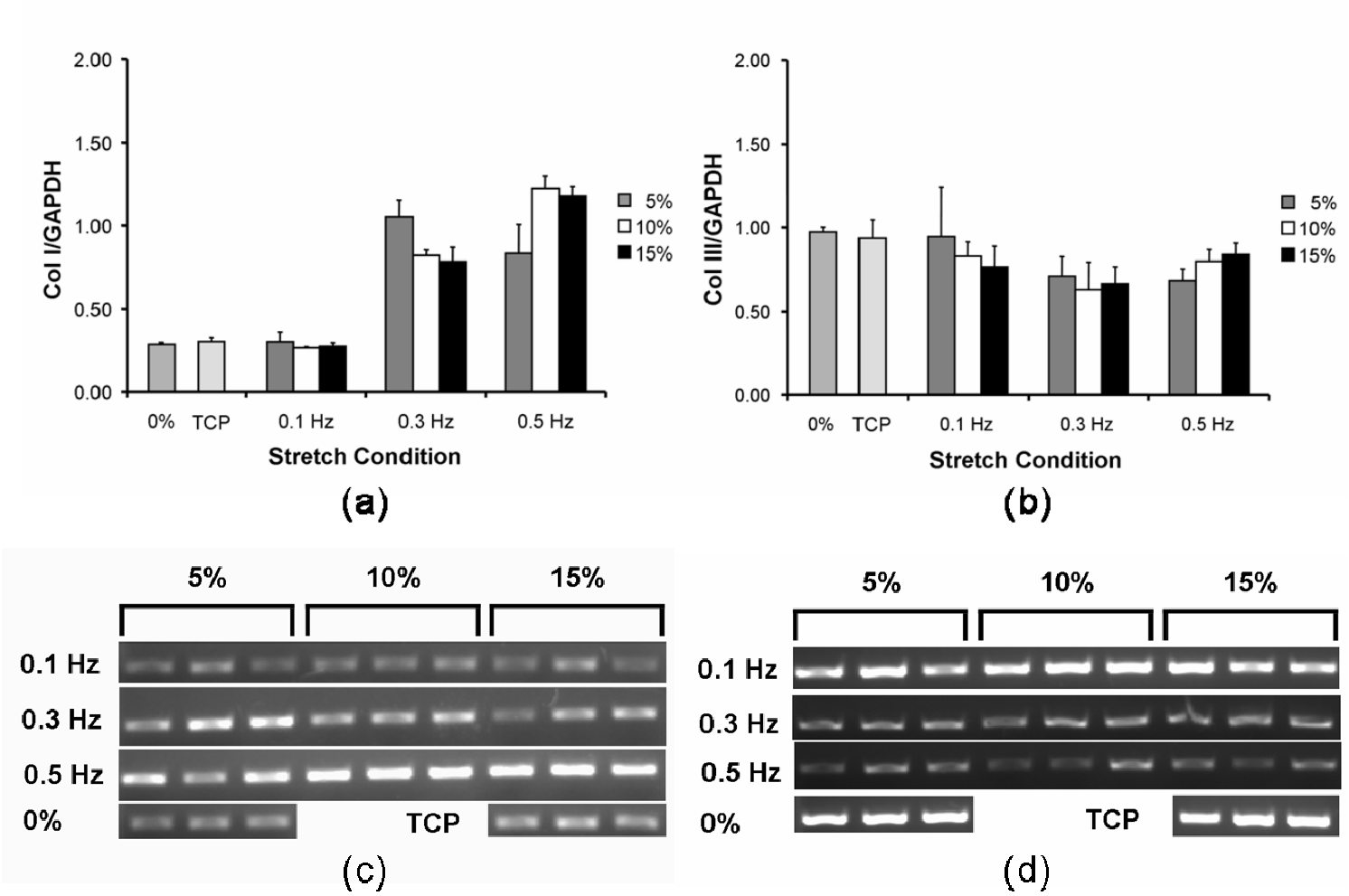

Figure 7-11. Relative expression of (A) collagen I (Col I) and (B) collagen III (Col III) to GAPDH for the NIH-3T3 fibroblasts seeded on small intestinal submucosa in response to a number of stretching regimens (0%, 5%, 10%, 15%; 0.1Hz, 0.3 Hz, 0.5 Hz). Col I expression significantly increased in response increasing frequencies of stretch. Col III expression significantly decreased in response to stretch at a frequency of 0.3 Hz. Cells cultured on TCP were used to determine the basal level of Col I expression. The bands of (C) Col I and (D) Col III RT-PCR product from ethidium bromide gels are also shown.

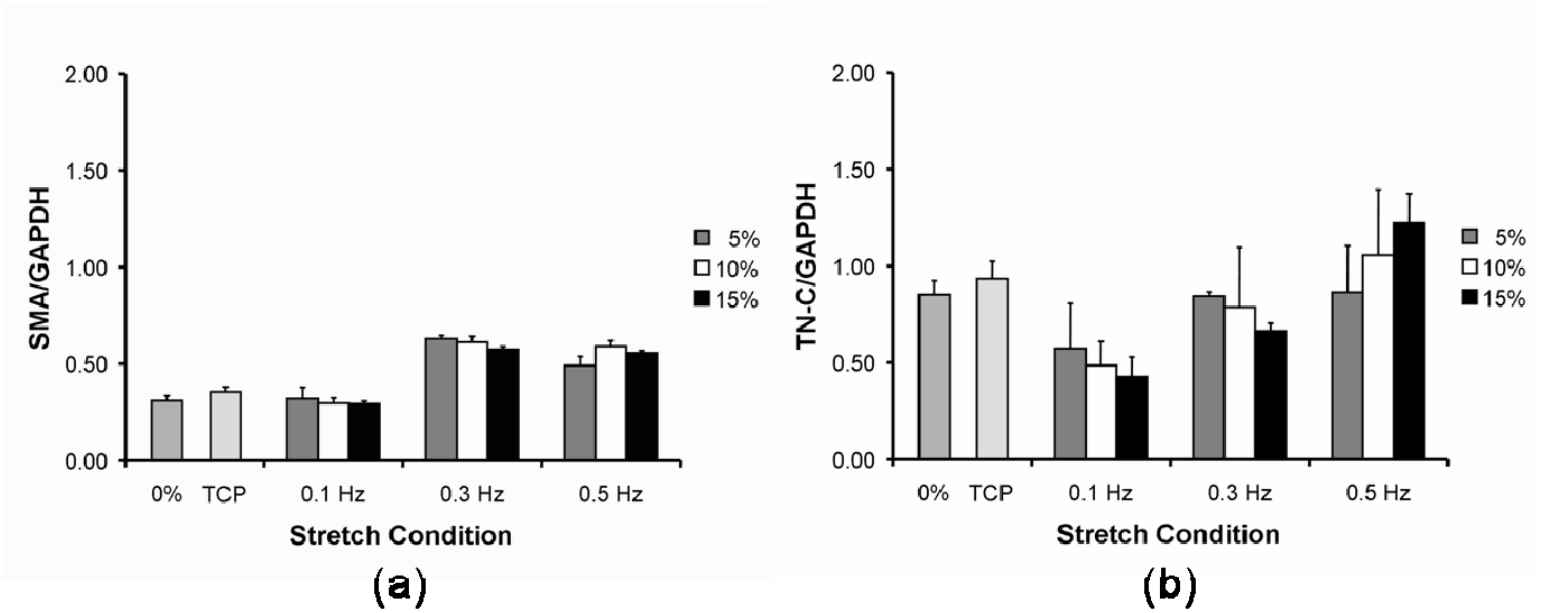

Figure 7-12. Relative expression of (A) smooth muscle actin (SMA) and (B) tenascin-C (TN-C) to GAPDH for the NIH-3T3 fibroblasts seeded on small intestinal submucosa in response to a number of stretching regimens (0%, 5%, 10%, 15%; 0.1Hz, 0.3 Hz, 0.5 Hz). SMA expression significantly increased in response increasing frequencies of stretch. TN-C expression tended to increase with an increase in the frequency to stretch. Cells cultured on TCP were used to determine the basal level of SMA and TN-C expression.

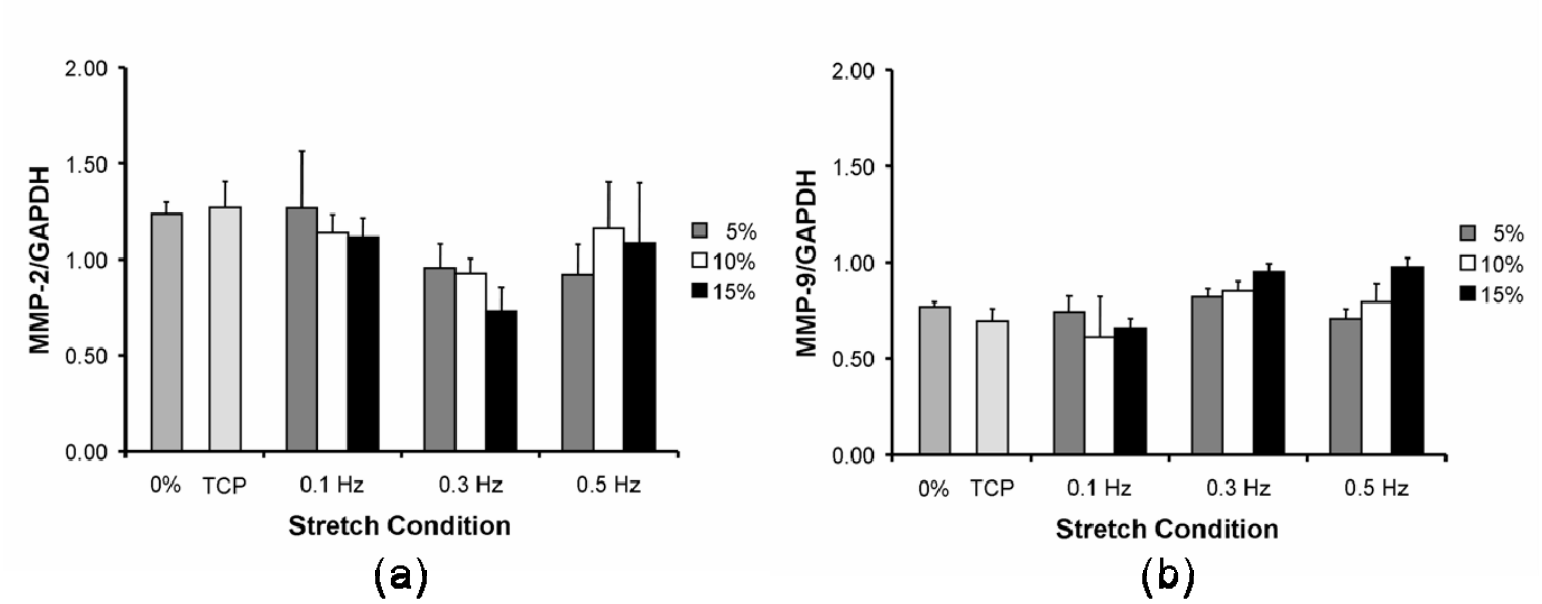

Figure 7-13. Relative expression of (A) matrix metalloprotease-2 (MMP-2) and (B) matrix metalloprotease-9 (MMP-9) to GAPDH for the NIH-3T3 fibroblasts seeded on small intestinal submucosa in response to a number of stretching regimens (0%, 5%, 10%, 15%; 0.1Hz, 0.3 Hz, 0.5 Hz). MMP-2 expression significantly decreased in response to stretch at a frequency of 0.3 Hz. MMP-9 expression tended to increase with increasing magnitude of stretch at frequencies of 0.3 Hz and 0.5 Hz. Cells cultured on TCP were used to determine the basal level of MMP-2 and MMP-9 expression.

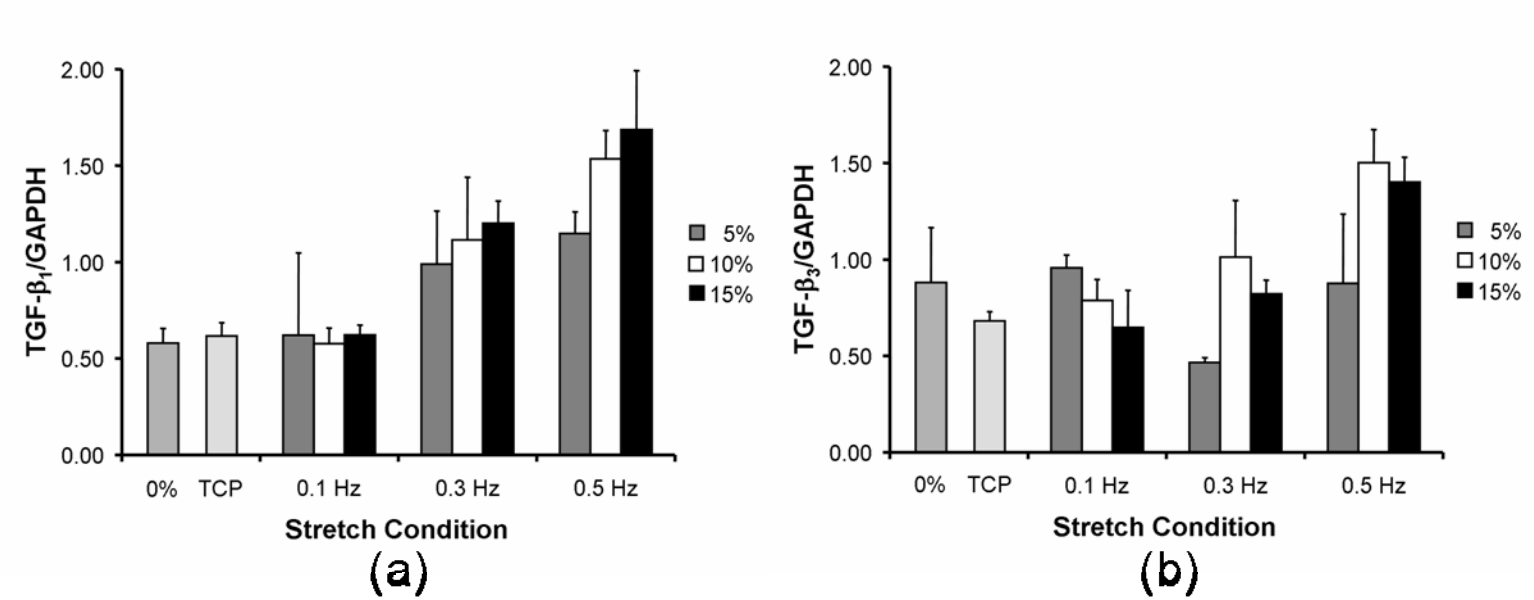

Figure 7-14. Relative expression of (A) transforming growth factor-β_1 (TGF-β_1) and (B) transforming growth factor-β_3 (TGF-β_3) to GAPDH for the NIH-3T3 fibroblasts seeded on small intestinal submucosa in response to a number of stretching regimens (0%, 5%, 10%, 15%; 0.1Hz, 0.3 Hz, 0.5 Hz). TGF-β_1 expression significantly increased in response increasing frequencies of stretch. TGF- β_3 expression tended to decrease at a frequency of 0.1 Hz, but tended to increase at frequencies of 0.3 Hz and 0.5 Hz. Cells cultured on TCP were used to determine the basal level of TGF-β_1 and TGF- β_3 expression.

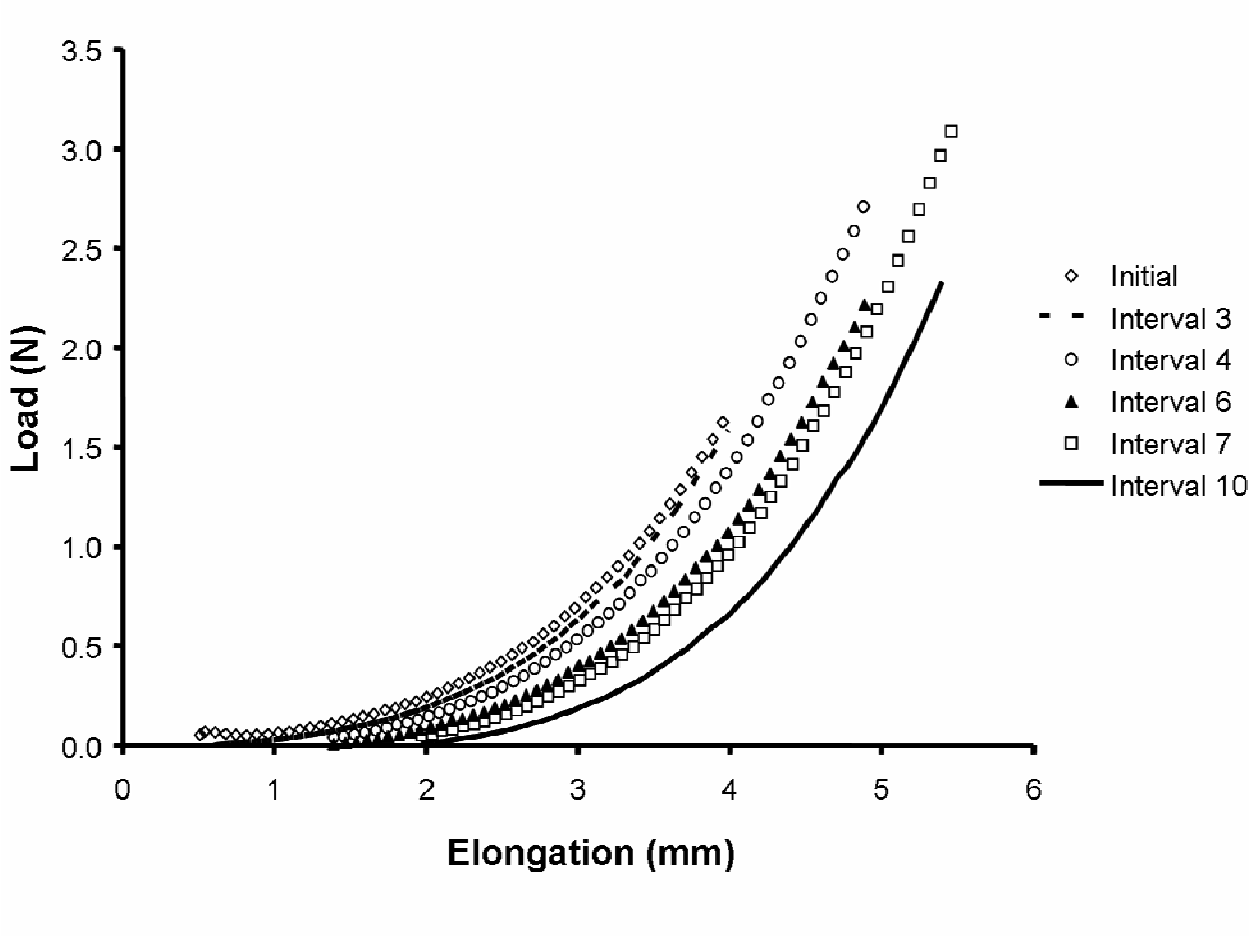

Figure 7-15. Load-elongation curves for one specimen subjected to cyclic stretch of 10% at a frequency of 0.1Hz. The maximum load and stiffness decreased during each 24 hour period (i.e., Initial to Interval 3, Interval 4 to Interval 6, Interval 7 to Interval 10), and subsequently increased upon reapplication of the preload. The initial elongation increased for the reapplication of the preload causing the curves to move to the right on the graph.

Table 7-5. Statistical comparisons from the Two-Way ANOVA for the effects of stretch frequency (A) and stretch magnitude (B) on the expression of matrix related genes. * indicates significant differences at a $p<0.05$.

A	0% - 0.1 Hz	0% - 0.3 Hz	0% - 0.5 Hz	0.1 Hz - 0.3 Hz	0.1 Hz - 0.5 Hz	0.3Hz - 0.5 Hz
Col I		*	*	*	*	*
Col III		*		*		
SMA		*	*	*	*	*
TN-C	*			*	*	*
MMP-2		*		*		
MMP-9			*	*		
TGF-β_1		*	*	*	*	*
TGF-β_3			*		*	
B	0% - 5%	0% - 10%	0% - 15%	5% - 10%	5% - 15%	10% - 15%
Col I	*	*	*			
Col III						
SMA	*	*	*			
TN-C						
MMP-2						
MMP-9						
TGF-β_1		*	*			
TGF-β_3				*		

Table 7-6. Mechanical characteristics of fibroblast seeded SIS-ECM under various cyclic mechanical stretching regimens.

	Initial Stiffness (N/mm)	Final Stiffness (N/mm)	%Δ Stiffness	% Elongation
		5%		
0.1 Hz	0.19 ± 0.06	0.22 ± 0.06	15.0% ± 17.5%	3.3% ± 0.6%
0.3 Hz	0.32 ± 0.29	0.46 ± 0.45	44.4% ± 42.4%	2.7% ± 1.9%
0.5 Hz	0.15 ± 0.03	0.19 ± 0.11	23.7% ± 39.8%	1.7% ± 0.9%
		10%		
0.1 Hz	0.83 ± 0.34	1.06 ± 0.54	10.1% ± 17.2%	2.9% ± 0.7%
0.3 Hz	0.99 ± 0.66	1.03 ± 0.46	12.8% ± 27.1%	3.5% ± 2.1%
0.5 Hz	0.33 ± 0.24	0.57 ± 0.19	116.7% ± 108.2%	4.6% ± 0.5%
		15%		
0.1 Hz	0.63 ± 0.85	0.79 ± 0.82	69.0% ± 76.4%	8.6% ± 4.3%
0.3 Hz	0.56 ± 0.45	0.70 ± 0.49	40.8% ± 77.0%	11.4% ± 3.4%
0.5 Hz	0.28 ± 0.20	0.45 ± 0.26	94.6% ± 90.0%	7.4% ± 4.6%

7.3 RECRUITMENT AND MECHANICAL LOADING OF FIBROCYTES SEEDED ON SIS-ECM

Some of the preceding studies have shown that SIS-ECM scaffolds used to repair a musculotendinous injury degraded within 60 days of implantation in a dog model and that there was an abundant infiltration of mononuclear cells that persists for more than one month. The cells produced a dense organized collagenous tissue that was histologically similar to the normal Achilles tendon. In a similar mouse study, it was shown that a portion of the mononuclear cells that were recruited to the site of ECM remodeling were derived from the bone marrow and remained as part of the new tissue even after 16 weeks of remodeling. Although the exact fate of these cells was unclear, they showed some fibroblastic characteristics, including expression of Col I and Col III. It is hypothesized that this phenotypic fate was a result, at least in part, of appropriate mechanical cues.

A second set of studies focused on the role of mechanical loading in the remodeling of SIS-ECM *in vitro*. First, the collagen fiber kinematics of SIS-ECM was determined to provide a basis for the magnitudes of stretch that should be applied to the SIS-ECM in vitro. Second, the gene expression of NIH-3T3 cells seeded on SIS-ECM was evaluated in response to various magnitudes and frequencies of stretch using a new Cyclic Stretching Tissue Culture System. Despite being an immortalized cell line rather than a primary cell, mechanical stretching of these cells on SIS-ECM led to changes in the gene expression that were consistent with the constructive, site-specific remodeling response that was observed in the *in vivo* studies. Obviously, it would be desirable to evaluate the changes in gene expression by the same cells that are recruited *in vivo* to the site of ECM remodeling in response to mechanical loading.

The goal of the present study was to evaluate the response to cyclic stretching by a population of cells that may be representative of the cells that are recruited from the bone marrow to the site of ECM remodeling, specifically the fibrocyte. The fibrocyte is a bone marrow derived mesenchymal cell that has been suggested to play an important role in wound repair.[1, 46] Fibrocytes exhibit unique surface markers (Col I^+, $CD11b^+$, $CD13^+$, $CD34^+$, $CD45RO^+$, MHC class II^+, $CD86^+$), have been shown to enter a wound bed from circulating

blood, and have been found in connective tissue scars. These cells have also been shown to home to the site of injury, potentially due to recruitment by secondary lymphoid chemokine.[1] Fibrocytes express α-smooth muscle actin (SMA), and have been shown to contract collagen gels *in vitro*, suggesting that they may play a role to tissue organization.[1] Fibrocytes also promote angiogenesis by secretion of proangiogenic factors such as VEGF, bFGF, interleukin-8, and platelet derived growth factor, and by releasing matrix metalloprotease-9 (MMP-9) to allow endothelial cell migration into tissue.[112] An *in vivo* Matrigel study showed that fibrocytes and fibrocyte conditioned media both promote blood vessel formation.[112] Many of these characteristics of fibrocytes are consistent with the behavior of cells that participate in remodeling of an ECM scaffold (i.e., recruitment of a bone marrow derived cell population, deposition and organization of collagen, promotion of angiogenesis). To simulate the *in vivo* ECM remodeling situation, fibrocytes will be isolated and a chemoattractant assay will be used to isolate fibrocytes that are recruited to the degradation products of SIS-ECM. The recruited fibrocytes will then be seeded on SIS-ECM and subjected to cyclic stretching and the gene expression by those cells will be assessed.

7.3.1 Fibrocyte Isolation

Mouse perpherial blood (PB) was collected four times and bone marrow (BM) was harvested eight times. All PB samples were collected in heparinized collection tubes while bones were gently crushed with a mortar and pestle to liberate the marrow. All samples were then spun (at 2,000 RPM for 30 min. at RT) through a density gradient (Lymphocyte Separation Medium) to isolate the buffy coat. The low density mononuclear cells were then plated onto either collagen type I or fibronectin coated plates (2 PB and 6 BM on collagen and 2 PB and 2 BM on fibronectin) at densities ranging from 720,000 to 1,536,000 PB cells per well of a 6-well plate and from 3,090,000 to 95,000,000 BM cells per well. Cells were then cultured at 37ºC with non-adherent cells removed after 48 hours. All cultures were maintained for at least 7 weeks with medium (DMEM + 10% FBS + 2% Pen./Strep.) changed 2-3 times per week.

7.3.2 Chemical and Physical Methods of ECM Degradation

Lyophilized SIS-ECM was ground into a particulate form using a Wiley Mill as previously descibed.[97] The resulting particulate SIS-ECM was then hydrated with phosphate buffered saline (PBS) plus Protease Inhibitors. The hydrated particulate SIS-ECM was then be digested in 0.5N acetic acid at 120^{o}C under 2 atmospheres of pressure. The temperature was ramped to 120^{o}C in 55 minutes, held at 120^{o}C for 30 minutes, and was brought down to 60^{o}C in 2 minutes and to room temperature within an additional 15 mintues. The resulting digest was sequentially filtered through cheesecloth, Reeve Angel filter paper, and Whatman No.42 filter paper and then lyophilized and stored at -80^{o}C. The digest was resuspended at 200mg dry weight per ml in [0.1M sodium phosphate / 0.15M sodium chloride], pH 6.8 buffer, centrifuged at 12,000 RPM for 1 hour at room temperature, and then filtered through a 45μm syringe filter to recover the solubilized material. Total protein concentration were estimated with a BCA protein assay (Pierce Biotechnology) and the protein concentration was adjusted to 10mg/ml in [0.1M sodium phosphate / 0.15M sodium chloride], pH 6.8.

An ammonium sulfate precipitation step was then used to remove those components such as glycosaminoglycans that increase the viscosity of the digest. Extensive preliminary studies have been conducted evaluating the optimal concentration of ammonium sulfate to use in this precipitation step. Interestingly, while fractionating the ECM digest by precipitating at 0% - 100% saturation of ammonium sulfate at 10% intervals, we have identified biologic activities in fractions that precipitate at different ammonium sulfate concentrations. After precipitation, the pellets were resuspended in [0.1M sodium phosphate / 0.15M sodium chloride], pH 6.8 plus protease inhibitors, snap frozen on dry ice, and stored at -80^{o}C. The supernatant and suspended pellet samples were then desalted, concentrated using either a Microcon YM-3 centrifugal filter device (molecular weight cutoff of 3,000 daltons) or float-a-lyzer dialysis devices (MWCO of 3,000 daltons), and then assayed for total protein. These fractions were then ready for screening for bioactivity in our chemotactic assays described below.

7.3.3 Boyden chamber assay for Chemotaxis

The Boyden chamber assay was used for initial screening of ECM digest fractions. The fibrocytes was starved for 12-16 hours prior to the beginning of the assay. The filters used (will vary with each cell line) had a pore size of 3, 8 or 12 microns. The filters were uncoated or coated with either gelatin or collagen. A 48 well chamber was to be used for the assays. A sample of the unknown (i.e., a fraction of ECM) or a positive control chemoattractant was to be placed in each well beneath the filter, and then in the wells above the filter the fibrocytes were suspended in solution for 12 hours. The nonrecruited were to be scraped from the top of the filters, and in preliminary experiments the filters were to be stained and cells attached to the underside of the filter were to be counted. The stain used for this assay was DiffQuik. Assays were to be run as triplicates. In separate experiments, the recruited cells were to be harvested for use in a cyclic stretching experiment using the CSTC System as described in Section 7.2.2.

7.3.4 Fibrocyte Isolation Results

Only one of the twelve cultures appeared to contain fibrocytes, as detected by spindle-shaped cell morphology, and that culture was sorted in an attempt to isolate the fibrocytes. The cells were sorted using the phenotype of CD34+/CD45+/collagen type I+ using a FACSVantage cell sorter. Due to a lack of staining with the collagen type I antibody, we were unable to identify any cells positive for collagen type I expression, and so cells that were double positive for CD34 and CD45 were sorted. Following the sort the cells were replated onto a fibronectin coated plate. All of the cells died within one week. All other cultures developed mesenchymal-like cell morphology and were discarded. Since no fibrocytes were isolated, this experiment could not be completed. We are continuing our efforts to isolate fibrocytes so that this work can progress. We have been in contact with Dr. Richard Bucala, the investigator that first described the isolation and phenotypic characteristic of fibrocytes and he has offered suggestions on how to improve our results. This is not a trivial task, and the remainder of the dissertation work was completed with the exception of the successful isolation of this cell population.

8.0 CONCLUSIONS

This Dissertation examined two major aspects of the remodeling of a naturally occurring ECM scaffold, specifically the fate of bone marrow derived cells the site of ECM scaffold remodeling in a musculotendinous application and role of mechanical loading on the remodeling of an ECM scaffold using *in vitro* systems. The following section summarizes the major findings from the studies performed and addresses the Specific Aims that were not completed. Finally, potential future studies are described to extend this work.

8.1 DISSERTATION SYNOPSIS

8.1.1 Degradation of SIS-ECM in a Musculotendinous Application

The first component of this Aim was to quantify the rate of degradation of the SIS-ECM scaffold and relate the degradation to the remodeling events (i.e., cellularity, cell morphology, collagen organization). It was found that the profile for degradation of SIS-ECM in the Achilles tendon location was similar to the profile observed for implantation to the urinary bladder.[229] The rate of degradation appeared be slightly faster for the Achilles tendon with no scaffold detected by 60 days after implantation. Degradation was noted as early as 3 days post implantation, although the extent of degradation was only a few percent. The degradation rate increased after 7 days of remodeling, which corresponded to the time that was required for an abundance of mononuclear cells consistent with macrophage morphology to enter the scaffold. The 14 day time point was the peak for cellularity, and the time frame from 7 – 14 days represented the period of most rapid ECM scaffold degradation. Beyond 14 days, the cellularity of the scaffold began to decrease, and the rate of degradation also began to slow down. By 28

days, the mononuclear cells begin to show site specific cell morphology, primarily as fibroblasts. The origin of the cells was not definitively determined in this study, nor did these cells show any fibroblastic markers. A number of attempts were made to examine the phenotype of the cells (CD68 staining for macrophages, RNA isolation for Col I RT-PCR), but these analyses were conducted in retrospect and the specimens had already been fixed in 10% neutral buffered formalin which limited our options. By 60 days, the scaffold was not detectable, and the organization and cellularity of the tissue approached that of the normal tendon. An important factor in the remodeling response was the external bracing of the Achilles tendon during the early stage after surgery that immobilized the joint but still allowed the limb to bear load. After the splint was removed, the animals were allowed unrestricted cage activity. Based on previous studies, we speculate that without the presence of an appropriate mechanical environment, a constructive, site specific remodeling response would not have occurred.

8.1.2 Recruitment and Fate of Bone Marrow Derived Cells

In the early phase of ECM remodeling, a massive cell infiltration occurs with most of the cells originating in the bone marrow. In a mouse Achilles tendon model, it was shown that a portion of these bone marrow derived cells remain at the site of ECM remodeling for at least 4 months; a finding that is at least contrary to normal mammalian wound healing. In this model of tendon repair, the bone marrow derived cells generally did not express CD45 and expressed Col I, Col III, and SMA, suggesting several possiblilities. First, these cells could be myofibroblastic cells or circulating fibrocytes that were recruited from the bone marrow. Another interpretation is that these cells represent the remnants of blood vessels that formed during the initial phase of remodeling. The facts that these cells were spindle shaped in appearance and were found within the body of the tendon favors the former explanation. It is possible that the bone marrow derived cells responded to local environmental cues to become site specific cells. Appropriate mechanical and biochemical cues would have led the cells to be fibroblastic cells. In other locations, the cells differentiate into other cells types, such as endothelial cells as has been shown previously. This site specific cell differentiation would help to explain, at least in part, the constructive remodeling process that occurs at the site of ECM remodeling.

8.1.3 Fiber Kinematics of SIS-ECM

In order to develop a better understanding of the role of mechanical loading in the remodeling of an ECM scaffold, we first studied the collagen fiber kinematics of SIS-ECM under a number of loading regimens. In general, the fiber kinematics behaved as expected, with increases in the degree of collagen fiber alignment when the scaffold was stretched along the preferred collagen fiber direction of the tissue, and with decreases in the alignment with stretch in the cross preferred direction. In the initial phase of stretch, rotation of the collagen fiber population was observed towards the direction of stretch, and this was particularly noticeable for uniaxial stretch along the longitudinal axis of the intestinal. Under equibiaxial and strip biaxial stretch, the ECM scaffold behaved in an affine manner, so the fiber kinematics could be modeled. However, under uniaxial stretch, the fiber kinematics deviated from the affine deformation model. For stretch along the preferred fiber direction, the experimentally obtained collagen fiber distribution was less aligned than the predicted value, which suggested a greater level of interconnectedness between the collagen fibers than assumed by the affine model. The results for uniaxial stretch in the cross-preferred direction suggested a dramatic global fiber rotation towards the direction of stretch as opposed to a separation of the two subpopulations that have been identified in the SIS-ECM. It is suspected that these results are an artifact of the experimental procedure. It is possible that the lateral contraction that occurred in the unconfined direction led to a form of collagen buckling. In this case, the fibers would fold forming a zig-zag arrangement. At the size scale of the laser, this zig-zag arrangement could lead to a diffraction pattern that would appear to be aligned in the direction of stretch as opposed to the global longitudinal axis of the collagen fiber; however, this was not confirmed experimentally.

The results for the fiber kinematics of SIS-ECM under uniaxial stretch along the longitudinal axis of the SIS-ECM formed the basis for the selection of stretch magnitudes for *in vitro* mechanical loading studies of SIS-ECM seeded with fibroblasts. The fiber kinematics results showed that at 5% stretch, the collagen fiber population experienced a global fiber rotation toward the direction of stretch with no increase in the degree of alignment. It was assumed that this would translate to minimal stretch to the fibroblasts seeded on the SIS-ECM. At 10% stretch, the degree of orientation had increased by approximately 3%, and 15% stretch caused a 6% increase in the degree of orientation. Above 15% stretch, the degree of alignment

did not increase. It was assumed that 10% stretch would therefore cause a moderate stretch to the fibroblasts and a stretch of 15% would cause excessive stretch. Future work will be necessary to determine the exact relationship between scaffold stretch and cell stretch.

8.1.4 Cyclic Stretching of SIS-ECM Seeded with Fibroblasts

The Cyclic Stretching Tissue Culture (CSTC) system was developed to apply a variety of cyclic stretching regimens to SIS-ECM seeded with fibroblasts. Each of the 8 stations can apply a different loading regimen simultaneously, while a load cell monitors the force developed within the scaffold. The CSTC system was used to evaluate the effects of magnitude and frequency of stretch on the expression of several genes that are involved ECM remodeling. In addition, load vs. elongation behavior was obtained and the stiffness of the scaffold was calculated over time. The findings showed that cyclic mechanical loading of SIS-ECM seeded with fibroblasts led to significant changes in the gene expression. The greatest change in expression level was for Col I, which showed a five-fold increase in expression at 0.3 Hz and 15% stretch compared to the non-stretched control. SMA, TN-C, TGF-β_1, and MMP-9 expression also tended to increase in response to cyclic loading. Col III expression tended to decrease with cyclic stretching, which is contrary to other findings in literature. However, decreased Col III expression is consistent with a constructive remodeling response since Col III is elevated in scar tissue. Along with the increase in Col I, this *in vitro* study suggests that an ECM scaffold might restore the normal Col III/Col I ratio of remodeling tissue. The increased expressions of SMA, TN-C, and TGF-β_1 suggest that the fibroblasts exhibit a contractile phenotype, such as that associated with myofibroblasts, which might contribute to the development of tissue organization. Finally, the increased expression of MMP-9 suggests that the scaffold itself is degraded and removed from the site of remodeling, which is consistent with the *in vivo* degradation studies that have shown complete removal of the scaffold from the implant site within 60-90 days.

Interestingly, the changes in gene expression tended to be more dependent on the frequency of stretch rather than the magnitude of stretch. This finding supports the need for additional work to determine the relationship between the magnitude of scaffold strain and the magnitude of cell strain. Furthermore, it leads to questions regarding the importance of cycle

number and strain in the gene expression. Additional studies are currently underway to attempt to address these questions.

Another Specific Aim was to examine the changes in the collagen fiber architecture and kinematics of the SIS-ECM scaffold after seeding with fibroblasts and subjecting the scaffold to a regimen of long-term cyclic stretch. A series of four experiments (n=8 per experiment) was attempted in order to accomplish this Aim, but technical difficulties forced reconsideration of this Specific Aim. The first problem was that after 1-2 weeks of culture, there was a high incidence of scaffold damage due to cyclic stretch. Another issue was cell proliferation that occurred over the period of the experiment. After 2 weeks of culture, the media became acidic prior to the three day standard media change. It is likely that the media would have to be changed daily, which was not economically feasible at this time. Given the interesting results of the gene expression after a few days, it was decided that a better use of time and resources would be to begin looking at alternative stretching parameters and other cell types.

8.1.5 Effects of Mechanical Loading on Fibrocytes

Specific Aim 3 was designed to determine if one group of cells from the bone marrow, the circulating fibrocyte, is included in the population of bone marrow cells that are recruited to the site of ECM remodeling, eventually becoming a site specific cell. These cells have been found to circulate through the body and are well characterized. Due to technical difficulties in isolating these cells from circulating blood (mouse and human) and from bone marrow (mouse only), these studies were not completed (see Section 7.3.4). If we can successfully isolate circulating fibrocytes, we will systematically address this question.

8.2 FUTURE STUDIES

A number of future studies are suggested. From the *in vitro* mechanical stretching experiments, a limited number of magnitudes, frequencies, and stretch/rest intervals were evaluated. Future studies should expand on these parameters in order to development of a clearer understanding of the effects of mechanical loading on the behavior of cells on the scaffold. Of particular interest is whether cycle number or strain rate has a greater effect on the behavior of cells seeded on SIS-ECM, since it was found that frequency has a significant effect on the gene expression by cells.

In addition, the analysis should be expanded beyond gene expression of subset of matrix related proteins to include protein synthesis, integrin expression, stress fiber formation, cell traction forces, cell migration, and matrix degradation. A specific example of a future study that could contribute to the understanding of the mechanisms of ECM remodeling would be to investigate the effects of mechanical loading on the rate of cell migration into the scaffold. As described in Section 2.3.1, when an ECM scaffold is implanted *in vivo* and immobilized, one key observation was that the interior of the scaffold was devoid of cells, whereas the scaffold subject to load had cells distributed throughout the remodeling ECM. It would be interesting to determine whether cells migrate into an ECM scaffold faster *in vitro* when the scaffolds are cyclically loaded as opposed to static cell culture.

Further study is also needed to understand the signals that cells receive from the SIS-ECM both in the static condition and in response to mechanical loading. It is possible that stretch exposes different motifs in the protein structure that signal the cells to behave in a different way. In addition, additional study is needed to determine how the SIS-ECM scaffold is remodeled by the cells. Specifically, analysis of the collagen fiber architecture and kinematics and biomechanical characterization of the remodeled SIS-ECM are needed.

It will also be necessary to expand the studies to include other cell types that are involved in the remodeling of ECM scaffolds. This could include primary fibroblasts from adjacent injured tissues, macrophages, and bone marrow derived cells.

Future studies should also be conducted in order to determine the specific mechanisms by which the bone marrow derived cells are recruited to the site of ECM remodeling and the specific cells that are recruited. There is now substantial evidence, albeit circumstantial, that the degradation of ECM scaffolds plays an important role in the constructive remodeling response

through the release of small peptides that exhibit bioactivity. It is important to determine which peptides are involved in the recruitment of bone marrow derived cells and to verify these peptides form naturally.

It will also be important to determine the role of different environmental cues on the differentiation of those cells. Specifically, the effects of the mechanical environment on the process of ECM remodeling is worthy of detailed study. It is clear that the absence of mechanical loading is extremely detrimental to the remodeling process, but the advantages of an appropriate mechanical environment are not specifically understood. It will be important to perform detailed studies comparing ECM remodeling under appropriate and deficient loading environments, including biomechanical analysis (passive and active, depending on the tissue), tissue architecture analysis, degradation rate, cell migration and phenotype, and others. Based on the existing literature using ECM scaffolds for repair of tissues, it seems that these studies would be best performed in the Achilles tendon, urinary bladder, or body wall.

APPENDIX A

PRODUCTION OF ECM SCAFFOLDS

Developing the methods necessary to produce scaffolds derived from naturally derived ECM is challenging. The scaffold must be completely decellularized and of a form that can be used surgically for a variety of pre-clinical and clinical applications. This must be done in the most benign way possible to reduce adverse affects on the scaffold that might compromise its ability to promote a constructive remodeling response (e.g., compromised mechanical behavior, loss of collagen, glycosaminoglycans, and growth factors, etc.). Furthermore, it is possible to modify the ECM material in such a way that allows us to answer important questions about the remodeling process. This Appendix presents two sections describing different aspects of ECM scaffold production. The first section deals with decellularization of tissues to obtain an ECM scaffold.[99] The second section details the methodology for labeling ECM with ^{14}C for subsequent use in degradation studies.[102] The efficiency of labeling for a number of tissues that may be of interest for tissue engineering applications is described.

A.1 DECELLULARIZATION OF TISSUES

Biologic scaffolds derived from decellularized tissues and organs have been successfully used in both pre-clinical animal studies and in human clinical applications.[24, 57, 77, 110, 153, 173, 199, 277] Removal of cells from a tissue or an organ leaves the complex mixture of structural and functional proteins that constitute the ECM. The tissues from which the ECM is harvested, the species of origin, the decellularization methods and the methods of terminal sterilization for

these biologic scaffolds have varied widely. Each of these variables affects the composition and ultrastructure of the ECM and accordingly, affects the host tissue response to the ECM scaffold following implantation. The objective of this manuscript is to provide an overview of the various methods that have been used to decellularize tissues, and the potential effects of the various decellularization protocols on the biochemical composition, ultrastructure, and mechanical behavior of the ECM scaffold materials.

A.1.1 Rationale for Decellularization of ECM

Xenogeneic and allogeneic cellular antigens are, by definition, recognized as foreign by the host and therefore induce an inflammatory response or an immune-mediated rejection of the tissue. However, components of the ECM are generally conserved among species and are tolerated well even by xenogeneic recipients.[29, 30, 67, 82] ECM from a variety of tissues, including heart valves,[10, 37, 107, 143, 157, 231, 243] blood vessels,[66, 72, 245, 267] skin,[58] nerves,[129, 148] skeletal muscle,[38] tendons,[53] ligaments,[290], small intestinal submucosa,[11, 13, 162], urinary bladder,[57, 90, 97], and liver[182] have been studied for tissue engineering and regenerative medicine applications. The goal of a decellularization protocol is to efficiently remove all cellular and nuclear material while minimizing any adverse effect on the composition, biological activity, and mechanical integrity of the remaining ECM.

Any processing step intended to remove cells will alter the native 3-dimensional architecture of the ECM. The most commonly utilized methods for decellularization of tissues involve a combination of physical and chemical treatments. The physical treatments can include agitation or sonication, mechanical massage or pressure, or freezing and thawing. These methods disrupt the cell membrane, release cell contents, and facilitate subsequent rinsing and removal of the cell contents from the ECM. These physical treatments are generally insufficient to achieve complete decellularization and must be combined with a chemical treatment. Enzymatic treatments, such as trypsin, and chemical treatment, such as ionic solutions and detergents, disrupt cell membranes and the bonds responsible for intercellular and extracellular connections. Tissues are composed of both cellular material and ECM arranged in variable degrees of compactness depending on the source of the tissue. The ECM must be adequately disrupted during the decellularization process to allow for adequate exposure of all cells to the

chaotropic agents and to provide a path for cellular material to be removed from the tissue. The intent of most decellularization processes is to minimize the disruption and thus retain native mechanical properties and biologic properties.

A.1.2 Description of Decellularization Protocols

The most robust and effective decellularization protocols include a combination of physical, chemical, and enzymatic approaches. A decellularization protocol generally begins with lysis of the cell membrane using physical treatments or ionic solutions, followed by separation of cellular components from the ECM using enzymatic treatments, solubilization of cytoplasmic and nuclear cellular components using detergents, and finally removal of cellular debris from the tissue. These steps can be coupled with mechanical agitation to increase their effectiveness. Following decellularization, all residual chemicals must be removed to avoid an adverse host tissue response to the chemical. The efficiency of decellularization and preservation of the extracellular matrix can be assessed by several methods. The mechanisms of physical, enzymatic, and chemical decellularization for a variety of tissues are reviewed in the following sections and in Table A-1.

Table A-1. Commonly used decellularization methods and chaotropic agents.

Method	Mode of Action	Effects on ECM	References
Physical			
Snap Freezing	Intracellular ice crystals disrupt cell membrane	ECM can be disrupted or fractured during rapid freezing	108, 132-136, 232
Mechanical force	Pressure can burst cells and tissue removal eliminates cells	Mechanical force can cause damage to ECM	90, 182
Mechanical Agitation	Can cause cell lysis, but more commonly used to facilitate chemical exposure and cellular material removal	Aggressive agitation or sonication can disrupt ECM as the cellular material is removed	72, 90, 182, 243
Chemical			
Alkaline; Acid	Solubilizes cytoplasmic components of cells; disrupts nucleic acids	Removes GAGs	74, 83, 90, 223, 295
Non-Ionic Detergents			
Triton X-100	Disrupts lipid-lipid and lipid-protein interactions, while leaving protein-protein interactions intact	Mixed results; efficiency dependent on tissue, removes GAGs	53, 57, 72, 74, 106, 182, 290
Ionic Detergents			
Sodium Dodecyl Sulfate (SDS)	Solubilize cytoplasmic and nuclear cellular membranes; tend to denature proteins	Removes nuclear remnants and cytoplasmic proteins; tends to disrupt native tissue structure, remove GAGs and damage collagen	58, 129, 130, 146, 182, 231, 290
Sodium Deoxycholate		More disruptive to tissue structure than SDS	58, 129, 130, 146, 182, 231, 290
Triton X-200		Yielded efficient cell removal when used with zwitterionic detergents	58, 129, 130, 146, 182, 231, 290
Zwitterionic Detergents			
CHAPS	Exhibit properties of non-ionic and ionic detergents	Efficient cell removal with ECM disruption similar to that of Triton X-100	72
Sulfobetaine-10 and -16 (SB-10, SB-16)		Yielded cell removal and mild ECM disruption with Triton X-200	58, 129, 130, 146, 182, 231, 290

Table A-1. Continued.

Method	Mode of Action	Effects on ECM	References
Chemical (cont'd.)			
Tri(n-butyl)phosphate	Organic solvent that disrupts protein-protein interactions	Variable cell removal; loss of collagen content, although effect on mechanical properties was minimal	53, 290
Hypotonic and Hypertonic Solutions	Cell lysis by osmotic shock	Efficient for cell lysis, but does not effectively remove the cellular remnants	72, 104, 193, 276, 290
EDTA, EGTA	Chelating agents that bind divalent metallic ions, thereby disrupting cell adhesion to ECM	No isolated exposure, typically used with enzymatic methods (e.g. trypsin)	10, 95, 198, 262
Enzymatic			
Trypsin	Cleaves peptide bonds on the C- side of Arg and Lys	Prolonged exposure can disrupt ECM structure, removes laminin, fibronectin, elastin, and GAGs	10, 95, 198, 262
Endonucleases	Catalyze the hydrolysis of the interior bonds of ribonucleotide and deoxyribonucleotide chains	Difficult to remove from the tissue and could invoke an immune response	68, 72, 231, 290
Exonucleases	Catalyze the hydrolysis of the terminal bonds of ribonucleotide and deoxyribonucleotide chains		

A.1.3 Physical Methods

Physical methods that can be used to facilitate decellularization of tissues include freezing, direct pressure, sonication, and agitation. Snap freezing has been used frequently for decellularization of tendinous and ligamentous tissue [132-136, 232] and nerve tissue.[108] By rapidly freezing a tissue, intracellular ice crystals form that disrupt cellular membranes and cause cell lysis. The rate of temperature change must be carefully controlled to prevent the ice formation from disrupting the ECM as well. While freezing can be an effective method of cell lysis, it must be followed by processes to remove the cellular material from the tissue.

Cells can be lysed by applying direct pressure to tissue, but this method is only effective for tissues or organs that are not characterized by densely organized ECM (e.g. liver, lung). Mechanical force has also been used to delaminate layers of tissue from organs that are characterized by natural planes of dissection such as the small intestine and the urinary bladder. These methods are effective, and cause minimal disruption to the 3-D architecture of the ECM within these tissues.

Mechanical agitation and sonication have been utilized simultaneously with chemical treatment to assist in cell lysis and removal of cellular debris. Mechanical agitation can be applied by using a magnetic stir plate, an orbital shaker, or a low profile roller. There have been no studies performed to determine the optimal magnitude or frequency of sonication for disruption of cells, but a standard ultrasonic cleaner appears to be as effective at removing cellular material as placing the tissue on an orbital shaker. In all of these procedures, the optimal speed, volume of reagent, and length of mechanical agitation is dependent on the composition, volume, and density of the tissue.

A.1.4 Chemical Methods: Alkaline and acid treatments

Alkaline and acid treatments are also used in decellularization protocols to solubilize the cytoplasmic component of the cells as well as remove nucleic acids such as RNA and DNA. For example, acetic acid, peracetic acid (PAA), hydrochloric acid, sulfuric acid, and ammonium hydroxide (NH_4OH) can effectively disrupt cell membranes and intracellular organelles [74, 83, 90,

[223, 295]. However, these chemicals also dissociate important molecules such as GAGs from collagenous tissues.

A variety of porcine tissues including small intestinal submucosa (SIS) and layers of the urinary bladder [e.g., submucosal layer (UBS) and the basement membrane plus tunica propria (UBM)] have been decellularized using peracetic acid at concentrations of approximately 0.10 to 0.15% (v/v). This treatment is highly efficient at removing cellular material from these thin ECM structures, and simultaneously also disinfects the material by entering microorganisms and oxidizing microbial enzymes.[121, 225] The effects of PAA treatment on the ECM components have been studied extensively. Several types of collagen including types I, III, IV, V, VI, and VII have been identified in SIS and/or UBM following treatment with PAA,[13, 41] however, the microstructure of the collagen fibers has not been closely examined following such treatment. The ECM retains many of the native GAGs including hyaluronic acid, heparin, heparin sulfate, chondroitin sulfate A, and dermatan sulfate following PAA treatment.[118] It has also been shown that laminin and fibronectin are present in the ECM scaffolds following exposure to PAA.[41, 122] PAA treatment preserves the structure and function of many of the growth factors that are resident in the ECM, including TGF-β, b-FGF, and VEGF.[120, 274] PAA does not appear to have any adverse effect on the mechanical behavior of the biologic scaffold.[90] Both SIS and UBM have been shown repeatedly to serve as excellent substrates for *in vitro* cell culture,[15, 17, 122, 123] and have been successfully used for many tissue engineering applications *in vivo* following decellularization and disinfection with PAA.

A.1.5 Chemical Methods: Non-ionic detergents

Non-ionic detergents have been used extensively in decellularization protocols because of their relatively mild effects upon tissue structure. Non-ionic detergents disrupt lipid-lipid and lipid-protein interactions, but leave protein-protein interactions intact so that proteins within a tissue or organ following non-ionic detergent treatment should be left in a functional conformation.[248]

Triton X-100 is the most widely studied non-ionic detergent for decellularization protocols. Exposure of tissue to Triton X-100 for periods ranging from several hours to 14 days.[53, 57, 72, 74, 106, 182, 290] Decellularization of tissues with Triton X-100 has shown mixed results. When Triton X-100 was used to decellularize a heart valve, complete removal of nuclear

material was observed with maintenance of the valvular structure after 24 hours. However, cellular material was found in the adjacent myocardium and aortic wall.[107] With regard to the ECM components, Triton X-100 led to a nearly a complete loss of GAGs and decreases in the laminin and fibronectin content of the valve tissue.[107] Other studies showed that Triton X-100 was not effective at completely removing cellular material from a blood vessel, tendon, and ligament after exposure for up to 4 days.[53, 72, 290] Nuclear material was observed by histological staining in all of the tissues and immunohistochemical staining showed the presence of the cytoskeletal protein vimentin in the anterior cruciate ligament after treatment with Triton X-100. It was found that treatment with Triton severely altered the tendon with respect to the tensile strength of collagen fibers isolated from the tendon. Conversely, treatment with Triton showed no effect on the collagen content in the anterior cruciate ligament. Treatment with Triton X-100 also showed mixed results with regards to GAG content. All GAGs were removed from a heart valve after treatment with Triton X-100 for 24 hours, while there was no difference in the sulfated GAG content in the ACL after treatment with Triton X-100 for 4 days. Although Triton X-100 can be an effective decellularization method, its efficacy is dependent upon the tissue being decellularized and the other methods with which it is combined in a given decellularization protocol.

A.1.6 Chemical Methods: Ionic detergents

Ionic detergents are effective for solubilizing both cytoplasmic and nuclear cellular membranes, but tend to denature proteins by disrupting protein-protein interactions.[248] The most commonly used ionic detergents are sodium dodecyl sulfate (SDS) and sodium deoxycholate and Triton X-200.[58, 129, 130, 146, 182, 231, 290]

SDS is very effective for removal of cellular components from tissue. Compared to other detergents, SDS yields more complete removal of nuclear remnants and cytoplasmic proteins, such as vimentin.[290] SDS tends to disrupt the native tissue structure, and causes a decrease in the GAG concentration and a loss of collagen integrity. However, it does not appear that SDS removes collagen from the tissue.

Sodium deoxycholate is also very effective for removing cellular remnants, but tends to cause greater disruption to the native tissue architecture when compared to SDS. There are no

reports of tissue decellularization using sodium deoxycholate alone, so it is difficult to isolate its effect on the remaining ECM of a tissue. Sodium deoxycholate was also combined with several zwitterionic detergents to decellularize nerve tissue, however, it was found that only a combination of Triton X-200 with the zwitterionic detergents yielded a completely decellularized nerve ECM.[129, 130]

A.1.7 Chemical Methods: Zwitterionic detergents

Zwitterionic detergents exhibit the properties of both nonionic and ionic detergents. Zwitterionic detergents have a greater tendency to denature proteins than nonionic detergents. Examples of zwitterionic detergents include 3-[(3-cholamidopropyl)dimethylammonio]-1-propanesulfonate (CHAPS), which has been studied for decellularization of blood vessels,[72] and sulfobetaine-10 (SB-10) and -16 (SB-16), which have been used for decellularization of nerves.[129, 130] CHAPS treated artery tissue has histologically normal collagen and elastin morphology and the collagen content appears to remain similar to that of the native artery. CHAPS treatment results in a significant decrease in the burst pressure and maximum stress of arterial tissue, but the decrease is comparable to the burst pressure of arteries subjected to treatment with Triton X-100 and hypotonic/hypertonic solutions.[72] Nerves have been decellularized with SB-10 and SB-16 in combination with Triton X-200, an ionic detergent. The combined treatments had a less detrimental effect on the structure of the nerve ECM than combined treatments with Triton X-100 and sodium deoxycholate.[129, 130]

A.1.8 Chemical Methods: Tri(n-butyl)phosphate

Tri(n-butyl)phosphate (TBP) is an organic solvent that is used to inactivate viruses in blood with out compromising the coagulation factor activity. Recently, TBP has been used as a chaotropic agent for decellularization of tendon and ligament grafts. Treatment with TBP yielded complete removal of nuclear remnants from rat tail tendon and the midsubstance of an anterior cruciate ligament (ACL) graft, although the removal of cellular material was incomplete at the insertion of the ligament to bone. TBP treatment did not have an effect on the tensile strength of collagen fibers isolated from the rat tail tendon as compared to native control, but for the ACL, treatment

with TBP led to a decrease in collagen content.[53, 290] TBP appears to be a promising chaotropic agent for decellularization that has minimal effect on the mechanical behavior of the ECM and is worthy of further study.

A.1.9 Chemical Methods: Hypotonic and hypertonic treatments

Osmotic shock with a hypotonic or hypertonic solution such as deionized water or low ionic strength solution is used to lyse the cells within tissues and organs.[72, 104, 193, 276, 290] A treatment in a hypotonic solution (10mM Trizma HCl, 5mM EDTA) for 11 hours followed by an 11 hour treatment in a hypertonic solution (50mM Trizma HCl, 1M NaCl, 10mM EDTA) can cause cell lysis, but does not generally remove the resultant cellular remnants from the tissue. Additional enzymatic or chemical treatments are typically necessary to facilitate removal of cellular debris. Removal of DNA remnants from the tissue can be particularly difficult due to the "sticky" nature of DNA and its tendency to adhere to ECM proteins.

A.1.10 Chemical Methods: Chelating agents

Chelating agents, such as EDTA and EGTA, form a ring-shaped molecular complex that firmly binds and isolates a central metal ion. It has been shown that divalent cations, such as Ca^{2+} and Mg^{2+}, are necessary for cell attachment to collagen and fibronectin at the Arg-Gly-Asp receptor.[93, 150, 151, 201]. By binding the divalent cations that are present at the cell adhesions to the ECM, these agents facilitate removal of the cellular material from the tissue. EDTA is typically used in combination with trypsin.

A.1.11 Enzymatic Methods

Enzymatic techniques of decellularization include the use of protease digestion, calcium chelating agents, and nucleases.[10, 95, 198, 262] Trypsin is one of the most commonly used proteolytic enzymes in decellularization protocols. Trypsin is a highly specific enzyme that cleaves the peptide bonds on the carbon side of arginine and lysine if the next residue is not

proline.[273] The maximal enzymatic activity of trypsin occurs at 37°C and at a pH of 8. Nucleases such as endonucleases catalyze the hydrolysis of the interior bonds of the ribonucleotide or deoxyribonucleotide chains whereas exonucleases catalyze the hydrolysis of the terminal bonds of deoxyribonucleotide or ribonucleotide ultimately leading to the degradation of RNA or DNA.

The efficacy of enzymatic treatments for removal or separation of the cellular material from the ECM has been studied for a variety of tissues. Some studies show efficient removal of cellular material from porcine pulmonary valves after treatment with 0.05% trypsin/0.02% EDTA for 24 hours with agitation,[243] while other studies show less efficient decellularization. For example, porcine aortic valves subjected to treatment with 0.5% trypsin, 0.05% EDTA, 0.02% Gentamicin, 0.02 mg/ml DNase and 20 μg/ml RNAse-A in Milli-Q water for up to 17 hours at 37°C with agitation rendered the cells non-viable, but did not lead to removal of cellular material from the tissue.[107]

Enzymatic methods of decellularization are not without an adverse effect upon the extracellular components of tissues and organs. Prolonged treatment with trypsin/EDTA causes disruption of the normal pulmonary valve ECM structure, but does not affect the amount of collagen in the tissue.[243] Trypsin/EDTA did, however, substantially reduce the laminin and fibronectin content of the ECM. Prolonged exposure to trypsin/EDTA greatly decreases the elastin content and GAGs over time, with o-sulfated GAGs (chondroitin sulfates, keratin sulfates, and dermatan sulfates) showing the greatest decrease. Such treatments can contribute to a decrease in tensile strength of up to 50%. The remaining ECM after such enzymatic decellularization protocols still supports endothelial cell growth *in vitro* despite the removal of ECM components.[107, 243] It is desirable to limit the duration of exposure to trypsin/EDTA treatments to minimize the disruptive effects upon the ultrastructure and composition of the ECM.

A.1.12 Protease Inhibitors

During the decellularization protocols, a number of proteases can be released from the disrupted cells. For long duration chemical treatments, the presence of proteases can cause damage to the native ECM ultrastructure. For this reason, it may be desirable to include protease inhibitors

such as phenylmethylsulfonylfluoride (PMSF), aprotonin, and leupeptin to the solutions in which the tissue is immersed. A buffered solution of pH 7 to 8 further inhibits many proteases, and the control of temperature and time of exposure to the lysis solutions can also limit the activity of the proteases.

A.1.13 Antibiotics

One concern for long duration chemical decellularization methods is the presence of bacteria which can contaminate the remaining ECM material. A number of protocols have therefore included antibiotic solutions such as penicillin, streptomycin, or amphotericin B [3, 116, 146, 167, 290]. However, if antibiotics or antibiotic residues remain in the scaffold material after the decellularization protocol, regulatory agencies may consider the material a drug rather than a medical device, which increases the complexity of regulatory approval.

A.1.14 Effects of Tissue Variability upon Decellularization

The efficiency of a given decellularization method or protocol is dependent upon the tissue of interest. Despite identical times of exposure and a greater concentration of trypsin (0.5% vs. 0.05%), Grauss et al.[107] found that a trypsin based decellularization protocol was ineffective at removing the cellular material from the rat aortic heart valve, while Schenke-Layland, et al.[243] showed complete removal of cells from a porcine pulmonary valve. It is likely that subtle nuances in the application of the protocols had an effect on the efficiency of removal that are not entirely clear, such as the application of three-dimensional agitation by Schenke-Layland, et al. [243]. Studies by Cartmell and Dunn [53] and Woods and Gratzer,[290] which studied decellularization of rat tail tendon and porcine ACL, respectively, showed differences in the decellularization results that cannot be easily explained by differences in the protocols studied. These studies show that the effectiveness of decellularization and the alterations to the ECM vary depending on the source of the tissue, the composition of the tissue, the tissue density, and other factors. For each tissue that is studied, it will be necessary to optimize the decellularization protocol to obtain acceptable cell removal.

A.1.15 Verification of Cell Removal

There are a number of methods available to determine the efficiency of the removal of cellular material from tissues. Standard histological staining with Hematoxylin and Eosin can serve as a first line of inspection to determine if nuclear structures can be observed. Alternative histological stains such as Masson's Trichrome, Movat's Pentachrome, or Safrin O can be used to examine tissues for the presence of various cytoplasmic and extracellular molecules. Immunohistochemical methods can also be utilized for specific intracellular proteins, such as actin and vimentin.[290]

Inspection for the presence of DNA can be performed by staining the specimen with DAPI or Hoechst, which are both fluorescent molecules that bind to the AT clusters in the minor groove of DNA.[140, 142, 172, 226] In addition, assays using propidium iodide and PicoGreen have been developed to provide quantitative data regarding the presence of DNA within a specimen.[160] DNA probe techniques have been utilized to track the fate of DNA from allografts after implantation, and could also be utilized to determine whether any DNA is present in the decellularized tissue.[137] Polymerase chain reaction (PCR) or electron microscopic methods are possible but not typically used to examine for the presence of remnant nuclear material or cytoplasmic debris due to the technical complexity and expense of these procedures for routine work.

In addition, to determining what has been removed, it is also necessary to confirm that desirable components of the ECM are retained, such as adhesion proteins like fibronectin and laminin, GAGs, growth factors, elastic fibers, and collagens which will be required for infiltration of the matrix by cells of choice *in vitro* or *in vivo*. Mechanical testing of the ECM after treatment provides insight into presence and integrity of the structural proteins within the scaffold.

Although the above methods provide important information regarding the effectiveness of the decellularization methods, the biologic consequences of small amounts of nuclear material or cytoplasmic debris within the remaining scaffold materials is unclear. There are no reports showing a direct cause-effect relationship between such cellular remnants and an adverse host response to date.

A.1.16 Removal of Residual Chemicals

The decellularization methods described above include a wide variety of chemicals which are used because of their inherent abilities to damage cells. If the chemicals remain within the tissue in high concentrations after treatment, then it is likely that they will be toxic to host cells when the scaffold is implanted *in vivo*. There is a need for development of assays to quantify the presence of residual chemicals in the decellularized scaffold material. Similarly, some of the processes that have been described above include enzymes commonly derived from bovine sources (i.e., DNase, RNase, and trypsin). These enzymes can potentially invoke an adverse immune response by the host.

A.1.17 Conclusion

Complete decellularization of most tissues will require a combination of physical, enzymatic, and chemical treatments, and the protocol will be dependent on the tissue of interest. It is generally desirable to use the mildest protocol possible that yields an acellular material without disruption of the structural and functional component of the ECM. A typical progressive approach would be to start with treatment in a hypotonic or hypertonic solution followed by a mild nonionic or zwitterionic detergent. If necessary, an enzymatic treatment of tryspin/EDTA can be added prior to the detergent treatment to assist in breaking the bonds between the cell membranes and the ECM. Finally, if these treatments are still inadequate to remove the cellular material, an ionic detergent such as SDS, deoxycholate, or Triton X-200 can be added to the decellularization protocol.

It is clear that physical, enzymatic, and chemical treatments can have substantial effects on the composition, mechanical behavior, and host response to biologic scaffolds derived from the decellularization of native tissue and organs, and could have important implications for subsequent use for *in vitro* and *in vivo* applications. The removal of adhesive proteins and GAGs from the scaffold could slow cell migration onto the scaffold and the bioactivity of the scaffold itself. Disruption of the collagen network can change the mechanical behavior and collagen fiber kinematics of the scaffold, which can have an effect on the load bearing capacity of the scaffold and alter the mechanical environment to which the cells are exposed. Degradation is another

important factor that relates to the mechanical behavior and bioactivity of the scaffold that could be affected by decellularization treatments. The chemical treatments could compromise the ECM scaffold in a way that makes it more susceptible to enzymatic degradation *in vivo*, which would lead to a rapid decrease in the strength of the scaffold.

It is unlikely that any combination of methods will remove 100% of all cell components from a tissue or organ. However, it seems apparent that methods which remove most or all of the visible cellular material result in biologic scaffold materials that are safe for implantation. A number of naturally occurring ECM devices and related decellularization protocols have received regulatory approval for use in human patients, including human dermis (Alloderm®, LifeCell, Corp.), porcine SIS (SurgiSIS®, Cook Biotech, Inc.; Restore®, DePuy Orthopaedics, Inc.), porcine urinary bladder (ACell, Inc.), and porcine heart valves (Synergraft®, CryoLife, Inc.).

All of the tissues that have been discussed thus far have been thin connective tissues which generally have a sheet-like shape. The major challenge for decellularization of ECM scaffolds that must be addressed is removal of cellular material from complex 3-D organs while retaining their native architecture and morphology, as this will be a necessary step for using this technology for tissue engineering of whole organs. One approach that has been considered is perfusing chaotropic agents through the existing vasculature of the intact organ. The growing list of biologic scaffolds used for tissue engineering/regenerative medicine applications makes the continued development of decellularization protocols a clinically relevant and important effort.

A.2 RADIOACTIVE LABELING OF ECM

Scaffolds derived from extracellular matrix (ECM) have been widely studied for tissue engineering/regenerative medicine applications. Pre-clinical studies have shown that many of these scaffolds facilitate constructive remodeling of injured tissues and circumvent the default process of scar tissue formation.[24] Several scaffolds composed of ECM are now commercially available for human clinical application.[57, 65, 110, 173, 196, 199, 203, 208, 277] The species of origin, tissue of origin, and processing techniques for the ECM can differ markedly for these devices. It is

well established that factors such as method of decellularization, use of a chemical crosslinking agent, and means of sterilization can substantially affect the host response to the scaffold and the rate of scaffold degradation.[99, 179, 205] The rate of ECM scaffold remodeling, the fate of scaffold degradation products, the source of cells that participate in the remodeling process, and the factors that influence the remodeling process are also important factors and are worthy of investigation.

As an ECM scaffold is remodeled *in vivo*, the fate of the ECM components is rarely considered and therefore poorly understood, and methodologies for investigating the *in vivo* degradation of ECM scaffolds and fate of the degradation products are needed. Radioactive labeling is commonly used in the pharmaceutical industry to determine the metabolic fate of developmental drugs.[42, 171] The most frequently utilized isotope is ^{14}C because it can be stably incorporated into organic compounds and has a long half-life of 5760 years.[42, 171] With advances in detection techniques, such as accelerator mass spectrometry (AMS), exceedingly small amounts of a drug can be tracked. ^{14}C levels on the order of 100 to 1000 times the environmental baseline level of $1.2x10^{-12}$ can be accurately determined with such methods.[42, 171] A similar approach may be useful when applied to *in vivo* ECM scaffold remodeling. The predominant protein within ECM scaffolds is Type I collagen, which in turn is rich in glycine, proline, and hydroxyproline. Proline is internalized by cells and converted to hydroxyproline during the intercellular production and maturation of collagens. Proline may be broken down into CO_2 or utilized for the synthesis of glutamine, glutamate, ornithine, and arginine.[229] Hydroxyproline released from tissue cannot be recycled biosynthetically into proteins,[255] but may be degraded to metabolic precursors and indirectly incorporated into other amino acids.[229] Therefore, ^{14}C labeled proline is a logical choice to incorporate radioactivity into ECM derived scaffolds. The present manuscript describes a method for labeling porcine ECM with ^{14}C for use in scaffold fabrication and quantifies the amount of radioactivity incorporated into a number of clinically interesting porcine tissues.

A.2.1 Study Design and Preparation of ^{14}C labeled ECM

A total of six pigs had ^{14}C labeled proline incorporated into most of their tissues during the first 6 months of life. After sacrifice, a number of organs were harvested, including the aorta, heart, urinary bladder, small intestine, mesenteric lymph nodes, liver, spleen, pancreas, and trachea, for isolation of extracellular matrix and determination of ^{14}C levels within each tissue. The specific methods for labeling the ECM with ^{14}C and quantifying the amount of ^{14}C within the recipient tissues are described below.

The production of radioactively labeled tissues by injection of ^{14}C labeled proline into growing pigs was performed as part of this study was approved by the University of Pittsburgh Radiation Safety Committee and Institutional Animal Care and Use Committee of the University Pittsburgh (protocol number 0309053). The animal care complied with the NIH Guidelines for the Care and Use of Laboratory Animals.

The methods for labeling the porcine tissues with ^{14}C have been reported previously,[100, 229]. Briefly, ^{14}C labeled proline (Amersham Life Science; 256mCi/mmol, 50μCi/ml) was diluted 1:10 in PBS. Piglets were given weekly intravenous injections (i.e., ear vein) of 10μCi of ^{14}C labeled proline from 3 to 26 weeks of age. The pigs were then sacrificed and a number of tissues were harvested including the heart, aorta, small intestine, urinary bladder, liver, lymph nodes, spleen, pancreas, heart, and trachea. These tissues were then processed (e.g., cleaned, decellularized, and disinfected) to isolate the desired ECM scaffold material. The ^{14}C levels of each ECM scaffold were then determined.

A.2.2 Liquid Scintillation Counting

The radioactivity in each sample of interest was measured by liquid scintillation counting (LSC) using a LS1800 B-counter (Beckman Coulter, Somerset, NJ). For the SIS-ECM graft at time zero, the remodeled SIS-urinary bladder tissue, the remodeled SIS-tendon tissue, and all other harvested tissues, approximately 80 mg of tissue was incubated with 1 ml of Solvable (Packard Instruments, Meriden, CT) at 50°C for 2-4 hours. Ten ml of scintillation fluid was then added to each sample and the radioactivity was determined. The tissue radioactivity was reported as CPM/g.

A.2.3 Efficiency of ^{14}C Labeling

Determination of the ^{14}C levels by liquid scintillation counting (LSC) in the tissues harvested from the pigs after 23 weekly injections of ^{14}C labeled proline showed variability in the level of labeling, with the tissues falling into three general groups (Table A-1). ECM from the aorta, liver stroma, SIS, and tracheal cartilage contained the highest levels of radioactive proline at a level of approximately 3500 CPM/g. The second group included ECM scaffolds prepared from the aortic valve, pulmonary valve, left ventricle wall, urinary bladder matrix, lymph node, pancreas, and tracheal mucosa. This second group showed ^{14}C levels at approximately 1500 CPM/g. The last group included only the ECM from the spleen, which showed ^{14}C at background levels despite weekly intravenous injections of radioactively labeled proline.

A.2.4 Significance of ^{14}C Labeling

Scaffolds derived from naturally occurring extracellular matrix proteins have received a great deal of attention in the field of tissue engineering due to their innate bioactivity and the fact that are completely degradable. In addition, site-specific, constructive remodeling occurs with minimal scar tissue formation.[13, 25, 76, 128, 152, 163] Even when ECM scaffolds are chemically treated to yield a more permanent, nondegradable device, the possibility of partial degradation still exists. The present manuscript describes a method for labeling ECM with ^{14}C such that the extent of degradation of scaffolds constructed from this ECM can be accurately determined and the fate of the degradation products can be followed.

The ^{14}C concentration of an ECM scaffold can be increased by at least three orders of magnitude by the intravenous injection of radiolabeled proline during the rapid growth period of pigs; however, not all tissues are labeled equally. ^{14}C was not detected above baseline levels in splenic ECM, while aorta, liver stroma, SIS, and tracheal cartilage and had ^{14}C concentrations approximately 500 times greater than baseline. This inter-tissue difference may be due to the extent of organ development at birth and/or the rate of collagen turnover for the specific tissues. The aorta, liver, and small intestine are organs with high metabolic activity so they are constantly depositing new collagen. The high levels of ^{14}C in tracheal cartilage were surprising since cartilage does not remodel very rapidly. However, the trachea must develop mechanical

integrity quickly, so an abundance of collagen may be synthesized early in life, and then remain at the site for a prolonged period of time. Due to the differences in labeling efficiency, it is necessary to evaluate the level of ^{14}C in each tissue of interest prior to implantation.

There are a number of advantages to labeling scaffolds with ^{14}C to monitor their degradation. First, the ^{14}C is integrally bound to the scaffold at the molecular level, so breakdown of the ECM is required for its release. By binding the radioactive isotope to proline, it is a specific and accurate determinate of ECM turnover. Due to the development of detection methods like accelerator mass spectrometry, this model is exceedingly sensitive to changes in the ^{14}C concentration. Therefore, this approach poses minimal to zero risk to the subject and the investigator.

The approach of labeling ECM with a radioactive isotope is not without limitations. First, this approach requires access to facilities that are able to house and properly handle radioactive materials. The processes to obtain sufficient amounts of labeled tissue and the follow up to monitor removal of the radioactive isotope from the body are time consuming, resource demanding, and expensive. Furthermore, while LSC is useful for tissues that are heavily labeled with ^{14}C, the ^{14}C concentrations are often below the sensitivity of LSC in the remodeling tissue as the scaffold degrades and in tissues that accumulate the degradation products. In these cases, it is necessary to have access to AMS equipment. AMS has increased sensitivity for detection of ^{14}C because the actual molecules of ^{14}C are counted and compared to the number of ^{12}C molecules, as opposed to counting individual radioactive decay events as in LSC. A detailed description of the specimen preparation and methodology for AMS can be found in several comprehensive reviews.[42, 117, 171]

The degradation of scaffolds for tissue engineering/regenerative medicine affects the mechanical integrity of a scaffold and the host response to the scaffold. As a result, the rate of degradation and the fate of the degradation products is a concern to regulatory agencies that must evaluate the safety and efficacy of such devices. Radioactive labeling of a scaffold with ^{14}C is one option to track the degradation products. There may be other approaches that could incorporate other radioactive labels into tissues to track their degradation, including ^{3}H, ^{26}Al, ^{41}Ca, or ^{129}I, which have found use in other biomedical applications.[42] ^{3}H labeling would be advantageous in the current model due to its relative safety and short half-life, but the concern would be that the as a reactive side group, the ^{3}H might be hydrolyzed or otherwise removed

from the proline independent of ECM degradation. If the target tissue was bone, the ^{41}Ca could be an obvious choice to track degradation. Another non-radioactive approach that has been recently reported involved genetically engineering cells so that they tag all elastin fibers with an oligohistidine (His(6)) epitope that can be tracked independent of new tissue formation.[214] Any of these approaches would require extensive time and resources in order to produce sufficient scaffolding material to do appropriate *in vivo* studies. Development of additional novel methodologies will be needed as new applications for ECM scaffolds are investigated and as our need to understand the rate of scaffold degradation and fate of degradation products increases.

A.2.5 Conclusions

Intravenous injection of ^{14}C labeled proline into an animal during the early phase of life is an effective means to incorporate radioactivity into tissues that are utilized to make scaffolds derived from ECM. Radioactive labeling allows for accurate and sensitive determination of the rate of degradation of the scaffold and the fate of the degradation products, which are important considerations for tissue engineering applications. While this approach is attractive due to its sensitivity and safety, it requires access to AMS facilities and is expensive. Development of additional approaches to track the degradation of scaffolds will be necessary for widespread use.

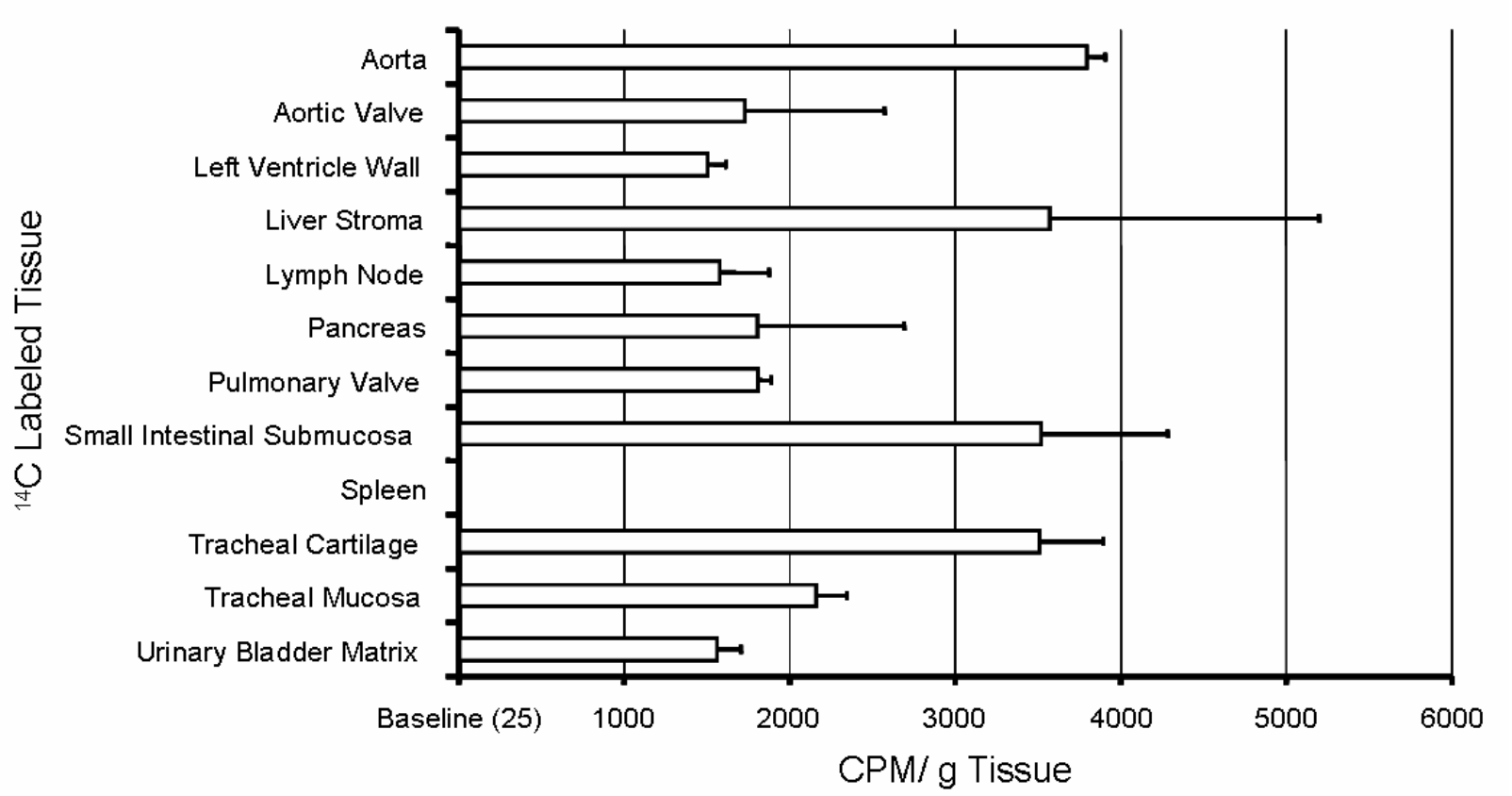

Table A-1. Counts of ^{14}C per minute per gram of labeled porcine tissues using liquid scintillation counting. The more metabolic tissues (aorta, liver, small intestine) tended to have higher levels of ^{14}C at approximately 3500 CPM/g. Interestingly, splenic ECM was not found to have an elevated ^{14}C concentration.

BIBLIOGRAPHY

1. Abe R, Donnelly SC, Peng T, Bucala R, Metz CN, 2001. Peripheral blood fibrocytes: differentiation pathway and migration to wound sites. J Immunol 166,7556-62.

2. Abraham GA, Murray J, Billiar K, Sullivan SJ, 2000. Evaluation of the porcine intestinal collagen layer as a biomaterial. J Biomed Mater Res 51,442-52.

3. Affonso da Costa FD, Dohmen PM, Lopes SV, Lacerda G, Pohl F, Vilani R, Affonso Da Costa MB, Vieira ED, Yoschi S, Konertz W, Affonso da Costa I, 2004. Comparison of cryopreserved homografts and decellularized porcine heterografts implanted in sheep. Artif Organs 28,366-70.

4. Agoram B, Barocas VH, 2001. Coupled macroscopic and microscopic scale modeling of fibrillar tissues and tissue equivalents. J Biomech Eng 123,362-9.

5. Allman AJ, McPherson TB, Badylak SF, Merrill LC, Kallakury B, Sheehan C, Raeder RH, Metzger DW, 2001. Xenogeneic extracellular matrix grafts elicit a TH2-restricted immune response. Transplantation 71,1631-40.

6. Altman GH, Horan RL, Martin I, Farhadi J, Stark PR, Volloch V, Richmond JC, Vunjak-Novakovic G, Kaplan DL, 2002. Cell differentiation by mechanical stress. FASEB J 16,270-2.

7. Androjna C, Spragg RK, Derwin KA, 2006. Mechanical conditioning of cell-seeded small intestine submucosa (SIS): A potential tissue-engineering strategy for tendon repair. Tissue Eng In Press.

8. Arner O, Lindholm A, Orell SR, 1959. Histologic changes in subcutaneous rupture of the Achilles tendon; a study of 74 cases. Acta Chir Scand 116,484-90.

9. Atala A, 1999. Creation of bladder tissue *in vitro* and *in vivo*. A system for organ replacement. Adv Exp Med Biol 462,31-42.

10. Bader A, Schilling T, Teebken OE, Brandes G, Herden T, Steinhoff G, Haverich A, 1998. Tissue engineering of heart valves--human endothelial cell seeding of detergent acellularized porcine valves. Eur J Cardiothorac Surg 14,279-84.

11. Badylak SF, Lantz GC, Coffey A, Geddes LA, 1989. Small intestinal submucosa as a large diameter vascular graft in the dog. J Surg Res 47,74-80.

12. Badylak SF, Coffey AC, Lantz GC, Tacker WA, Geddes LA, 1994. Comparison of the resistance to infection of intestinal submucosa arterial autografts versus polytetrafluoroethylene arterial prostheses in a dog model. J Vasc Surg 19,465-72.

13. Badylak SF, Tullius R, Kokini K, Shelbourne KD, Klootwyk T, Voytik SL, Kraine MR, Simmons C, 1995. The use of xenogeneic small intestinal submucosa as a biomaterial for Achilles tendon repair in a dog model. J Biomed Mater Res 29,977-85.

14. Badylak SF, Kropp B, McPherson T, Liang H, Snyder PW, 1998. Small intestinal submucosa: a rapidly resorbed bioscaffold for augmentation cystoplasty in a dog model. Tissue Eng 4,379-87.

15. Badylak SF, Record R, Lindberg K, Hodde JP, Park K, 1998. Small intestinal submucosa: a substrate for *in vitro* cell growth. J Biomater Sci Polym Ed 9,863-78.

16. Badylak SF, Arnoczky S, Plouhar P, Haut R, Mendenhall V, Clarke R, Horvath C, 1999. Naturally occurring extracellular matrix as a scaffold for musculoskeletal repair. Clin Orthop,S333-43.

17. Badylak SF, Liang A, Record R, Tullius R, Hodde JP, 1999. Endothelial cell adherence to small intestinal submucosa: an acellular bioscaffold. Biomaterials 20,2257-63.

18. Badylak SF, Meurling S, Chen M, Spievack A, Simmons-Byrd A, 2000. Resorbable bioscaffold for esophageal repair in a dog model. J Pediatr Surg 35,1097-103.

19. Badylak SF, Kokini K, Tullius B, Whitson B, 2001. Strength over time of a resorbable bioscaffold for body wall repair in a dog model. J Surg Res 99,282-7.

20. Badylak SF, Park K, Peppas N, McCabe G, Yoder M, 2001. Marrow-derived cells populate scaffolds composed of xenogeneic extracellular matrix. Exp Hematol 29,1310-8.

21. Badylak SF, Kokini K, Tullius B, Simmons-Byrd A, Morff R, 2002. Morphologic study of small intestinal submucosa as a body wall repair device. J Surg Res 103,190-202.

22. Badylak SF, Obermiller J, Geddes L, Matheny R, 2003. Extracellular matrix for myocardial repair. Heart Surg Forum 6,E20-6.

23. Badylak SF, Wu CC, Bible M, McPherson E, 2003. Host protection against deliberate bacterial contamination of an extracellular matrix bioscaffold versus Dacron mesh in a dog model of orthopedic soft tissue repair. J Biomed Mater Res B Appl Biomater 67,648-54.

24. Badylak SF, 2004. Xenogeneic extracellular matrix as a scaffold for tissue reconstruction. Transpl Immunol 12,367-77.

25. Badylak SF, Vorp DA, Spievack AR, Simmons-Byrd A, Hanke J, Freytes DO, Thapa A, Gilbert TW, Nieponice A, 2005. Esophageal reconstruction with ECM and muscle tissue in a dog model. J Surg Res 128,87-97.

26. Badylak SF, Kochupura PV, Cohen IS, Doronin SV, Saltman AE, Gilbert TW, Kelly DJ, Ignotz RA, Gaudette GR, 2006. The use of extracellular matrix as an inductive scaffold for the partial replacement of functional myocardium. Cell Transplant 15 Suppl 1,S29-40.

27. Barocas VH, Tranquillo RT, 1997. An anisotropic biphasic theory of tissue-equivalent mechanics: the interplay among cell traction, fibrillar network deformation, fibril alignment, and cell contact guidance. J Biomech Eng 119,137-45.

28. Bell E, Ivarsson B, Merrill C, 1979. Production of a tissue-like structure by contraction of collagen lattices by human fibroblasts of different proliferative potential *in vitro*. Proc Natl Acad Sci U S A 76,1274-8.

29. Bernard MP, Chu ML, Myers JC, Ramirez F, Eikenberry EF, Prockop DJ, 1983. Nucleotide sequences of complementary deoxyribonucleic acids for the pro alpha 1 chain of human type I procollagen. Statistical evaluation of structures that are conserved during evolution. Biochemistry 22,5213-23.

30. Bernard MP, Myers JC, Chu ML, Ramirez F, Eikenberry EF, Prockop DJ, 1983. Structure of a cDNA for the pro alpha 2 chain of human type I procollagen. Comparison with chick cDNA for pro alpha 2(I) identifies structurally conserved features of the protein and the gene. Biochemistry 22,1139-45.

31. Bey MJ, Song HK, Wehrli FW, Soslowsky LJ, 2002. Intratendinous strain fields of the intact supraspinatus tendon: the effect of glenohumeral joint position and tendon region. J Orthop Res 20,869-74.

32. Billiar K, Murray J, Laude D, Abraham G, Bachrach N, 2001. Effects of carbodiimide crosslinking conditions on the physical properties of laminated intestinal submucosa. J Biomed Mater Res 56,101-8.

33. Billiar KL, Sacks MS, 1997. A method to quantify the fiber kinematics of planar tissues under biaxial stretch. J Biomech 30,753-6.

34. Birk DE, Fitch JM, Babiarz JP, Doane KJ, Linsenmayer TF, 1990. Collagen fibrillogenesis *in vitro*: interaction of types I and V collagen regulates fibril diameter. J Cell Sci 95 (Pt 4),649-57.

35. Birk DE, Mayne R, 1997. Localization of collagen types I, III and V during tendon development. Changes in collagen types I and III are correlated with changes in fibril diameter. Eur J Cell Biol 72,352-61.

36. Birk DE, 2001. Type V collagen: heterotypic type I/V collagen interactions in the regulation of fibril assembly. Micron 32,223-37.

37. Booth C, Korossis SA, Wilcox HE, Watterson KG, Kearney JN, Fisher J, Ingham E, 2002. Tissue engineering of cardiac valve prostheses I: development and histological characterization of an acellular porcine scaffold. J Heart Valve Dis 11,457-62.

38. Borschel GH, Dennis RG, Kuzon WM, Jr., 2004. Contractile skeletal muscle tissue-engineered on an acellular scaffold. Plast Reconstr Surg 113,595-602; discussion 603-4.

39. Brennan EP, Reing J, Chew D, Myers-Irvin J, Young EJ, Badylak SF, 2006. Antibacterial activity within degradation products of biological scaffolds composed of extracellular matrix. Tissue Eng 12,2949-55.

40. Brittan M, Hunt T, Jeffery R, Poulsom R, Forbes SJ, Hodivala-Dilke K, Goldman J, Alison MR, Wright NA, 2002. Bone marrow derivation of pericryptal myofibroblasts in the mouse and human small intestine and colon. Gut 50,752-7.

41. Brown B, Lindberg K, Reing J, Stolz DB, Badylak SF, 2006. The basement membrane component of biologic scaffolds derived from extracellular matrix. Tissue Eng 12,519-26.

42. Brown K, Tompkins EM, White IN, 2006. Applications of accelerator mass spectrometry for pharmacological and toxicological research. Mass Spectrom Rev 25,127-45.

43. Brown RA, Talas G, Porter RA, McGrouther DA, Eastwood M, 1996. Balanced mechanical forces and microtubule contribution to fibroblast contraction. J Cell Physiol 169,439-47.

44. Brown RA, Prajapati R, McGrouther DA, Yannas IV, Eastwood M, 1998. Tensional homeostasis in dermal fibroblasts: mechanical responses to mechanical loading in three-dimensional substrates. J Cell Physiol 175,323-32.

45. Brown SA, Merritt K, Woods TO, McNamee SG, Hitchins VM, 2002. Effects of different disinfection and sterilization methods on tensile strength of materials used for single use devices. Biomed Instrum Technol 36,23-7.

46. Bucala R, Spiegel LA, Chesney J, Hogan M, Cerami A, 1994. Circulating fibrocytes define a new leukocyte subpopulation that mediates tissue repair. Mol Med 1,71-81.

47. Buchholz BA, Arjomand A, Dueker SR, Schneider PD, Clifford AJ, Vogel JS, 1999. Intrinsic erythrocyte labeling and attomole pharmacokinetic tracing of 14C-labeled folic acid with accelerator mass spectrometry. Anal Biochem 269,348-52.

48. Butler DL, Juncosa N, Dressler MR, 2004. Functional efficacy of tendon repair processes. Annu Rev Biomed Eng 6,303-29.

49. Butler JP, Tolic-Norrelykke IM, Fabry B, Fredberg JJ, 2002. Traction fields, moments, and strain energy that cells exert on their surroundings. Am J Physiol Cell Physiol 282,C595-605.

50. Cacou C, Palmer D, Lee DA, Bader DL, Shelton JC, 2000. A system for monitoring the response of uniaxial strain on cell seeded collagen gels. Med Eng Phys 22,327-33.

51. Campbell BH, Agarwal C, Wang JH-C, 2004. TGF-β1, TGF-β3, and PGE-2 regulate contraction of human patellar tendon fibroblasts. Biomech Model Mechanobiol 2,239-45.

52. Caplan AI, 1991. Mesenchymal stem cells. J Orthop Res 9,641-50.

53. Cartmell JS, Dunn MG, 2000. Effect of chemical treatments on tendon cellularity and mechanical properties. J Biomed Mater Res 49,134-40.

54. Carver W, Molano I, Reaves TA, Borg TK, Terracio L, 1995. Role of the alpha 1 beta 1 integrin complex in collagen gel contraction in vitro by fibroblasts. J Cell Physiol 165,425-37.

55. Catena F, Ansaloni L, Leone A, De Cataldis A, Gagliardi S, Gazzotti F, Peruzzi S, Agrusti S, D'Alessandro L, Taffurelli M, 2005. Lichtenstein repair of inguinal hernia with Surgisis inguinal hernia matrix soft-tissue graft in immunodepressed patients. Hernia 9,29-31.

56. Chandran PL, Barocas VH, 2006. Affine versus non-affine fibril kinematics in collagen networks: theoretical studies of network behavior. J Biomech Eng 128,259-70.

57. Chen F, Yoo JJ, Atala A, 1999. Acellular collagen matrix as a possible "off the shelf" biomaterial for urethral repair. Urology 54,407-10.

58. Chen RN, Ho HO, Tsai YT, Sheu MT, 2004. Process development of an acellular dermal matrix (ADM) for biomedical applications. Biomaterials 25,2679-86.

59. Chesney J, Bucala R, 1997. Peripheral blood fibrocytes: novel fibroblast-like cells that present antigen and mediate tissue repair. Biochem Soc Trans 25,520-4.

60. Chesney J, Bucala R, 2000. Peripheral blood fibrocytes: mesenchymal precursor cells and the pathogenesis of fibrosis. Curr Rheumatol Rep 2,501-5.

61. Chiquet-Ehrismann R, Tannheimer M, Koch M, Brunner A, Spring J, Martin D, Baumgartner S, Chiquet M, 1994. Tenascin-C expression by fibroblasts is elevated in stressed collagen gels. J Cell Biol 127,2093-101.

62. Chiquet M, Renedo AS, Huber F, Fluck M, 2003. How do fibroblasts translate mechanical signals into changes in extracellular matrix production? Matrix Biol 22,73-80.

63. Clayton ML, Weir GJ, Jr., 1959. Experimental investigations of ligamentous healing. Am J Surg 98,373-8.

64. Clayton ML, Miles JS, Abdulla M, 1968. Experimental investigations of ligamentous healing. Clin Orthop Relat Res 61,146-53.

65. Colvert JR, 3rd, Kropp BP, Cheng EY, Pope JC, 4th, Brock JW, 3rd, Adams MC, Austin P, Furness PD, 3rd, Koyle MA, 2002. The use of small intestinal submucosa as an off-the-shelf urethral sling material for pediatric urinary incontinence. J Urol 168,1872-5; discussion 1875-6.

66. Conklin BS, Richter ER, Kreutziger KL, Zhong DS, Chen C, 2002. Development and evaluation of a novel decellularized vascular xenograft. Med Eng Phys 24,173-83.

67. Constantinou CD, Jimenez SA, 1991. Structure of cDNAs encoding the triple-helical domain of murine alpha 2 (VI) collagen chain and comparison to human and chick homologues. Use of polymerase chain reaction and partially degenerate oligonucleotide for generation of novel cDNA clones. Matrix 11,1-9.

68. Courtman DW, Pereira CA, Kashef V, McComb D, Lee JM, Wilson GJ, 1994. Development of a pericardial acellular matrix biomaterial: biochemical and mechanical effects of cell extraction. J Biomed Mater Res 28,655-66.

69. Cowin SC, 2000. How is a tissue built? J Biomech Eng 122,553-69.

70. Criscione JC, Sacks MS, Hunter WC, 2003. Experimentally tractable, pseudo-elastic constitutive law for biomembranes: I. Theory. J Biomech Eng 125,94-9.

71. Criscione JC, Sacks MS, Hunter WC, 2003. Experimentally tractable, pseudo-elastic constitutive law for biomembranes: II. Application. J Biomech Eng 125,100-5.

72. Dahl SL, Koh J, Prabhakar V, Niklason LE, 2003. Decellularized native and engineered arterial scaffolds for transplantation. Cell Transplant 12,659-66.

73. Dallon JC, Sherratt JA, Maini PK, 1999. Mathematical modelling of extracellular matrix dynamics using discrete cells: fiber orientation and tissue regeneration. J Theor Biol 199,449-71.

74. De Filippo RE, Yoo JJ, Atala A, 2002. Urethral replacement using cell seeded tubularized collagen matrices. J Urol 168,1789-92; discussion 1792-3.

75. de la Fuente SG, Gottfried MR, Lawson DC, Harris MB, Mantyh CR, Pappas TN, 2003. Evaluation of porcine-derived small intestine submucosa as a biodegradable graft for gastrointestinal healing. J Gastrointest Surg 7,96-101.

76. Dejardin LM, Arnoczky SP, Ewers BJ, Haut RC, Clarke RB, 2001. Tissue-engineered rotator cuff tendon using porcine small intestine submucosa. Histologic and mechanical evaluation in dogs. Am J Sports Med 29,175-84.

77. Dellgren G, Eriksson M, Brodin LA, Radegran K, 1999. The extended Biocor stentless aortic bioprosthesis. Early clinical experience. Scand Cardiovasc J 33,259-64.

78. Dembo M, Wang YL, 1999. Stresses at the cell-to-substrate interface during locomotion of fibroblasts. Biophys J 76,2307-16.

79. Eastwood M, McGrouther DA, Brown RA, 1994. A culture force monitor for measurement of contraction forces generated in human dermal fibroblast cultures: evidence for cell-matrix mechanical signalling. Biochim Biophys Acta 1201,186-92.

80. Eastwood M, Mudera VC, McGrouther DA, Brown RA, 1998. Effect of precise mechanical loading on fibroblast populated collagen lattices: morphological changes. Cell Motil Cytoskeleton 40,13-21.

81. Enwemeka CS, 1989. Inflammation, cellularity, and fibrillogenesis in regenerating tendon: implications for tendon rehabilitation. Phys Ther 69,816-25.

82. Exposito JY, D'Alessio M, Solursh M, Ramirez F, 1992. Sea urchin collagen evolutionarily homologous to vertebrate pro-alpha 2(I) collagen. J Biol Chem 267,15559-62.

83. Falke G, Yoo JJ, Kwon TG, Moreland R, Atala A, 2003. Formation of corporal tissue architecture in vivo using human cavernosal muscle and endothelial cells seeded on collagen matrices. Tissue Eng 9,871-9.

84. Fathke C, Wilson L, Hutter J, Kapoor V, Smith A, Hocking A, Isik F, 2004. Contribution of bone marrow-derived cells to skin: collagen deposition and wound repair. Stem Cells 22,812-22.

85. Finni T, Hodgson JA, Lai AM, Edgerton VR, Sinha S, 2003. Nonuniform strain of human soleus aponeurosis-tendon complex during submaximal voluntary contractions in vivo. J Appl Physiol 95,829-37.

86. Flück M, Tunc-Civelek V, Chiquet M, 2000. Rapid and reciprocal regulation of tenascin-C and tenascin-Y expression by loading of skeletal muscle. J Cell Sci 113,3583-91.

87. Frank C, Bray D, Rademaker A, Chrusch C, Sabiston P, Bodie D, Rangayyan R, 1989. Electron microscopic quantification of collagen fibril diameters in the rabbit medial collateral ligament: a baseline for comparison. Connect Tissue Res 19,11-25.

88. Frank C, McDonald D, Bray D, Bray R, Rangayyan R, Chimich D, Shrive N, 1992. Collagen fibril diameters in the healing adult rabbit medial collateral ligament. Connect Tissue Res 27,251-63.

89. Frank C, McDonald D, Shrive N, 1997. Collagen fibril diameters in the rabbit medial collateral ligament scar: a longer term assessment. Connect Tissue Res 36,261-9.

90. Freytes DO, Badylak SF, Webster TJ, Geddes LA, Rundell AE, 2004. Biaxial strength of multilaminated extracellular matrix scaffolds. Biomaterials 25,2353-61.

91. Freytes DO, Tullius RS, Badylak SF, 2006. Effect of storage upon material properties of lyophilized porcine extracellular matrix derived from the urinary bladder. J Biomed Mater Res B Appl Biomater 78,327-33.

92. Fung YC. Foundations of Solid Mechanics. Englewood Cliffs, NJ, Prentice-Hall, Inc., 1965.

93. Gailit J, Ruoslahti E, 1988. Regulation of the fibronectin receptor affinity by divalent cations. J Biol Chem 263,12927-32.

94. Galbraith CG, Sheetz MP, 1997. A micromachined device provides a new bend on fibroblast traction forces. Proc Natl Acad Sci U S A 94,9114-8.

95. Gamba PG, Conconi MT, Lo Piccolo R, Zara G, Spinazzi R, Parnigotto PP, 2002. Experimental abdominal wall defect repaired with acellular matrix. Pediatr Surg Int 18,327-31.

96. Giddings VL, Beaupre GS, Whalen RT, Carter DR, 2000. Calcaneal loading during walking and running. Med Sci Sports Exerc 32,627-34.

97. Gilbert TW, Stolz DB, Biancaniello F, Simmons-Byrd A, Badylak SF, 2005. Production and characterization of ECM powder: implications for tissue engineering applications. Biomaterials 26,1431-5.

98. Gilbert TW, Sacks MS, Grashow JS, Woo SL-Y, Badylak SF, Chancellor MB, 2006. Fiber kinematics of small intestinal submucosa subjected to uniaxial and biaxial stretch. J Biomech Eng 128.

99. Gilbert TW, Sellaro TL, Badylak SF, 2006. Decellularization of tissues and organs. Biomaterials 27,3675-83.

100. Gilbert TW, Stewart-Akers AM, Simmons-Byrd A, Badylak SF, 2006. Degradation and remodeling of small intestinal submucosa in Achilles tendon repair. J Bone Joint Surg Am In Press.

101. Gilbert TW, Stewart-Akers AM, Sydeski J, Nguyen TD, Badylak SF, Woo SL-Y, 2006. Gene expression by fibroblasts seeded on small intestinal submucosa and subjected to cyclic stretching. Tissue Eng Submitted.

102. Gilbert TW, Stewart-Akers AM, Badylak SF, 2007. A quantitative method for evaluating the degradation of biologic scaffold materials. Biomaterials 28,147-50.

103. Gloeckner DC, Sacks MS, Billiar KL, Bachrach N, 2000. Mechanical evaluation and design of a multilayered collagenous repair biomaterial. J Biomed Mater Res 52,365-73.

104. Goissis G, Suzigan S, Parreira DR, Maniglia JV, Braile DM, Raymundo S, 2000. Preparation and characterization of collagen-elastin matrices from blood vessels intended as small diameter vascular grafts. Artif Organs 24,217-23.

105. Gourevitch D, Clark L, Chen P, Seitz A, Samulewicz SJ, Heber-Katz E, 2003. Matrix metalloproteinase activity correlates with blastema formation in the regenerating MRL mouse ear hole model. Dev Dyn 226,377-87.

106. Grauss RW, Hazekamp MG, van Vliet S, Gittenberger-de Groot AC, DeRuiter MC, 2003. Decellularization of rat aortic valve allografts reduces leaflet destruction and extracellular matrix remodeling. J Thorac Cardiovasc Surg 126,2003-10.

107. Grauss RW, Hazekamp MG, Oppenhuizen F, van Munsteren CJ, Gittenberger-de Groot AC, DeRuiter MC, 2005. Histological evaluation of decellularised porcine aortic valves: matrix changes due to different decellularisation methods. Eur J Cardiothorac Surg 27,566-71.

108. Gulati AK, 1988. Evaluation of acellular and cellular nerve grafts in repair of rat peripheral nerve. J Neurosurg 68,117-23.

109. Hamilton DW, Maul TM, Vorp DA, 2004. Characterization of the response of bone marrow-derived progenitor cells to cyclic strain: implications for vascular tissue-engineering applications. Tissue Eng 10,361-9.

110. Harper C, 2001. Permacol: clinical experience with a new biomaterial. Hosp Med 62,90-5.

111. Hart RA, Woo SL-Y, Newton PO, 1992. Ultrastructural morphometry of anterior cruciate and medial collateral ligaments: an experimental study in rabbits. J Orthop Res 10,96-103.

112. Hartlapp I, Abe R, Saeed RW, Peng T, Voelter W, Bucala R, Metz CN, 2001. Fibrocytes induce an angiogenic phenotype in cultured endothelial cells and promote angiogenesis *in vivo*. FASEB J 15,2215-24.

113. Head DA, Levine AJ, MacKintosh FC, 2003. Distinct regimes of elastic response and deformation modes of cross-linked cytoskeletal and semiflexible polymer networks. Phys Rev E Stat Nonlin Soft Matter Phys 68,061907.

114. Head DA, Levine AJ, MacKintosh FC, 2003. Deformation of cross-linked semiflexible polymer networks. Phys Rev Lett 91,108102.

115. Helton WS, Fisichella PM, Berger R, Horgan S, Espat NJ, Abcarian H, 2005. Short-term outcomes with small intestinal submucosa for ventral abdominal hernia. Arch Surg 140,549-60; discussion 560-2.

116. Hilbert SL, Yanagida R, Souza J, Wolfinbarger L, Jones AL, Krueger P, Stearns G, Bert A, Hopkins RA, 2004. Prototype anionic detergent technique used to decellularize allograft valve conduits evaluated in the right ventricular outflow tract in sheep. J Heart Valve Dis 13,831-40.

117. Hillegonds DJ, Record R, Rickey FA, Badylak SF, Jackson GS, Simmons-Byrd A, Elmore D, Lipschutz ME, 2001. Prime Lab sample handling and data analysis for accelerator-based biomedical radiocarbon analysis. Radiocarbon 43,305-11.

118. Hodde JP, Badylak SF, Brightman AO, Voytik-Harbin SL, 1996. Glycosaminoglycan content of small intestinal submucosa: A bioscaffold for tissue replacement. Tissue Eng 2,209-217.

119. Hodde JP, Badylak SF, Shelbourne KD, 1997. The effect of range of motion on remodeling of small intestinal submucosa (SIS) when used as an Achilles tendon repair material in the rabbit. Tissue Eng 3,27-37.

120. Hodde JP, Record RD, Liang HA, Badylak SF, 2001. Vascular endothelial growth factor in porcine-derived extracellular matrix. Endothelium 8,11-24.

121. Hodde JP, Hiles M, 2002. Virus safety of a porcine-derived medical device: evaluation of a viral inactivation method. Biotechnol Bioeng 79,211-6.

122. Hodde JP, Record R, Tullius R, Badylak SF, 2002. Fibronectin peptides mediate HMEC adhesion to porcine-derived extracellular matrix. Biomaterials 23,1841-8.

123. Hodde JP, Record RD, Tullius RS, Badylak SF, 2002. Retention of endothelial cell adherence to porcine-derived extracellular matrix after disinfection and sterilization. Tissue Eng 8,225-34.

124. Hodde JP, Ernst DM, Hiles MC, 2005. An investigation of the long-term bioactivity of endogenous growth factor in OASIS Wound Matrix. J Wound Care 14,23-5.

125. Holtom PD, Shinar Z, Benna J, Patzakis MJ, 2004. Porcine small intestine submucosa does not show antimicrobial properties. Clin Orthop,18-21.

126. Hristov M, Erl W, Weber PC, 2003. Endothelial progenitor cells: mobilization, differentiation, and homing. Arterioscler Thromb Vasc Biol 23,1185-9.

127. Huang D, Chang TR, Aggarwal A, Lee RC, Ehrlich HP, 1993. Mechanisms and dynamics of mechanical strengthening in ligament-equivalent fibroblast-populated collagen matrices. Ann Biomed Eng 21,289-305.

128. Huber JE, Spievack A, Simmons-Byrd A, Ringel RL, Badylak S, 2003. Extracellular matrix as a scaffold for laryngeal reconstruction. Ann Otol Rhinol Laryngol 112,428-33.

129. Hudson TW, Liu SY, Schmidt CE, 2004. Engineering an improved acellular nerve graft via optimized chemical processing. Tissue Eng 10,1346-58.

130. Hudson TW, Zawko S, Deister C, Lundy S, Hu CY, Lee K, Schmidt CE, 2004. Optimized acellular nerve graft is immunologically tolerated and supports regeneration. Tissue Eng 10,1641-51.

131. Ingram DA, Mead LE, Tanaka H, Meade V, Fenoglio A, Mortell K, Pollok K, Ferkowicz MJ, Gilley D, Yoder MC, 2004. Identification of a novel hierarchy of endothelial progenitor cells using human peripheral and umbilical cord blood. Blood 104,2752-60.

132. Jackson DW, Grood ES, Arnoczky SP, Butler DL, Simon TM, 1987. Freeze dried anterior cruciate ligament allografts. Preliminary studies in a goat model. Am J Sports Med 15,295-303.

133. Jackson DW, Grood ES, Arnoczky SP, Butler DL, Simon TM, 1987. Cruciate reconstruction using freeze dried anterior cruciate ligament allograft and a ligament augmentation device (LAD). An experimental study in a goat model. Am J Sports Med 15,528-38.

134. Jackson DW, Grood ES, Wilcox P, Butler DL, Simon TM, Holden JP, 1988. The effects of processing techniques on the mechanical properties of bone-anterior cruciate ligament-bone allografts. An experimental study in goats. Am J Sports Med 16,101-5.

135. Jackson DW, Windler GE, Simon TM, 1990. Intraarticular reaction associated with the use of freeze-dried, ethylene oxide-sterilized bone-patella tendon-bone allografts in the reconstruction of the anterior cruciate ligament. Am J Sports Med 18,1-10; discussion 10-1.

136. Jackson DW, Grood ES, Cohn BT, Arnoczky SP, Simon TM, Cummings JF, 1991. The effects of in situ freezing on the anterior cruciate ligament. An experimental study in goats. J Bone Joint Surg Am 73,201-13.

137. Jackson DW, Simon TM, 2002. Donor cell survival and repopulation after intraarticular transplantation of tendon and ligament allografts. Microsc Res Tech 58,25-33.

138. Jernigan TW, Croce MA, Cagiannos C, Shell DH, Handorf CR, Fabian TC, 2004. Small intestinal submucosa for vascular reconstruction in the presence of gastrointestinal contamination. Ann Surg 239,733-8; discussion 738-40.

139. Juncosa N, West JR, Galloway MT, Boivin GP, Butler DL, 2003. *In vivo* forces used to develop design parameters for tissue engineered implants for rabbit patellar tendon repair. J Biomech 36,483-8.

140. Kakkar R, Grover SR, 2005. Theoretical study of molecular recognition by Hoechst 33258 derivatives. J Biomol Struct Dynam 23,37-47.

141. Kanda K, Matsuda T, 1994. Mechanical stress-induced orientation and ultrastructural change of smooth muscle cells cultured in three-dimensional collagen lattices. Cell Transplant 3,481-92.

142. Kapuscinski J, Skoczylas B, 1978. Fluorescent complexes of DNA with DAPI 4',6-diamidine-2-phenyl indole.2HCl or DCI 4',6-dicarboxyamide-2-phenyl indole. Nucleic Acids Res 5,3775-99.

143. Kasimir MT, Rieder E, Seebacher G, Silberhumer G, Wolner E, Weigel G, Simon P, 2003. Comparison of different decellularization procedures of porcine heart valves. Int J Artif Organs 26,421-7.

144. Kato Y, Yamataka A, Miyahara K, Sueyoshi N, Hayakawa J, Hayashida M, Migita M, Shimada T, Kobayashi H, Lane GJ, Miyano T, 2004. Recipient non-hematopoietic bone marrow cells in the intestinal graft after fetal small intestinal transplantation. Pediatr Surg Int 20,1-4.

145. Ker RF, Alexander RM, Bennett MB, 1988. Why are mammalian tendons so thick? J Zool 216,309-24.

146. Ketchedjian A, Jones AL, Krueger P, Robinson E, Crouch K, Wolfinbarger L, Jr., Hopkins R, 2005. Recellularization of decellularized allograft scaffolds in ovine great vessel reconstructions. Ann Thorac Surg 79,888-96; discussion 896.

147. Kim BS, Nikolovski J, Bonadio J, Mooney DJ, 1999. Cyclic mechanical strain regulates the development of engineered smooth muscle tissue. Nat Biotechnol 17,979-83.

148. Kim BS, Yoo JJ, Atala A, 2004. Peripheral nerve regeneration using acellular nerve grafts. J Biomed Mater Res A 68,201-9.

149. Kim SG, Akaike T, Sasagaw T, Atomi Y, Kurosawa H, 2002. Gene expression of type I and type III collagen by mechanical stretch in anterior cruciate ligament cells. Cell Struct Funct 27,139-44.

150. Klebe RJ, 1974. Isolation of a collagen-dependent cell attachment factor. Nature 250,248-51.

151. Klebe RJ, 1975. Cell attachment to collagen: the requirement for energy. J Cell Physiol 86,231-6.

152. Kochupura PV, Azeloglu EU, Kelly DJ, Doronin SV, Badylak SF, Krukenkamp IB, Cohen IS, Gaudette GR, 2005. Tissue-engineered myocardial patch derived from extracellular matrix provides regional mechanical function. Circulation 112,I144-9.

153. Kolker AR, Brown DJ, Redstone JS, Scarpinato VM, Wallack MK, 2005. Multilayer reconstruction of abdominal wall defects with acellular dermal allograft (AlloDerm) and component separation. Ann Plast Surg 55,36-41; discussion 41-2.

154. Komatsu K, Viidik A, 1996. Changes in the fibre arrangement of the rat incisor periodontal ligament in relation to various loading levels in vitro. Arch Oral Biol 41,147-59.

155. Komatsu K, Chiba M, 2001. Synchronous recording of load-deformation behaviour and polarized light-microscopic images of the rabbit incisor periodontal ligament during tensile loading. Arch Oral Biol 46,929-37.

156. Komi PV, Fukashiro S, Jarvinen M, 1992. Biomechanical loading of Achilles tendon during normal locomotion. Clin Sports Med 11,521-31.

157. Korossis SA, Booth C, Wilcox HE, Watterson KG, Kearney JN, Fisher J, Ingham E, 2002. Tissue engineering of cardiac valve prostheses II: biomechanical characterization of decellularized porcine aortic heart valves. J Heart Valve Dis 11,463-71.

158. Koumas L, Smith TJ, Phipps RP, 2002. Fibroblast subsets in the human orbit: Thy-1+ and Thy-1- subpopulations exhibit distinct phenotypes. Eur J Immunol 32,477-85.

159. Koumas L, Smith TJ, Feldon S, Blumberg N, Phipps RP, 2003. Thy-1 expression in human fibroblast subsets defines myofibroblastic or lipofibroblastic phenotypes. Am J Pathol 163,1291-300.

160. Kral T, Widerak K, Langner M, Hof M, 2005. Propidium iodide and PicoGreen as dyes for the DNA fluorescence correlation spectroscopy measurements. J Fluoresc 15,179-83.

161. Krause DS, Theise ND, Collector MI, Henegariu O, Hwang S, Gardner R, Neutzel S, Sharkis SJ, 2001. Multi-organ, multi-lineage engraftment by a single bone marrow-derived stem cell. Cell 105,369-77.

162. Kropp BP, Eppley BL, Prevel CD, Rippy MK, Harruff RC, Badylak SF, Adams MC, Rink RC, Keating MA, 1995. Experimental assessment of small intestinal submucosa as a bladder wall substitute. Urology 46,396-400.

163. Kropp BP, Rippy MK, Badylak SF, Adams MC, Keating MA, Rink RC, Thor KB, 1996. Regenerative urinary bladder augmentation using small intestinal submucosa: urodynamic and histopathologic assessment in long-term canine bladder augmentations. J Urol 155,2098-104.

164. Kropp BP, Sawyer BD, Shannon HE, Rippy MK, Badylak SF, Adams MC, Keating MA, Rink RC, Thor KB, 1996. Characterization of small intestinal submucosa regenerated canine detrusor: assessment of reinnervation, in vitro compliance and contractility. J Urol 156,599-607.

165. Kropp BP, Cheng EY, Pope JCt, Brock JW, 3rd, Koyle MA, Furness PD, 3rd, Weigel ND, Keck RW, Kropp KA, 2002. Use of small intestinal submucosa for corporal body grafting in cases of severe penile curvature. J Urol 168,1742-5; discussion 1745.

166. Lambert CA, Soudant EP, Nusgens BV, Lapiere CM, 1992. Pretranslational regulation of extracellular matrix macromolecules and collagenase expression in fibroblasts by mechanical forces. Lab Invest 66,444-51.

167. Lange P, Hopkins R, Brockbank K. Allograft valve banking: techniques and technology. In: Cardiac reconstructions wiht allograft valves, pp 37-64. Ed by R Hopkins. New York, Springer-Verlag, 1989.

168. Langelier E, Rancourt D, Bouchard S, Lord C, Stevens PP, Germain L, Auger FA, 1999. Cyclic traction machine for long-term culture of fibroblast-populated collagen gels. Ann Biomed Eng 27,67-72.

169. Lanir Y, 1979. A structural theory for the homogeneous biaxial stress-strain relationships in flat collagenous tissues. J Biomech 12,423-36.

170. Lapiere CM, Nusgens B, Pierard GE, 1977. Interaction between collagen type I and type III in conditioning bundles organization. Connect Tissue Res 5,21-9.

171. Lappin G, Garner RC, 2004. Current perspectives of ^{14}C-isotope measurement in biomedical accelerator mass spectrometry. Anal Bioanal Chem 378,356-64.

172. Latt SA, Wohlleb JC, 1975. Optical studies of the interaction of 33258 Hoechst with DNA, chromatin, and metaphase chromosomes. Chromosoma 52,297-316.

173. Lee MS, 2004. GraftJacket augmentation of chronic Achilles tendon ruptures. Orthopedics 27,s151-3.

174. Leferovich JM, Bedelbaeva K, Samulewicz S, Zhang XM, Zwas D, Lankford EB, Heber-Katz E, 2001. Heart regeneration in adult MRL mice. Proc Natl Acad Sci U S A 98,9830-5.

175. Li F, Li W, Johnson S, Ingram D, Yoder M, Badylak S, 2004. Low-molecular-weight peptides derived from extracellular matrix as chemoattractants for primary endothelial cells. Endothelium 11,199-206.

176. Li F, Li W, Johnson S, Ingram D, Yoder M, Badylak SF, 2004. Low-molecular-weight peptides derived from extracellular matrix as chemoattractants for primary endothelial cells. Endothelium 11,199-206.

177. Li Z, Yang G, Khan M, Stone D, Woo SL-Y, Wang JH-C, 2004. Inflammatory response of human tendon fibroblasts to cyclic mechanical stretching. Am J Sports Med 32,435-40.

178. Lian Q, Samuel TS, Dheen ST, 2003. Enhanced expression of transforming growth factor-β isoforms in the neural tube of embryos derived from diabetic mice exposed to cyclophosphamide. Neurosci Lett 351,51-5.

179. Liang HC, Chang Y, Hsu CK, Lee MH, Sung HW, 2004. Effects of crosslinking degree of an acellular biological tissue on its tissue regeneration pattern. Biomaterials 25,3541-52.

180. Liang R, Woo SL-Y, Takakura Y, Moon DK, Jia F, Abramowitch SD, 2006. Long-term effects of porcine small intestine submucosa on the healing of medial collateral ligament: a functional tissue engineering study. J Orthop Res 24,811-9.

181. Liechty KW, MacKenzie TC, Shaaban AF, Radu A, Moseley AM, Deans R, Marshak DR, Flake AW, 2000. Human mesenchymal stem cells engraft and demonstrate site-specific differentiation after in utero transplantation in sheep. Nat Med 6,1282-6.

182. Lin P, Chan WC, Badylak SF, Bhatia SN, 2004. Assessing porcine liver-derived biomatrix for hepatic tissue engineering. Tissue Eng 10,1046-53.

183. Linsenmayer TF, Gibney E, Igoe F, Gordon MK, Fitch JM, Fessler LI, Birk DE, 1993. Type V collagen: molecular structure and fibrillar organization of the chicken alpha 1(V) NH2-terminal domain, a putative regulator of corneal fibrillogenesis. J Cell Biol 121,1181-9.

184. Loesberg WA, Walboomers XF, van Loon JJ, Jansen JA, 2005. The effect of combined cyclic mechanical stretching and microgrooved surface topography on the behavior of fibroblasts. J Biomed Mater Res A 75,723-32.

185. Lokiec F, Ezra E, Khermosh O, Wientroub S, 1996. Simple bone cysts treated by percutaneous autologous marrow grafting. A preliminary report. J Bone Joint Surg Br 78,934-7.

186. Lu SH, Cannon TW, Chermanski C, Pruchnic R, Somogyi G, Sacks M, de Groat WC, Huard J, Chancellor MB, 2003. Muscle-derived stem cells seeded into acellular scaffolds develop calcium-dependent contractile activity that is modulated by nicotinic receptors. Urology 61,1285-91.

187. Lu SH, Sacks MS, Chung SY, Gloeckner DC, Pruchnic R, Huard J, de Groat WC, Chancellor MB, 2005. Biaxial mechanical properties of muscle-derived cell seeded small intestinal submucosa for bladder wall reconstitution. Biomaterials 26,443-9.

188. Lyman J, Weinhold PS, Almekinders LC, 2004. Strain behavior of the distal Achilles tendon: implications for insertional Achilles tendinopathy. Am J Sports Med 32,457-61.

189. MacLeod TM, Sarathchandra P, Williams G, Sanders R, Green CJ, 2004. Evaluation of a porcine origin acellular dermal matrix and small intestinal submucosa as dermal replacements in preventing secondary skin graft contraction. Burns 30,431-7.

190. Maffulli N, Tallon C, Wong J, Lim KP, Bleakney R, 2003. Early weightbearing and ankle mobilization after open repair of acute midsubstance tears of the Achilles tendon. Am J Sports Med 31,692-700.

191. Mantovani A, Sica A, Sozzani S, Allavena P, Vecchi A, Locati M, 2004. The chemokine system in diverse forms of macrophage activation and polarization. Trends Immunol 25,677-86.

192. Manwaring ME, Walsh JF, Tresco PA, 2004. Contact guidance induced organization of extracellular matrix. Biomaterials 25,3631-8.

193. Martins-Green M, Bissel MF, 1995. Cell-extracellular matrix interactions in development. Semin Dev Biol 6,149-159.

194. Masuda H, Kalka C, Asahara T, 2000. Endothelial progenitor cells for regeneration. Hum Cell 13,153-60.

195. Matziolis G, Tuischer J, Kasper G, Thompson M, Bartmeyer B, Krocker D, Perka C, Duda G, 2006. Simulation of cell differentiation in fracture healing: mechanically loaded composite scaffolds in a novel bioreactor system. Tissue Eng 12,201-8.

196. McCready RA, Hodde J, Irwin RJ, Coffey AC, Divelbiss JL, Bryant MA, Chitwood RW, Paget DS, Chess BA, 2005. Pseudoaneurysm formation in a subset of patients with small intestinal submucosa biologic patches after carotid endarterectomy. J Vasc Surg 41,782-8.

197. McDevitt CA, Wildey GM, Cutrone RM, 2003. Transforming growth factor-beta1 in a sterilized tissue derived from the pig small intestine submucosa. J Biomed Mater Res A 67,637-40.

198. McFetridge PS, Daniel JW, Bodamyali T, Horrocks M, Chaudhuri JB, 2004. Preparation of porcine carotid arteries for vascular tissue engineering applications. J Biomed Mater Res A 70,224-34.

199. Metcalf MH, Savoie FH, Kellum B, 2002. Surgical technique for xenograft (SIS) augmentation of rotator-cuff repairs. Oper Tech Orthop 12,204-8.

200. Monboisee JC, Borel JP, 1992. Oxidative damage in collagen. EXS 62,323-7.

201. Moore R, Madara JL, MacLeod RJ, 1994. Enterocytes adhere preferentially to collagen IV in a differentially regulated divalent cation-dependent manner. Am J Physiol 266,G1099-107.

202. Morlock M, Schneider E, Bluhm A, Vollmer M, Bergmann G, Muller V, Honl M, 2001. Duration and frequency of every day activities in total hip patients. J Biomech 34,873-81.

203. Mostow EN, Haraway GD, Dalsing M, Hodde JP, King D, 2005. Effectiveness of an extracellular matrix graft (OASIS Wound Matrix) in the treatment of chronic leg ulcers: a randomized clinical trial. J Vasc Surg 41,837-43.

204. Moulin V, Tam BY, Castilloux G, Auger FA, O'Connor-McCourt MD, Philip A, Germain L, 2001. Fetal and adult human skin fibroblasts display intrinsic differences in contractile capacity. J Cell Physiol 188,211-22.

205. Munting E, Wilmart JF, Wijne A, Hennebert P, Delloye C, 1988. Effect of sterilization on osteoinduction. Comparison of five methods in demineralized rat bone. Acta Orthop Scand 59,34-8.

206. Musahl V, Abramowitch SD, Gilbert TW, Tsuda E, Wang JH-C, Badylak SF, Woo SL-Y, 2004. The use of porcine small intestinal submucosa to enhance the healing of the medial collateral ligament--a functional tissue engineering study in rabbits. J Orthop Res 22,214-20.

207. Nakamura N, Hart DA, Boorman RS, Kaneda Y, Shrive NG, Marchuk LL, Shino K, Ochi T, Frank CB, 2000. Decorin antisense gene therapy improves functional healing of early rabbit ligament scar with enhanced collagen fibrillogenesis *in vivo*. J Orthop Res 18,517-23.

208. Niezgoda JA, Van Gils CC, Frykberg RG, Hodde JP, 2005. Randomized clinical trial comparing OASIS Wound Matrix to Regranex Gel for diabetic ulcers. Adv Skin Wound Care 18,258-66.

209. Niklason LE, Gao J, Abbott WM, Hirschi KK, Houser S, Marini R, Langer R, 1999. Functional arteries grown in vitro. Science 284,489-93.

210. Niyibizi C, Kavalkovich K, Yamaji T, Woo SL-Y, 2000. Type V collagen is increased during rabbit medial collateral ligament healing. Knee Surg Sports Traumatol Arthrosc 8,281-5.

211. Noda N, Minoura H, Nishiura R, Toyoda N, Imanaka-Yoshida K, Sakakura T, Yoshida T, 2000. Expression of tenascin-C in stromal cells of the murine uterus during early pregnancy: induction by interleukin-1α, prostaglandin E(2), and prostaglandin F(2α). Biol Reprod 63,1713-20.

212. O'Donoghue DH, Frank GR, Jeter GL, Johnson W, Zeiders JW, Kenyon R, 1971. Repair and reconstruction of the anterior cruciate ligament in dogs. Factors influencing long-term results. J Bone Joint Surg Am 53,710-8.

213. Ohland KJ, Woo SL-Y, Weiss JA. Healing of combined injuries of the rabbit medial collateral ligament and its insertions: a long term study of the effects of conservative vs. surgical treatment. In: ASME Adv Bioeng, pp 447-8, 1991.

214. Ong SR, Trabbic-Carlson KA, Nettles DL, Lim DW, Chilkoti A, Setton LA, 2006. Epitope tagging for tracking elastin-like polypeptides. Biomaterials 27,1930-5.

215. Orberg J, Baer E, Hiltner A, 1983. Organization of collagen fibers in the intestine. Connect Tissue Res 11,285-97.

216. Orberg JW, Klein L, Hiltner A, 1982. Scanning electron microscopy of collagen fibers in intestine. Connect Tissue Res 9,187-93.

217. Pedersen JA, Swartz MA, 2005. Mechanobiology in the third dimension. Ann Biomed Eng 33,1469-1490.

218. Peperzak KA, Gilbert TW, Wang JH-C, 2004. A multi-station dynamic-culture force monitor system to study cell mechanobiology. Med Eng Phys 26,355-8.

219. Petersen W, Varoga D, Zantop T, Hassenpflug J, Mentlein R, Pufe T, 2004. Cyclic strain influences the expression of the vascular endothelial growth factor (VEGF) and the hypoxia inducible factor 1 alpha (HIF-1alpha) in tendon fibroblasts. J Orthop Res 22,847-53.

220. Prajapati RT, Chavally-Mis B, Herbage D, Eastwood M, Brown RA, 2000. Mechanical loading regulates protease production by fibroblasts in three-dimensional collagen substrates. Wound Repair Regen 8,226-37.

221. Prajapati RT, Eastwood M, Brown RA, 2000. Duration and orientation of mechanical loads determine fibroblast cyto-mechanical activation: monitored by protease release. Wound Repair Regen 8,238-46.

222. Prevel CD, Eppley BL, Summerlin DJ, Sidner R, Jackson JR, McCarty M, Badylak SF, 1995. Small intestinal submucosa: utilization as a wound dressing in full-thickness rodent wounds. Ann Plast Surg 35,381-8.

223. Probst M, Dahiya R, Carrier S, Tanagho EA, 1997. Reproduction of functional smooth muscle tissue and partial bladder replacement. Br J Urol 79,505-15.

224. Prockop DJ, 1997. Marrow stromal cells as stem cells for nonhematopoietic tissues. Science 276,71-4.

225. Pruss A, Kao M, Kiesewetter H, von Versen R, Pauli G, 1999. Virus safety of avital bone tissue transplants: evaluation of sterilization steps of spongiosa cuboids using a peracetic acid-methanol mixture. Biologicals 27,195-201.

226. Quintana JR, Lipanov AA, Dickerson RE, 1991. Low-temperature crystallographic analyses of the binding of Hoechst 33258 to the double-helical DNA dodecamer C-G-C-G-A-A-T-T-C-G-C-G. Biochemistry 30,10294-306.

227. Raghavan D, Kropp BP, Lin HK, Zhang Y, Cowan R, Madihally SV, 2005. Physical characteristics of small intestinal submucosa scaffolds are location-dependent. J Biomed Mater Res A 73,90-6.

228. Ratajczak MZ, Kucia M, Majka M, Reca R, Ratajczak J, 2004. Heterogeneous populations of bone marrow stem cells--are we spotting on the same cells from the different angles? Folia Histochem Cytobiol 42,139-46.

229. Record RD, Hillegonds D, Simmons C, Tullius R, Rickey FA, Elmore D, Badylak SF, 2001. In vivo degradation of ^{14}C-labeled small intestinal submucosa (SIS) when used for urinary bladder repair. Biomaterials 22,2653-9.

230. Reilly P, Amis AA, Wallace AL, Emery RJ, 2003. Mechanical factors in the initiation and propagation of tears of the rotator cuff. Quantification of strains of the supraspinatus tendon in vitro. J Bone Joint Surg Br 85,594-9.

231. Rieder E, Kasimir MT, Silberhumer G, Seebacher G, Wolner E, Simon P, Weigel G, 2004. Decellularization protocols of porcine heart valves differ importantly in efficiency of cell removal and susceptibility of the matrix to recellularization with human vascular cells. J Thorac Cardiovasc Surg 127,399-405.

232. Roberts TS, Drez D, Jr., McCarthy W, Paine R, 1991. Anterior cruciate ligament reconstruction using freeze-dried, ethylene oxide-sterilized, bone-patellar tendon-bone allografts. Two year results in thirty-six patients. Am J Sports Med 19,35-41.

233. Robinson KA, Li J, Mathison M, Redkar A, Cui J, Chronos NA, Matheny RG, Badylak SF, 2005. Extracellular matrix scaffold for cardiac repair. Circulation 112,I135-43.

234. Sacks MS, Smith DB, Hiester ED, 1997. A small angle light scattering device for planar connective tissue microstructural analysis. Ann Biomed Eng 25,678-89.

235. Sacks MS, Chuong CJ, 1998. Orthotropic mechanical properties of chemically treated bovine pericardium. Ann Biomed Eng 26,892-902.

236. Sacks MS, 1999. A method for planar biaxial mechanical testing that includes in-plane shear. J Biomech Eng 121,551-5.

237. Sacks MS, Gloeckner DC, 1999. Quantification of the fiber architecture and biaxial mechanical behavior of porcine intestinal submucosa. J Biomed Mater Res 46,1-10.

238. Sacks MS, 2003. Incorporation of experimentally-derived fiber orientation into a structural constitutive model for planar collagenous tissues. J Biomech Eng 125,280-7.

239. Sandusky GE, Jr., Badylak SF, Morff RJ, Johnson WD, Lantz G, 1992. Histologic findings after *in vivo* placement of small intestine submucosal vascular grafts and saphenous vein grafts in the carotid artery in dogs. Am J Pathol 140,317-24.

240. Sarikaya A, Record R, Wu CC, Tullius B, Badylak S, Ladisch M, 2002. Antimicrobial activity associated with extracellular matrices. Tissue Eng 8,63-71.

241. Sarikaya A, Record R, Wu CC, Tullius B, Badylak SF, Ladisch M, 2002. Antimicrobial activity associated with extracellular matrices. Tissue Eng 8,63-71.

242. Sawhney RK, Howard J, 2002. Slow local movements of collagen fibers by fibroblasts drive the rapid global self-organization of collagen gels. J Cell Biol 157,1083-91.

243. Schenke-Layland K, Vasilevski O, Opitz F, Konig K, Riemann I, Halbhuber KJ, Wahlers T, Stock UA, 2003. Impact of decellularization of xenogeneic tissue on extracellular matrix integrity for tissue engineering of heart valves. J Struct Biol 143,201-8.

244. Schiro JA, Chan BM, Roswit WT, Kassner PD, Pentland AP, Hemler ME, Eisen AZ, Kupper TS, 1991. Integrin alpha 2 beta 1 (VLA-2) mediates reorganization and contraction of collagen matrices by human cells. Cell 67,403-10.

245. Schmidt CE, Baier JM, 2000. Acellular vascular tissues: natural biomaterials for tissue repair and tissue engineering. Biomaterials 21,2215-31.

246. Schoenfeld JR, Vasser M, Jhurani P, Ng P, Hunter JJ, Ross J, Jr., Chien KR, Lowe DG, 1998. Distinct molecular phenotypes in murine cardiac muscle development, growth, and hypertrophy. J Mol Cell Cardiol 30,2269-80.

247. Screen HR, Lee DA, Bader DL, Shelton JC, 2003. Development of a technique to determine strains in tendons using the cell nuclei. Biorheology 40,361-8.

248. Seddon AM, Curnow P, Booth PJ, 2004. Membrane proteins, lipids and detergents: not just a soap opera. Biochim Biophys Acta 1666,105-17.

249. Seliktar D, Black RA, Vito RP, Nerem RM, 2000. Dynamic mechanical conditioning of collagen-gel blood vessel constructs induces remodeling in vitro. Ann Biomed Eng 28,351-62.

250. Seliktar D, Nerem RM, Galis ZS, 2001. The role of matrix metalloproteinase-2 in the remodeling of cell-seeded vascular constructs subjected to cyclic strain. Ann Biomed Eng 29,923-34.

251. Sethi KK, Mudera V, Sutterlin R, Baschong W, Brown RA, 2002. Contraction-mediated pinocytosis of RGD-peptide by dermal fibroblasts: inhibition of matrix attachment blocks contraction and disrupts microfilament organisation. Cell Motil Cytoskeleton 52,231-41.

252. Shell DH, 4th, Croce MA, Cagiannos C, Jernigan TW, Edwards N, Fabian TC, 2005. Comparison of small-intestinal submucosa and expanded polytetrafluoroethylene as a vascular conduit in the presence of gram-positive contamination. Ann Surg 241,995-1001; discussion 1001-4.

253. Skutek M, van Griensven M, Zeichen J, Brauer N, Bosch U, 2001. Cyclic mechanical stretching modulates secretion pattern of growth factors in human tendon fibroblasts. Eur J Appl Physiol 86,48-52.

254. Skutek M, van Griensven M, Zeichen J, Brauer N, Bosch U, 2001. Cyclic mechanical stretching enhances secretion of Interleukin 6 in human tendon fibroblasts. Knee Surg Sports Traumatol Arthrosc 9,322-6.

255. Stetten MR, 1949. Some aspects of the metabolism of hydroxyproline, studied with the aid of isotopic nitrogen. J Biol Chem 181,31-7.

256. Strange PS, 2003. Small intestinal submucosa for laparoscopic repair of large paraesophageal hiatal hernias: a preliminary report. Surg Technol Int 11,141-3.

257. Suchak AA, Spooner C, Reid DC, Jomha NM, 2006. Postoperative rehabilitation protocols for Achilles tendon ruptures: a meta-analysis. Clin Orthop Relat Res 445,216-21.

258. Suckow MA, Voytik-Harbin SL, Terril LA, Badylak SF, 1999. Enhanced bone regeneration using porcine small intestinal submucosa. J Invest Surg 12,277-87.

259. Sumpio BE, Banes AJ, Link WG, Johnson G, Jr., 1988. Enhanced collagen production by smooth muscle cells during repetitive mechanical stretching. Arch Surg 123,1233-6.

260. Sumpio BE, Banes AJ, Link GW, Iba T, 1990. Modulation of endothelial cell phenotype by cyclic stretch: inhibition of collagen production. J Surg Res 48,415-20.

261. Sun W, Sacks MS, Scott MJ, 2005. Effects of boundary conditions on the estimation of the planar biaxial mechanical properties of soft tissues. J Biomech Eng 127,709-15.

262. Teebken OE, Bader A, Steinhoff G, Haverich A, 2000. Tissue engineering of vascular grafts: human cell seeding of decellularised porcine matrix. Eur J Vasc Endovasc Surg 19,381-6.

263. Tepper OM, Capla JM, Galiano RD, Ceradini DJ, Callaghan MJ, Kleinman ME, Gurtner GC, 2005. Adult vasculogenesis occurs through in situ recruitment, proliferation, and tubulization of circulating bone marrow-derived cells. Blood 105,1068-77.

264. Tipton CM, James SL, Mergner W, Tcheng TK, 1970. Influence of exercise on strength of medial collateral knee ligaments of dogs. Am J Physiol 218,894-902.

265. Tomasek JJ, Haaksma CJ, Eddy RJ, Vaughan MB, 1992. Fibroblast contraction occurs on release of tension in attached collagen lattices: dependency on an organized actin cytoskeleton and serum. Anat Rec 232,359-68.

266. Tower TT, Neidert MR, Tranquillo RT, 2002. Fiber alignment imaging during mechanical testing of soft tissues. Ann Biomed Eng 30,1221-33.

267. Uchimura E, Sawa Y, Taketani S, Yamanaka Y, Hara M, Matsuda H, Miyake J, 2003. Novel method of preparing acellular cardiovascular grafts by decellularization with poly(ethylene glycol). J Biomed Mater Res A 67,834-7.

268. Ueno T, Pickett LC, de la Fuente SG, Lawson DC, Pappas TN, 2004. Clinical application of porcine small intestinal submucosa in the management of infected or potentially contaminated abdominal defects. J Gastrointest Surg 8,109-12.

269. Valentin JE, Badylak JS, McCabe GP, Badylak SF, 2006. Extracellular matrix bioscaffolds for orthopaedic applications: a comparative histologic study. J Bone Joint Surg Am In Press.

270. Valentin JE, Stewart-Akers AM, Ravindra A, Badylak SF. A comparison of macrophage phenotype response to different commercially available ECM-based scaffolds. In: Regenerate - World Congress of Tissue Engineering. Pittsburgh, PA, 2006.

271. van Wachem PB, van Luyn MJ, Olde Damink LH, Dijkstra PJ, Feijen J, Nieuwenhuis P, 1994. Tissue regenerating capacity of carbodiimide-crosslinked dermal sheep collagen during repair of the abdominal wall. Int J Artif Organs 17,230-9.

272. Vaught JD, Kropp BP, Sawyer BD, Rippy MK, Badylak SF, Shannon HE, Thor KB, 1996. Detrusor regeneration in the rat using porcine small intestinal submucosal grafts: functional innervation and receptor expression. J Urol 155,374-8.

273. Voet D, Voet JG, Pratt CW. Fundamentals of Biochemistry. New York, John Wiley & Sons, Inc., 2002.

274. Voytik-Harbin SL, Brightman AO, Kraine MR, Waisner B, Badylak SF, 1997. Identification of extractable growth factors from small intestinal submucosa. J Cell Biochem 67,478-91.

275. Voytik-Harbin SL, Roeder BA, Sturgis JE, Kokini K, Robinson JP, 2003. Simultaneous mechanical loading and confocal reflection microscopy for three-dimensional microbiomechanical analysis of biomaterials and tissue constructs. Microsc Microanal 9,74-85.

276. Vyavahare N, Hirsch D, Lerner E, Baskin JZ, Schoen FJ, Bianco R, Kruth HS, Zand R, Levy RJ, 1997. Prevention of bioprosthetic heart valve calcification by ethanol preincubation. Efficacy and mechanisms. Circulation 95,479-88.

277. Wainwright DJ, 1995. Use of an acellular allograft dermal matrix (AlloDerm) in the management of full-thickness burns. Burns 21,243-8.

278. Walter DH, Dimmeler S, 2002. Endothelial progenitor cells: regulation and contribution to adult neovascularization. Herz 27,579-88.

279. Wang JH-C, Jia F, Gilbert TW, Woo SL-Y, 2003. Cell orientation determines the alignment of cell-produced collagenous matrix. J Biomech 36,97-102.

280. Wang JH-C, Li Z, Yang G, Khan M, 2004. Repetitively stretched tendon fibroblasts produce inflammatory mediators. Clin Orthop Relat Res,243-50.

281. Wang JH-C, 2006. Mechanobiology of tendon. J Biomech 39,1563-82.

282. Wang N, Tolic-Norrelykke IM, Chen J, Mijailovich SM, Butler JP, Fredberg JJ, Stamenovic D, 2002. Cell prestress. I. Stiffness and prestress are closely associated in adherent contractile cells. Am J Physiol Cell Physiol 282,C606-16.

283. Waykole P, Heidemann E, 1976. Dityrosine in collagen. Connect Tissue Res 4,219-22.

284. Weiss JA, Woo SL-Y, Ohland KJ, Horibe S, Newton PO, 1991. Evaluation of a new injury model to study medial collateral ligament healing: primary repair versus nonoperative treatment. J Orthop Res 9,516-28.

285. Wenstrup RJ, Florer JB, Brunskill EW, Bell SM, Chervoneva I, Birk DE, 2004. Type V collagen controls the initiation of collagen fibril assembly. J Biol Chem 279,53331-7.

286. Whitson BA, Cheng BC, Kokini K, Badylak SF, Patel U, Morff R, O'Keefe CR, 1998. Multilaminate resorbable biomedical device under biaxial loading. J Biomed Mater Res 43,277-81.

287. Wientroub S, Goodwin D, Khermosh O, Salama R, 1989. The clinical use of autologous marrow to improve osteogenic potential of bone grafts in pediatric orthopedics. J Pediatr Orthop 9,186-90.

288. Woo SL-Y, Inoue M, McGurk-Burleson E, Gomez MA, 1987. Treatment of the medial collateral ligament injury. II: Structure and function of canine knees in response to differing treatment regimens. Am J Sports Med 15,22-9.

289. Woo SL-Y, Takakura Y, Liang R, Jia F, Moon DK, 2006. Treatment with bioscaffold enhances the fibril morphology and the collagen composition of healing medial collateral ligament in rabbits. Tissue Eng 12,159-66.

290. Woods T, Gratzer PF, 2005. Effectiveness of three extraction techniques in the development of a decellularized bone-anterior cruciate ligament-bone graft. Biomaterials 26,7339-7349.

291. Wren TA, Yerby SA, Beaupre GS, Carter DR, 2001. Mechanical properties of the human Achilles tendon. Clin Biomech (Bristol, Avon) 16,245-51.

292. Yang G, Crawford RC, Wang JH-C, 2004. Proliferation and collagen production of human patellar tendon fibroblasts in response to cyclic uniaxial stretching in serum-free conditions. J Biomech 37,1543-50.

293. Yang Z, Lin JS, Chen J, Wang JH-C, 2006. Determining substrate displacement and cell traction fields-a new approach. J Theor Biol.

294. Yoder MC, Cumming JG, Hiatt K, Mukherjee P, Williams DA, 1996. A novel method of myeloablation to enhance engraftment of adult bone marrow cells in newborn mice. Biol Blood Marrow Transplant 2,59-67.

295. Yoo JJ, Meng J, Oberpenning F, Atala A, 1998. Bladder augmentation using allogenic bladder submucosa seeded with cells. Urology 51,221-5.

296. Zantop T, Gilbert TW, Yoder MC, Badylak SF, 2006. Extracellular matrix scaffolds are repopulated by bone marrow-derived cells in a mouse model of Achilles tendon reconstruction. J Orthop Res 24,1299-309.

297. Zeng YJ, Qiao AK, Yu JD, Zhao JB, Liao DH, Xu XH, Hans G, 2003. Collagen fiber angle in the submucosa of small intestine and its application in Gastroenterology. World J Gastroenterol 9,804-7.

298. Zimmerman RA, Tomasek JJ, McRae J, Haaksma CJ, Schwartz RJ, Lin HK, Cowan RL, Jones AN, Kropp BP, 2004. Decreased expression of smooth muscle alpha-actin results in decreased contractile function of the mouse bladder. J Urol 172,1667-72.